BIOMEMS GLUCOSE SENSORS

BIOMEMS GLUCOSE SENSORS

By

Andrey Zdanovich, B.Sc.

A Thesis

Submitted to the School of Graduate Studies

in Partial Fulfilment of the Requirements

for the Degree

Master of Applied Sciences

McMaster University

MASTER OF APPLIED SCIENCES (2010)
(Engineering Physics)

McMaster University
Hamilton, Ontario

TITLE: BioMEMS Glucose Sensors

AUTHOR: Andrey Zdanovich, B.Sc.

SUPERVISOR: Dr. Rafael N. Kleiman

NUMBER OF PAGES: ix, 108

Abstract

Since creation of the first glucose sensor for diabetes management in the 1960s, there have been tremendous amount of research devoted to development of sensors suitable for continous *in vivo* measurement of blood glucose concentration. Such devices would significantly enhance life quality of patients allowing reliable continuous monitoring of their condition and timely administration of medications. Ultimately, it could be combined with an insulin pump to create automatic closed-loop system for tight control of blood glucose level.

Analysis of modern glucometers and issues with *in vivo* measurements suggests the need for a novel approach for glucose sensing. This thesis describes sensors that combine microcantilever transduction paradigm with two syntactic receptors for glucose, boronic acids and molecular imprinted polymers. These artificial ligands give invaluable advantages of being tunable and very resistant to harsh chemical conditions that would be beneficial for implantable devices. To validate the experiment design and compare results with literature, cantilever sensors with glucose oxidase, an enzyme used in conventional glucometers, were also tested.

Cantilever sensors have got a significant attention of the scientific community during last decade. Microcantilevers have an amazing capability to link physical, chemical and biological domains with easily assessable mechanical movements. Such microscopic devices hold a promise of being versatile and very sensitive detectors, which performance scales up with miniaturization. Fabrication process is compatible with CMOS technology opening up an opportunity for low cost mass production.

In this work, the developed glucose cantilever sensors are tested in aqueous solution of glucose and their deflections are measured using an optical lever setup.

Contents

List of Figures

List of Tables

1 Glucose sensors: an overview

Since the development of a glucose sensor for use in diabetic treatment in the 1960s, a number of papers have been published describing a variety of systems and methods to measure glucose *in vivo* in humans. Such a glucose sensor could be very beneficial for diabetic patients in the management of their blood glucose concentration. For example, real-time measurement of glucose may be used to notify the patient when his blood glucose is too low or in the automatic feedback-controlled administration of insulin when blood glucose exceeds normal levels. In spite of extensive research efforts devoted to this subject, still no robust glucose sensor for *in vivo* use has been introduced into the market for daily use.

This chapter gives an overview of the glucose sensing field. Different techniques are examined and problems associated with the development of continuous glucose monitoring system are presented.

1.1 Medical motivation

Glucose is an essential compound for many organisms being the major source of energy for cells and a precursor for synthesis of many important biomolecules. However, when present at high concentrations it poses a danger due to uncontrolled glycosilation that is irreversible non-specific glucose binding to proteins leading to destruction of their activity. Abnormal levels can also cause disruption of highly interrelated metabolic process inducing damages to internal organs. Therefore, tight natural glucose control is very important and any malfunctions lead to severe complications.

In people, optimum blood glucose concentration is within a narrow range of 4 to 6 mM (70 to 110 mg/dL) that should be kept independently of food intake. However, in people suffering from Diabetes Mellitus it is constantly elevated and can be as high as 30 mM even under treatment. On the other hand, some patients suffer from chronic hypoglycemia, when glucose concentration is below required. Hypoglycemia condition frequently occurs in people with diabetes type 1 after extensive physical work, fasting or improper administration of insulin. Hypoglycemic attacks can lead to loss of consciousness. Nocturnal hypoglycemia is especially dangerous because the patient is usually asleep and not aware of his low blood glucose level putting the patient in the danger of coma and death. At the same time, it is very difficult to prevent a hypoglycemic attack if only two or three glucose measurements are made

per day. Moreover, most glucose meters for home use are not optimized for detection of very low glucose concentrations.

As of today, there is no cure of diabetes, approximately 2.1% of world population are affected by this disease. The inability for diabetic patients to appropriately control blood glucose level has long-term health consequences such as cardiovascular problems, renal complications, blindness, nerve damages, foot and skin complications. These consequences are the direct results of elevated glucose level for a prolonged period of time. Recently it has been proved in long-term studies that near normoglycaemia can prevent or delay the onset of these long-term symptoms of diabetes [1]. Consequently, the proper control of blood glucose concentration is the key to reduce complications and improve life quality.

A critical step in blood glucose management is appropriate monitoring. At present, it requires regular finger pricking to draw a blood sample. The frequency of measurement and as result the quality of the disease management is usually low, because the procedure is painful, boring and sometimes is not appropriate.

Continuous glucose monitoring (CGM)

Continuous measurement of glucose has been a focus of extensive research for three decades. The advantage of this type of glycemic control over conventional one is that such measurements are real-time and continuous whereas blood glucose testing with finger-prick method is intermittent and infrequent. The use of a continuous glucose measurement system would therefore be an improvement in the self-monitoring of blood glucose and can especially be helpful in the prevention of nocturnal hypoglycemic attacks.

The ultimate solution for diabetes would a closed-loop system of an insulin delivery pump controlled by a continuous glucose sensor. Such a system, so-called an *artificial pancreas*, can be an efficient pancreas substitute. On the market there are a few commercially available insulin pumps, however there is still no reliable continuous sensor for glucose.

Measuring principles for biosensors can be classified into two main groups based on the interaction between the patient's body and sensors: invasive and non-invasive. *Invasive* glucose sensors require direct mechanical contact with the biological tissues or fluids. On other hand, *non-invasive* glucose sensors obtain information without mechanical intervention, using characteristic properties (for example, optical) of glucose, which can be detected remotely.

Non-invasive methods and related problems are discussed in Section 1.4. Despite availability of a few commercial devices, their performance is very limited and they cannot substitute conventional glucose testing at the present moment.

Therefore, a lot of research is devoted to *minimally-invasive* sensors for implantation in the body. The ultimate goal would be a glucose sensor applicable for

long time periods, at least a half to one year, and coupled with a telemetric system that transmits data to an external receiver. A long-term sensor could be used as a monitor but its ultimate application would be as a part of a implantable automatic feedback-controlled insulin delivery system.

At present, the following devices are FDA-approved for continuous glucose monitoring *in vivo*:

- Medtronic Guardian REAL-Time Continuous Glucose Monitoring System
- MiniMed Paradigm REAL-Time System
- Abbott FreeStyle Navigator
- Dexcom STS-7

All these devices use a small disposable sensor to be inserted into the subcutaneous tissues. This sensor continuously measures the change in glucose in interstitial fluids and sends the information to a transmitter outside the body for storage and display. However, the devices must be calibrated daily by entering blood glucose readings obtained using a standard blood glucose meter and cannot be a substitute for the traditional glucose testing. Moreover, the lifetime of sensors is limited to 7 days at best due to a significant decay in sensitivity over the implantation period.

The poor performance of current continuous glucose sensors is related to their sensing principle, enzymatic conversion of glucose with electrochemical transduction, and is discussed in detail in Section 1.5.2.

1.2 Basic concepts of sensing

The basic principle of all chemical and biochemical sensors is illustrated in Figure 1.1. The receptor is used for molecular recognition of the analyte determining the specificity of the sensor. The analyte is transformed by the recognition component into a quantifiable chemical or physical property (heat, change of pH, fluorescence, etc) and then converted by the transducer into an electrical signal or any other easily observable signal, like color change of a test strip. Each element of glucose sensing process is discussed in detail in the following sections.

There are three figures of merit related to sensing technology: selectivity, sensitivity and reversibility. First, selectivity attributes to responsiveness of the sensor to only one particular ligand and is determined by the recepting mechanism. This is especially important factor for biosensing in a highly inhomogeneous medium like blood. Second, reversibility refers to the possibility of multiple usage of the sensor. If the chemical reaction between target and probe molecules is too strong, the sensor

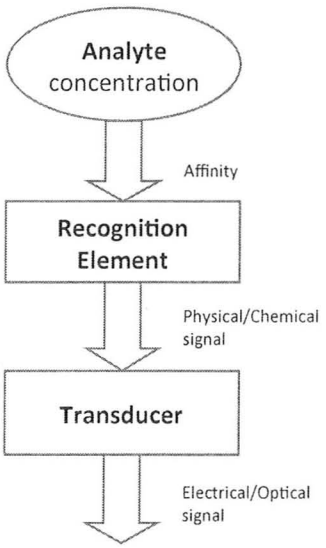

Figure 1.1: The principle of (bio)chemical sensing

cannot recover after it is exposed to a target, making it unavailable for further usage. To get a reversible sensor, weak interaction mechanisms, such as van der Waals forces and hydrogen binding, should be used as the molecular interaction mechanism. Third, sensitivity determines the level of response of a sensor to a target. Highly sensitive devices produce a large measurable response for a given target level. This property depends on employed transduction principle.

Reversibility is highly important requirement for long-term sensors of continuous glucose monitoring devices. The lengthy operation for many days demands usage of reversible chemical reactions for recognition and preferably no production or consumption of any reagents. Indeed, by-products are a big concern for implantable devices because they might cause foreign body reaction from surrounding tissues.

1.3 Chemistry of glucose

Glucose ($C_6H_{12}O_6$, MW 180.16 g/mol) is a monosaccharide with six carbon atoms, one of which is part of an aldehyde group ($-CH{=}O$). Therefore, glucose belongs to the class of aldohexoses with 16 possible stereoisomers (including D- and L- enantiomers). Only D-glucose, D-galactose and D-mannose have biological significance for people.

Glucose has a chiral center at C2. As result, there are two enantiomers, D-glucose and L-glucose, that are mirror-images of each other. In an aqueous solution, D-glucose causes polarized light to rotate clockwise (dextrorotary); in contrast, for L-enantiomer the direction of light rotation is opposite, counter-clockwise (levorotary). Commonly for all organisms, only D-glucose is biologically active; L-glucose does not

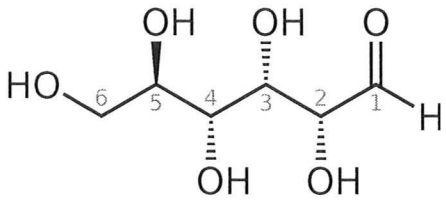

Figure 1.2: D-glucose in the chain form

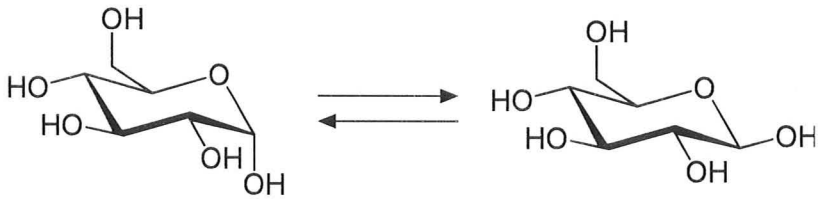

α-D-glucopyranose β-D-glucopyranose

Figure 1.3: Mutarotation of cyclic forms of glucose

occur naturally and cannot be metabolized due to high specificity of enzymes to D-isomers of carbohydrates.

Figure 1.2 illustrates open-chain (acyclic) form of glucose. In reality, glucose can also exist in a ring form as result of an intramolecular reaction between the aldehyde at C1 atom and the C5 hydroxyl group to form a six-membered cyclic hemiacetal so-called *glucopyranose*. In an aqueous solution the cyclic form is predominant.

An additional asymmetric center at C1 (called the anomeric carbon atom) is created when glucose cyclizes and two ring structures called anomers are formed as α-glucose and β-glucose (Figure 1.3). These forms differ structurally by the relative positioning of the hydroxyl group linked to C1 and the group at C6. In aqueous solution, the anomers interconvert in a process called mutarotation with equilibrium concentration ratio of 36:64 (α-D-glucopyranose:β-D-glucopyranose).

All monosaccharides containing accessible aldehyde (glucose) or ketone (fructose) functionalities are reducing sugars, because they are able to be oxidized by mild oxidizing agents and to conjugate with amines to form a Schiff's base. However, glucose in general has low reactivity because only rarely occurring open form is capable of reduction. Nevertheless, this form is believed to be responsible for non-enzymatic glycation of proteins and long-term complications of diabetes.

Low reactivity of glucose makes it problematic to be measured in a specific manner. It is even more complicated due to a lack of ionic functional groups capable of strong electrostatic interaction. Thus, monosaccharides can participate only in weak hydrogen bonds through hydroxyl groups and extremely weak hydrophobic interactions of the ring. In addition, in an aqueous environment glucose has to compete with water molecules to establish hydrogen bonds.

1.4 Direct (physical) methods

There are a few optical methods to measure glucose concentration, based on its optical activity, NIR spectrum and surface-enhanced Raman spectroscopy. Some of them even hold promise of non-invasive application as home-use devices, but optical methods are not yet well established and cannot be used reliably. The main problem is low selectivity and thus low accuracy due to highly complex composition of body fluids and presence of other optically active compounds beside glucose. Moreover, changes in the local blood circulation or the base-line variation in the spectra may affect the measurement accuracy substantially.

The optical approach seems to be completely impractical for implantable devices due to a number of technical reasons:

- It is still difficult to miniaturize both a light source and a detector in one small device.
- Usually different components of an optical device are made of different materials, like Si and III-V, limiting integration and leading to the need of assembling.
- High power consumption.
- High cost.

1.5 Receptors for glucose

(Bio)chemical receptors are recognition molecules that are able to bind specific ligands with high selectivity. The strength of ligand-binding interaction is called *affinity*. In general, the interaction is reversible (the notable exception is the enzymes) and the final ligand-binding complex is formed due to establishment of non-covalent bonds between the receptor and the substrate. Common examples of such intermolecular forces are hydrogen bonds, aromatic interaction (or π-π interaction), electrostatic forces between charged groups, van der Waals forces and hydrophobic interactions (see Figure 1.4). With the exception of ionic interactions, non-covalent bonds are very weak (energy of formation $1 - 5\,^{\mathrm{kcal}}/_{\mathrm{mol}}$) comparing to covalent bonds and on the same order of magnitude with thermal kinetic energy of molecules (about $0.6\,^{\mathrm{kcal}}/_{\mathrm{mol}}$ at $25\,^{\circ}$) [2]. Therefore, multiple noncovalent bonds are needed to produce highly stable and specific associations (complexes) between different molecules. The high selectivity of the receptor to the particular substrate requires a specific spatial arrangement of the bonds and as result, a specific conformation (shape) of receptor. This property is called molecular *complementarity*. The more complementary the binding sites of the molecule are to those of the target, the higher the binding energy.

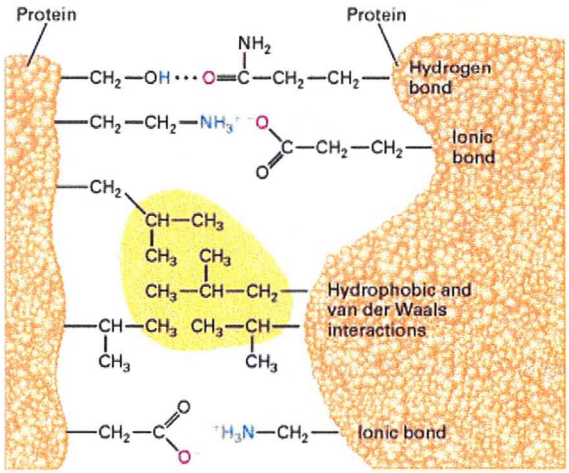

Figure 1.4: Noncovalent bonds and molecular complementarity [2]

Receptors may be classified depending on their origin as:

Natural recognizing agents are derived from biological systems. Most common types are proteins and nucleic acids (aptamers). These macromolecules are biopolymers composed of chains of repeating units, amino acids in case of proteins and nucleotides in nucleic acids. The sequence of different units determines conformation and chemical properties of molecule, giving its ability to interact with other molecules.

Not only recognition molecules are essential elements of living organisms being involved in signaling pathways and metabolism in case of enzymes, but also detection components of numerous biochemical sensors for almost any analyte. Such receptors can have extremely high affinity (K_d down to 10^{-15} M) and specificity (for example, glucose oxidase distinguishes α and β anomers of D-glucose). Moreover, properties of proteins can be further improved by protein engineering and combinatorial techniques. However, biomolecules are very sensitive to environmental conditions and most of them degrade at $40 - 70$°C. Usually, molecular biorecognition is efficient only in a narrow range of pH and temperature, and functional only in aqueous solutions.

Artificial receptors could be small molecules (boronic acids for monosaccharides) or polymers. Usually, artificial agents are very robust and can function in most demanding environments. Being small molecules or composed of highly repetitive units (polymers) such systems could be computer simulated and designed. Use of combinatorial and high-throughput screening techniques allows cost- and time-effective development of a receptor for particular needs. This approach seems to be most promising for sensing research and industry. However, the number of successful applications is still low. It is significantly complicated by

difficulties in construction of chemical structures with very specific arrangement of chemical bonds. For example, formation of polymers is statistically governed and on a microscale there is no well-defined order or conformation. In contrast, biomolecules are genetically programmed and produced in highly efficient and directional chemical reactions controlled by enzymes.

Affinity isotherm

In simplified version, a reversible reaction between a substrate S and a receptor R can be described by a two-state association process

$$\mathsf{S} + \mathsf{R} \rightleftharpoons \mathsf{SR}$$

where SR is the ligand-receptor complex.

In chemical equilibrium, concentrations for the species are interrelated through the equilibrium constants: *dissociation constant* K_d in units of moles per liter (denoted as M) and its inverse, *association (affinity) constant* K_a in units of M^{-1}. At low concentrations, the equilibrium constants can be defined as:

$$K_\mathrm{d} = {K_\mathrm{a}}^{-1} = \frac{[\mathsf{S}]\,[\mathsf{R}]}{[\mathsf{SR}]}, \tag{1.1}$$

where [R], [S] and [SR] represent the concentrations of the free receptor, free ligand and complex, respectively. The smaller the dissociation constant, the higher the affinity between the ligand and receptor.

The chemical equilibrium is attained when Gibbs free energy of the system reaches its minimum. As result the equilibrium constant K and the standard Gibbs energy change for the reaction $\Delta_r G^\circ$ are interrelated by equation

$$\ln K = \frac{-\Delta_r G^\circ}{RT},$$

where R is the gas constant and T is the absolute temperature.

If the dissociation constant is known, then the equilibrium concentration of the ligand-receptor complex [SR] can be calculated from equation (1.1) as

$$[\mathsf{SR}] = \frac{[\mathsf{S}]}{K_\mathrm{d} + [\mathsf{S}]}\,[\mathsf{R}]_0\ , \tag{1.2}$$

where $[\mathsf{R}]_0 = [\mathsf{R}] + [\mathsf{SR}]$ is the total concentration of the receptor molecules and [S] represents the concentration of the free molecules of the ligand. Usually, substrate is present at much higher concentrations than the receptor, as result [S] can be approximated by the total concentration of the substrate ($[\mathsf{S}] \approx [\mathsf{S}]_0$). Equation (1.2) is illustrated in Figure 1.5. It should be noted that the full receptor occupation is not

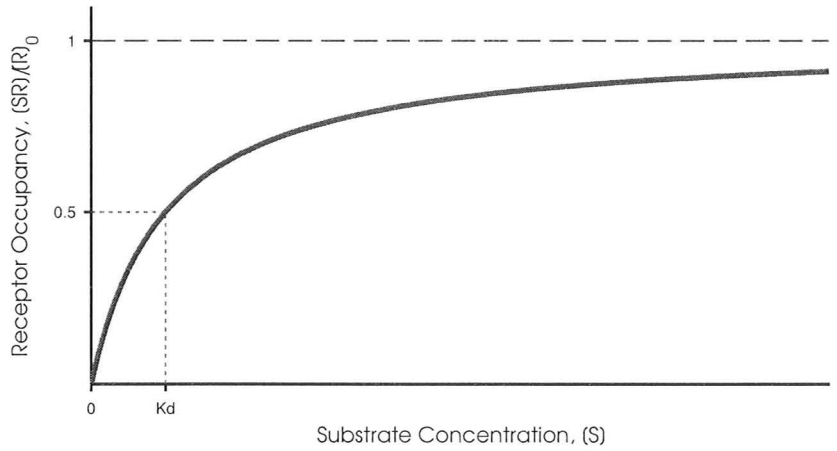

Figure 1.5: A saturation binding curve

attainable at any given ligand concentration, for instance the occupation is only 99% for $[\mathsf{S}] = 100K_\mathrm{d}$. When the concentration of the substrate is equal to the dissociation constant ($[\mathsf{S}] = K_\mathrm{d}$), receptors are half-saturated ($[\mathsf{SR}] = 1/2\,[\mathsf{R}]_0$).

Equation (1.2) is very important for selection of a suitable receptor for the sensor. At low ligand concentration ($[\mathsf{S}] \ll K_\mathrm{d}$), the occupancy of the receptors is proportional to the substrate concentration and the sensitivity is constant. On the other hand, at high ligand concentration ($[\mathsf{S}] \gg K_\mathrm{d}$), the receptors are saturated and their occupancy is independent of substrate concentration, as result the sensitivity of a sensor is near zero. Considering the physiologically important range of glucose, $2 - 30\,\mathrm{mM}$, the optimum affinity constant of the receptor is in the range $10 - 30\,\mathrm{mM}$.

Equation (1.2) is similar to Langmuir isotherm that is a relationship between the concentration of a compound adsorbing from a solution on a solid surface and the fractional occupancy of the binding sites (coverage) θ as

$$\theta = \frac{\alpha\,[\mathsf{S}]}{1 + \alpha\,[\mathsf{S}]}, \tag{1.3}$$

where $[\mathsf{S}]$ is the concentration of the adsorbate and α is the Langmuir adsorption constant.

1.5.1 Enzymes

Enzymes are highly specific bio-catalysts (mostly proteins), which speed up rate of chemical reactions without being consumed in the process. Similar to chemical catalysis, reaction rates of both the forward and reverse reactions are increased in the same way with no effect on the equilibrium constant of the process, but increase in the speed at which equilibrium is reached. The principal difference between enzymatic and

ordinary chemical catalysis is that enzymes can utilize noncovalent binding interactions with substrates to cause catalysis, in addition to the chemical mechanisms utilized by ordinary catalysts [3].

In contrast to ordinary catalysts, most enzymes are highly specific to particular substrates due to molecular recognition mechanism. While both receptor-ligand and enzyme-substrate interactions are specific and reversible, there is no chemical modification of the ligand as seen with the substrate upon binding to its enzyme. This catalytic activity makes observation of molecular interaction easier, which explains wide use of enzymes in biosensors and analytical chemistry. Substances produced or substances consumed during the chemical transformation may be easier detectable by a suitable transducer than the original analyte. By coupling of the main enzyme-catalyzed reaction with a second indicator reaction, very cheap strip assays can be fabricated for home use.

Enzymatic sensors in contrast to affinity-based assays consume the analyte. As result, the sensing is in not equilibrium (static) operation, but kinetics driven. It implies strong dependence of sensitivity on amount of active enzyme and on flux of the analyte and co-substrates if required. The latter could be strongly impacted in implantable sensors by membrane fouling and tissue encapsulation. Therefore, membrane design and biocompatibility are of high importance for *in vivo* glucose monitoring.

Michaelis–Menten kinetics

In the irreversible enzymatic reaction the substrates are transformed into reaction products according to the following general process:

$$\mathsf{E} + \mathsf{S} \rightleftharpoons \mathsf{ES} \longrightarrow \mathsf{E} + \mathsf{P}$$

where E represents the enzyme, S is the substrate(s), P is the product(s) and ES is the intermediate enzyme-substrate complex.

Many enzymes follow classical Michaelis–Menten kinetics and the initial velocity of enzymatic reaction V_0 is hyperbolically related to the substrate concentration $[\mathsf{S}]$:

$$\frac{d[\mathsf{P}]}{dt} = V_0 = \frac{V_{\max}[\mathsf{S}]}{K_{\mathrm{M}} + [\mathsf{S}]} \tag{1.4}$$

where K_{M} is the Michaelis constant of the enzyme and $V_{\max}$ is the asymptotic maximum rate of the reaction.

The reaction rate increases with an increase in substrate concentration $[\mathsf{S}]$, asymptotically approaching the maximum rate $V_{\max}$. At low substrate concentrations, the initial rate is proportional to the substrate concentration, referred to as first order kinetics. At high substrate concentrations, the initial rate is independent of

substrate concentration, referred to as saturation or zero order kinetics. At a substrate concentration equal to the Michaelis constant ($[\mathsf{S}] = K_{\mathrm{M}}$), the reaction rate reaches half of its maximum value ($^1/_2 V_{\max}$).

The Michaelis–Menten equation (1.4) results in a so-called *saturation curve*, analogous to affinity isotherm illustrated in Figure 1.5. Indeed, for some enzymatic reactions, when product formation is the rate-limiting step, the Michaelis constant is approximately equal to the dissociation constant of the enzyme-substrate complex (ES):

$$K_{\mathrm{M}} \approx K_{\mathrm{d}}.$$

Enzymes utilizing glucose as substrate

Glucose is an essential source of energy and precursor for synthesis of numerous biocompounds in all living organisms. It is not surprising that there are a number of enzymes targeting glucose as a substrate. But not all enzymes are suitable for creation of biosensors. For example, in human cells the first enzymatic transformation in glucose metabolism (glycolysis) is conducted by glucokinase (Enzyme Commision (EC) Number 2.7.1.2), an enzyme that catalyses phosphorylation of glucose to glucose-6-phosphate. It also requires a co-substrate, adenosine triphosphate (ATP), which is converted to adenosine diphosphate (ADP). As result, the need for constant supply of the co-substrate and the lack of easily measurable products make hexokinase unsuitable for a use in sensors.

For biosensing applications, the most targeted enzymes are *oxidoreductases*, proteins that catalyze the transfer of electrons from one molecule (glucose) to another (an *electron acceptor*). Such an enzymatic reaction can be conveniently coupled with an electrochemical transducer for measurement of the reaction rate related to the concentration of the analyte (glucose). There are four types of enzymes that oxidize glucose as a principal substrate acting on its alcohol groups:

- *Glucose 1-dehydrogenases* (GDH) (EC 1.1.1.47, EC 1.1.1.118, EC 1.1.1.119) are a broad class of enzymes (there are more than 450 enzymes of this type) that catalyses oxidation of D-glucose to D-glucono-1,5-lactone. The electron acceptor (a co-substrate of the reaction) is either NAD+ or NADP+. Specificity and activity varies significantly among species it is obtained from. The need for the co-substrate to perform the oxidation reaction prohibits long-term use of GDH in glucose electrochemical sensors. Although due to recent progress in development of artificial electron acceptors (mediators) theses enzymes have got significant research attention.

- *Quinoprotein glucose dehydrogenases* (PQQ-GDH) (EC 1.1.5.2) in similar fashion to glucose dehydrogenases convert D-glucose to D-glucono-1,5-lactone, except that the electron acceptor in the reaction is ubiquinone. PQQ-GDH contains a

bound pyrroloquinoline quinone (PQQ) cofactor and requires Mg^{2+} or Ca^{2+} for maximal activity. Due to low stability and selectivity, the enzyme has a very limited use.

- *Pyranose 2-oxidase* (EC 1.1.3.10) in the presence of oxygen oxidizes D-glucose at position C2 into D-glucosone producing also hydrogen peroxide. However, some other carbohydrates like gluconolactone are targeted by the enzyme as well.

- *Glucose 1-oxidase* (or just *glucose oxidase*, EC 1.1.3.4) catalyses the oxidation of specifically β-D-glucose at position C1 using molecular oxygen as an electron acceptor and producing D-glucono-1,5-lactone and hydrogen peroxide.

The basis of most glucose monitors used nowadays is glucose oxidase due to its moderate stability, specificity to glucose, high turnover and no need for any co-reagents except for oxygen that is naturally available (at least to some extent) in physiological fluids. Sensors based on glucose oxidase are described in the following section.

1.5.2 Glucose oxidase

Glucose oxidase (EC 1.1.3.4) is a secreted enzyme produced by different fungal species and honeybees with forms from *Aspergillus niger* and *Penicillium amagasakiense* (Figure 1.6) being most studied. Its normal biological function appears to be centered on the peroxide that is formed: hydrogen peroxide is a toxic compound that can be used to kill bacteria. For instance, glucose oxidase is found on the surface of fungi, where it helps protect against bacterial infection, and it is also found in honey, where it acts as a natural preservative. Glucose oxidase has become an important tool in several different industries, its uses ranging from a glucose biosensor for the control of diabetes, to a food preservative and colour stabilizer.

Glucose oxidase (GOx) is the most widely employed enzyme as analytical reagent being the central part of the majority of commercial glucose meters. The detection principle of these sensors is based on the monitoring of the enzyme-catalyzed oxidation of glucose according to the following reaction:

$$\beta\text{-D-glucose} + O_2 + H_2O \xrightarrow{\text{GOx}} \text{D-glucono-1,5-lactone} + H_2O_2 \quad + 19\,^{\text{kcal}}/_{\text{mol}}$$

D-glucono-1,5-lactone is then non-enzymatically hydrolyzed into gluconic acid with half-life of 10 min:

$$\text{D-glucono-1,5-lactone} + H_2O \longrightarrow \text{gluconic acid}$$

In this reaction the alcohol group (CH−OH) at position C1 of the glucopyranose ring is oxidized to produce D-glucono-1,5-lactone. Glucose oxidase acts temporarily

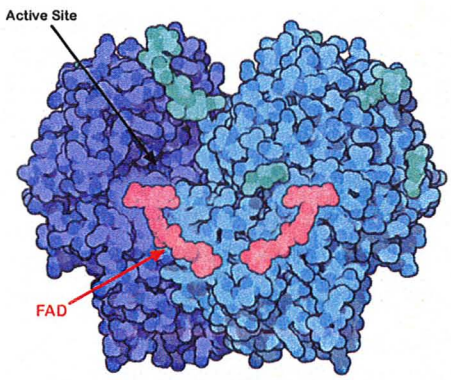

Figure 1.6: Glucose oxidase from *Penicillium amagasakiense* (PDB ID: 1GPE). The oxidation reaction is performed by FAD cofactor bound deep inside the enzyme, shown in red. The active site where glucose binds is just above the FAD, in a deep pocket [4].

Table 1.1: Types of transducers for glucose oxidase based sensors

Physical\Chemical parameter	**Detection method**
Heat release	Calorimetric
Change in pH due to gluconic acid formation	Potentiometric
Oxygen consumption	Amperometric
Hydrogen peroxide production	Amperometric, Spectrophotometric

as an electron acceptor, meaning that it is first reduced and subsequently reactivated by the reduction of oxygen to hydrogen peroxide.

Glucose oxidase is very specific to β-D-glucose whereas sensitivity to other carbohydrates including α-D-glucose is significantly smaller. The Michaelis constant K_M of commonly used GOx from *Aspergillus niger* is 33 mM [5] that is suitable for sensing of glucose in the physiological range of its concentrations.

There are many detection techniques such as amperometry, potentiometry, thermometry or photometry, all of which can function as transducer method in conjugation with this enzymatic reaction. Depending on the method used, different parameters can be measured and related to the concentration of glucose (Table 1.1). Of all transducer techniques, potentiometry and amperometry are mostly adopted. Both electrochemical methods are simple to use and offer excellent sensitivity, accuracy and low response time *in vitro*.

Potentiometric sensors measure the change in local pH due to the gluconic acid produced in the enzymatic reaction. The operation principle is based on measurement of the equilibrium potential between the working ion-selective electrode with immobilized glucose oxidase and the stable reference electrode under zero current conditions. An example of miniaturized potentiometric based systems is a pH-sensitive ion selective field effect transistor (ISFET). Main disadvantage is the low sensitivity of the sensor due to slow conversion and the small dissociation constant of the produced gluconic acid. Moreover, reliable measurements require a buffered sample solution. In addition, reducing agents present in blood such as ascorbic acid or uric acid can interfere with the detection. Therefore, this type of sensors has a very limited applicability in clinical practice.

Amperometric sensors measure the intensity of a current crossing the electrochemical cell under an applied electrical potential. Usually the cell consists of a working electrode where oxidation or reduction of the electrochemically active substances takes place and the second electrode that acts as reference electrode. The intensity of the current is a function of the concentration of the electro-active substrate. Major difference to a potentiometric electrode is the consumption of reaction products when an amperometric electrode is used. In glucose sensors a platinum working electrode is used either as cathode for reduction of oxygen or as anode for oxidation of hydrogen peroxide.
Amperometric electrodes have a high sensitivity, which allows detection of electro-active species at concentrations as low as 10^{-9} M and with a dynamic range of three to four orders of magnitude. However, such sensors are subject to electro-active interferents due to their oxidation or reduction at the applied operating potential. Common interferents present in blood are ascorbic acid, uric acid, acetaminophen, catechol, and hydroxyramine.

Amperometric electrodes are the most commonly used sensors for glucose management. There have been a few revisions to the basic concept outlined before [3, 6, 7]:

- The first generation of electrochemical sensors is based on measurement of oxygen uptake

$$O_2 + 4\,H^+ + 4\,e^- \xrightarrow{Pt} 2\,H_2O$$

or hydrogen peroxide production during enzymatic oxidation of glucose

$$H_2O_2 \longrightarrow O_2 + 2\,H^+ + 2\,e^-.$$

The biggest problem is strong dependence on oxygen concentration, which is relatively low and variable in tissues. Moreover, hydrogen peroxide itself is corrosive to a sensor and glucose oxidase. In addition, hydrogen peroxide is a toxic compound for the organism causing a rejection reaction, encapsulation in fibrous tissue and subsequent decrease of accessibility of glucose and oxygen.

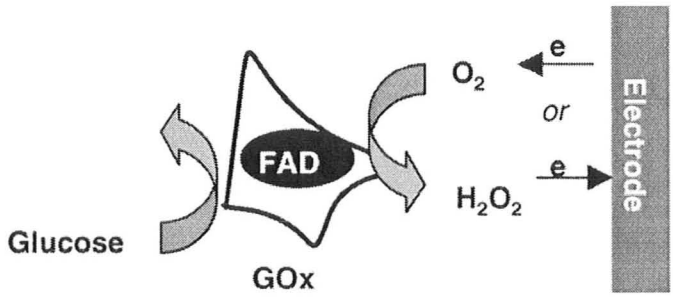

Figure 1.7: The first generation of electrochemical glucose sensors [7]

- In the second generation, oxygen is replaced by mediators as an artificial acceptor of electrons generated during oxidation. This approach eliminates most problems of original sensors and significantly increases sensitivity, but introduces a new problem. Most mediators are toxic and might leak out of the device making this type of sensors hardly possible to use *in vivo*.

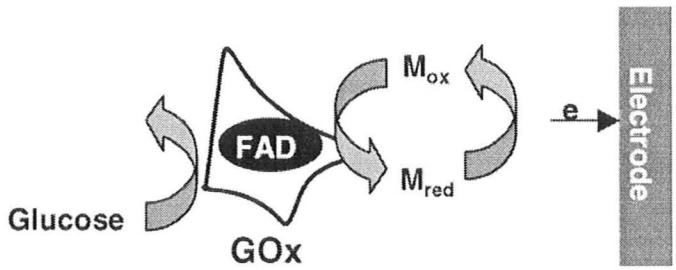

Figure 1.8: The second generation of electrochemical glucose sensors [7]

- In the third generation, mediators are replaced by conductive polymers directly wiring glucose oxidase to electrodes. However, such polymers are not reliable enough for *in vivo* use and the fabrication is very complicated. So far, there have been no reports of successful application of such devices for continuous glucose monitoring.

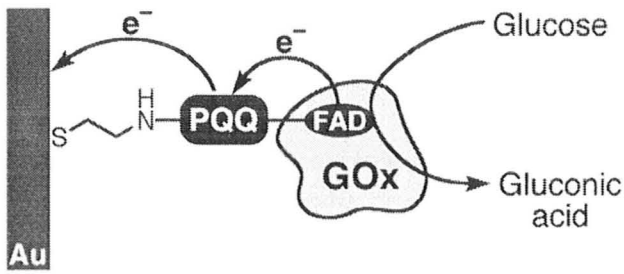

Figure 1.9: The third generation of electrochemical glucose sensors [7]

Electrochemical glucose sensors have excellent performance and long stability *in vitro*, but lose sensitivity extremely rapidly when placed in a tissue and require periodic re-calibration. The longest lifetime of commercially available devices is only 7 days. There is still no complete explanation of this phenomenon but some clues can be highlighted:

- After extraction from a tissue and thorough washing most sensors return their sensitivity, meaning that enzymatic activity is reversibly destroyed by unknown low weight molecules [8].
- Electrochemical sensors depend on diffusion rate of glucose through a membrane, which is altered *in vivo* due to biofouling.
- Enzymatic activity of sensors irreversibly consumes glucose, which can change local glucose concentration in a tissue. In addition, constant production of gluconic acid can decrease pH in tissue causing adverse reactions from the body.
- Electrodes suffer from biofouling and corrosion by low weight molecules that can diffuse through a protective membrane.

For *in vivo* application, a sensor must be of a size and shape that can be easily implanted and cause minimal discomfort. However, most reported devices have dimensions at least in millimeter range. Indeed, miniaturization of electrochemical sensors is problematic because the sensitivity of amperometric electrodes is directly related to amount of immobilized enzyme and surface area accessible for diffusion of glucose and oxygen. In this regard, potentiometric sensors like ISFETs are advantageous.

The concept of an electrochemical glucose sensor was first introduced by Clark and Lyons in 1962. Today, the majority of contemporary sensors is based on their idea and employ enzymes as biological components for molecular recognition coupled with an electrochemical cell. A number of attempts have been made to apply such sensors for *in vivo* measurement without significant success for almost 40 years. This has inspired the development of *in vivo* glucose sensing techniques based on methods other than the existing enzymatic ones. The most promising alternative sensing principles are described in the following sections.

1.5.3 Apo-enzymes

The redox catalytic function of glucose oxidase is performed by a tightly bound ($K_d \simeq 10^{-10}$ M) cofactor, flavin adenine dinucleotide (FAD). The FAD is not covalently attached to the protein and can be extracted to produce a so-called *apo-enzyme* (Figure 1.10). In contrast, an enzyme with bound cofactor is referred to as a *holo-enzyme*. The apo-enzyme missing the FAD cofactor is not biocatalytically active and is not able to conduct oxidation of glucose. However, the apo-glucose oxidase is still

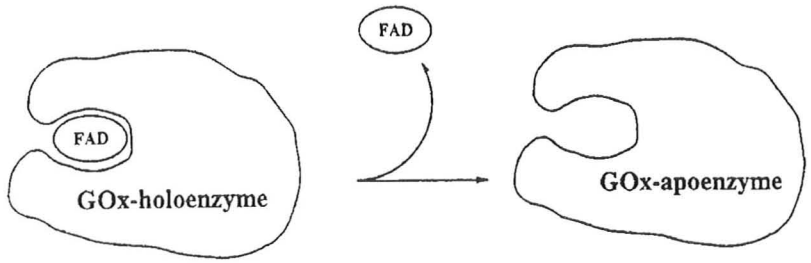

Figure 1.10: apo-Glucose oxidase [6]

capable of glucose complexation with an affinity comparable to the holo-enzyme. As result, the apo-enzyme can be used as a receptor with high affinity and specificity to glucose. But at the same time, it lacks the most important drawback of holo-GOx — it does not produce corrosive hydrogen peroxide that is harmful both to the enzyme itself and the sensor. Other problems of enzyme sensors — substrate consumption due to the irreversible chemical reaction and kinetics driven operation — are also eliminated.

There are a few problems associated with the use of apo-GOx for glucose sensing:

- Process of FAD extraction is complicated and leads to partial denaturation of the enzyme. At the current moment, it is hardly viable for fabrication of commercial devices.

- The apo-enzyme has very high affinity to FAD and can restore its enzymatic activity in the presence of the cofactor. It has even be exploited for detection of picomolar amounts of this compound [9]. FAD is a common component in biological oxidation-reduction reactions and may be present in physiological fluids in high enough concentrations to prohibit a long-term use of apo-glucose oxidase *in vivo*.

- Because of the lack of enzymatic activity, it is more difficult to detect complexation between the apo-enzyme and glucose. As result, more sophisticated transduction methods are required comparing to conventional electrochemical electrodes.

There have been a few attemptes to use apo-glucose oxidase as a recognition element in direct glucose sensors using various fluorescence schemes. For instance, weak intrinsic fluorescence of tryptophan residues has been reported to decrease with the addition of glucose [10]. Apo-GOx was also exploited in a competitive binding assay analogous to Con A–dextran systems (see Section 1.5.4) [11]. The other experiments were based on the apo-enzyme labeled with an environmentally sensitive fluorophore, which exhibited a decrease in intensity with the addition of glucose [10]. All reported results are based

on free apo-glucose oxidase in a solution phase and far from a practical application. In most cases, changes of the fluorescence signals upon ligand binding have been small and completely quenched in physiological liquids (serum and blood).

In a similar fashion, non-active forms of the thermostable enzymes from thermophilic bacteria, glucose dehydrogenase (GDH) from thermoacidophilic archaeon *Thermoplasma acidophilum* and glucokinase from *Bacillus stearothermophilus* have been used to measure glucose concentration by tagging with fluorophore ANS that displayed the decrease in emission upon glucose binding [10, 12]. Due to the nature of thermophilic microorganisms, these proteins are heat-, acid- and solvent-stable, for example, the performance of apo-GDH from *T. acidophilum* is optimum at elevated temperatures and in presence of small amounts of acetone. Such natural receptors could be ideal probes for creation of robust sensors for *in vivo* application.

1.5.4 Lectins

Lectins are a broad family of carbohydrate binding proteins. Plant lectins from *Canavalia ensiformis* (Concanavalin A), *Vicia cracca I*, *Pisum sativum*, *Lens culinaris*, *Vicia faba*, *Dioclea grandiflora* have been determined to have particular high affinity to glucose that might be utilized for construction of sensors. In this respect, Concanavalin A has received a significant attention from the research community.

Concanavalin A (Con A) is a sugar binding protein originally isolated from the Jack bean (*Canavalia ensiformis*). It has high affinity to glucose ($K_a = 400\,M^{-1}$), mannose and some oligosacharides. It should be noted that mannose is present in human blood at very low concentrations (on the order of a few μM), significantly less than glucose, hence mannose is not detrimental to measurements based on Con A.

A lot of research on Con A glucose sensors has been devoted to optical sensing with competitive binding being the most commonly used technique. In this case, a solution of Con A and high-molecular-weight dextran is entrapped in a hollow dialysis fiber accessible for diffusion of glucose from the external medium. Dextran is a branched polysaccharide made of glucose units, therefore in the absence of free glucose Con A is linked to dextran. Following introduction of glucose into the system, molecules of Con A detach from dextran and bind to free glucose. This process leads to easily observable signs like changes of viscosity of the solution or modulation of fluorescence if Con A and dextran are labeled with fluorophores. Depending on the fluorescence wavelength, the optical measurement can be conducted either by a directly attached optical fiber or remotely by interrogation through tissues. The viscosity of Con A–dextran solution may also be correlated to glucose concentration and measured by means of a microcantilever sensor [13].

Optical sensors based on Con A–dextran system have showed satisfactory performance in vitro and have even been demonstrated to be operational *in vivo*. It

has been reported that during 16 days of operation in the tissue the sensors had not showed decrease of sensitivity beside the raise of response time. These results are very encouraging, however some issues with the sensors based on competitive binding have to be addressed [12]:

- In plasma or serum, there is significant quenching of the fluorescence.
- The lack of an internal reference makes the sensor hardly usable for long-term applications due to significant drift and the need for frequent recalibration.
- High response time due to large volume of the system (required to achieve high signal-to-noise ratios) and slow displacement of Con A from dextran.
- Interaction between dextran and Con A is not completely reversible, which leads to steady decline of sensitivity.
- Free (not immobilized) molecules of Con A are susceptible to irreversible aggregation leading to eventual precipitation.
- The free lectins may leak out of the membrane capsule resulting causing adverse effects due to intrinsic toxicity of Con A.

1.5.5 Periplasmic glucose binding proteins

Periplasmic binding proteins (PBPs) constitute a large family of bacterial receptors that recognize a variety of small molecule ligands. The biological significance of these proteins is mediation in substrate transportation (as part of ABC transport systems) and chemotaxis.

Glucose/galactose-binding protein (GGBP) is a member of the sugar-binding protein subclass of PBPs. The most studied forms have been isolated from *Escherichia coli* and *Salmonella typhimurium*. Similar to all PBPs, it consists of two α/β globular domains connected by a hinge. Ligand binding induces a large-scale (approximately 31°) hinge-bending motion that clamps the ligand within the binding cleft and the protein undergoes transformation from a ligand-free open form to a closed conformation. Figure 1.11 illustrates the changes happening to GGBP as result of complexation with glucose. These reversible conformational changes between inactive and signaling-active states allow GGBP to communicate glucose/galactose levels in the periplasm to chemotaxis receptors of the cells [14].

High selectivity and sensitivity for glucose (concentrations of galactose are significantly lower in blood) coupled with large structural alterations make GGBP ideal for biosensor development. Site-specifically attached fluorophores have been reported to display spectral changes in response to micromolar concentrations of glucose with high sensitivity [12]. The main problem of real application of GGBPs in glucose meters

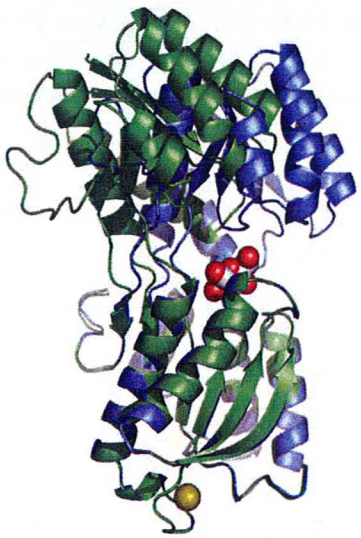

Figure 1.11: Glucose/galactose-binding protein from *Escherichia coli*. The superposition of glucose-bound (blue) and ligand-free (green) conformations reveals the 31° hinge opening movement [14].

Figure 1.12: The covalent and reversible complexation between a boronic acid and a diol [7]

is their extremely high affinity; the binding constant K_d lies in the micromolar range. As result, GGBPs can have a detection limit as low as 0.3 µM, but are completely saturated in the physiological range of glucose. However, genetically engineered proteins from *E. coli* with lower glucose affinity constant (10 mM versus original 0.2 µM) have been derived recently [15]. GGBP may also be used for ultrasensitive submillimolar measurements in laboratory and industrial environments.

1.5.6 Boronic acids

The ability of boronic acids to covalently and at the same time reversibly bind diols (chemical compounds containing two hydroxyl groups) has been well known since 1954 (illustrated in Figure 1.12). Upon complexation acidity of the medium increases and this effect has been applied in a number of chemosensors for different biomolecules such as carbohydrates and glycoproteins. The most popular transduction principle is adsorption or fluorescence measurement by incorporation of a dye or a fluorophore into the probe. A broad range of techniques has been used to study molecular recognition

by boronic acids including infrared and Raman spectroscopy, cyclic voltammetry, SPR and impedance spectroscopy.

The use of boronic acids for sugar sensing, including glucose, is very promising. The main advantages of this type of receptors are its simplicity and limitless possibilities to design such synthetic compounds for specific targets and with desired properties.

One of the simplest and well studied boronic acids—aminophenylboronic acid—has been applied as a sensitive coating for cantilevers in the thesis (see Chapter 6).

1.5.7 Molecular imprinted materials

Molecular imprinting is an emerging technology, which allows the synthesis of materials that contain highly specific receptor sites with an affinity for target compounds. It follows biomimetic approach to create structures with three-dimensional cavities of specific size and shape for molecular recognition of ligands. Such biomimetic materials can be rationally designed for almost any analyte, which is especially important for applications where natural receptors do not exist. Molecular imprinting has been achieved both in organic materials (polymers) and in totally inorganic substances like silica. As result, such receptors can be more versatile and robust than their natural counterparts and operate in extreme conditions like acids, organic solvents and high temperatures. These properties make molecular imprinted materials promising for various applications including (bio)chemical assays and sensors, separation materials, highly specific catalysts.

Seong *et al.* [16] demonstrated construction of a molecularly imprinted polymer (MIP) specific for D-glucose. It showed encouraging affinity results, however its applicability for sensing purposes was not well studied because the material was prepared using bulk polymerization and glucose-binding characteristics were examined by using an equilibrium dialysis technique.

Chapter 7 describes construction of a microcantilever sensor for glucose based on the MIP reported by Seong *et al.* [16].

1.6 Transducers

The function of a transducer is to translate a molecular recognition event happening at the nanoscale level into a measurement signal. This element converts a receptor into a functional sensor.

Considering the lack of fluorescent and electroactive properties in monosaccharides, direct measurement of glucose in highly complex media such as blood or interstitial fluids is hardly possible. The most commonly applied technique in contemporary glucose sensors is an enzymatic conversion of the analyte into more easily detectable substance like oxygen or hydrogen peroxide. Another popular approach is to use intrinsically fluorescent receptors or to couple a recognition element with an

environment sensitive fluorophore like in internal charge transfer (ICT) systems, for example. However, application of fluorescent sensors for *in vivo* use is still a challenge due to relatively low stability of fluorophores and difficulties in miniaturization of optical sensors that require both light sources and detectors.

Other common detection approaches are based on measurement of receptor-ligand system mass (gravimetric and cantilever sensors), changes of receptor conformation (cantilever and optical sensors) or changes in local medium around receptors (impedance spectroscopy, SPR, potentiometry) due to analyte binding.

A short overview of some transduction methods used for glucose detection is given in the following sections.

1.6.1 Electrochemical

Two most commonly applied electrochemical techniques, potentiometric and amperometric electrodes, measure concentration of electroactive species in a liquid medium. Glucose itself has low electroactivity, as result electrochemical transducers are frequently used in combination with enzymes to track production or consumption of electroactive subproducts of an enzymatic reaction. Such sensors are described in Section 1.5.2.

Glucose can also be directly oxidized on noble metal (such as platinum) electrodes without the use of an enzyme. However, electrocatalytic glucose sensors need application of moderately high potential resulting in the lack of specificity in biological fluids because of presence of substances electroactive at the applied electric potential. In addition, a gradual decline of electrode activity has been seen due to the absorption of reaction products on the electrode, reducing active surface area. Subproducts of electro-oxidation may also be toxic for surrounding tissues prohibiting *in vivo* use of electrocatalytic glucose sensors.

It should be noted that performance of most electrochemical sensors decreases with scaling down of their size because the signal (electrical current) depends on absolute value of electrode surface area and amount of the immobilized enzyme.

1.6.2 Gravimetric

Gravimetric sensors measure a change of mass due to adsorption of an analyte on sensors' surface with immobilized receptors. Such devices are usually realized in the form of microcantilever or quartz crystal resonators. The latter technique is referred to as quartz crystal microbalance (QCM).

Gravimetric method has a few serious issues with its application in glucose sensors:

- Detection limit is restricted by very small molecular weight of glucose ($180.16\,{}^{g}/_{mol}$).

- Gravimetric sensors are less efficient in viscous environment like blood or serum due to large damping. Moreover, viscosity has strong dependence on temperature and chemical composition of the media.
- Sensitivity is proportional to amount of immobilized receptors and therefore, proportional to surface area of the sensor. As result, performance of such devices suffers from miniaturization.

Some of these problems may be resolved by the use of nanostructured surfaces or receptors entrapped in hydrogen matrix at expense of complicated fabrication, increase in response time and limited repeatability.

1.6.3 Surface plasmon resonance

Surface plasmon resonance (SPR) is a charge-density oscillation that may exist at the interface of two media with dielectric constants of opposite signs, a metal and a dielectric. The charge-density wave is associated with an electromagnetic wave, the field vectors of which reach their maxima at the interface and decay evanescently into both media. The propagation constant of the surface plasmon wave propagating at the interface between a semi-infinite dielectric with the refractive index n_{D} and metal with the permittivity ε_{M} is given by the following dispersion expression:

$$\beta_{\mathrm{SP}} = \frac{\omega}{c} n_{\mathrm{eff}} = \frac{\omega}{c} \sqrt{\frac{\varepsilon_{\mathrm{M}} n_{\mathrm{D}}^2}{\varepsilon_{\mathrm{M}} + n_{\mathrm{D}}^2}}, \tag{1.5}$$

where ω is the angular frequency, c is the speed of light in vacuum and n_{eff} denotes the effective refractive index of the surface plasmon. As can be seen from equation (1.5), any change in the refractive index in the proximity of the metal surface results in a change in the velocity of the surface plasmon. This change in the propagation can be determined from the characteristics of the light wave coupled to the surface plasmon. This phenomenon is the basis of many instruments for measuring adsorption of material onto planar metal (typically gold and silver) surfaces or onto the surface of metal nanoparticles.

SPR affinity (bio)sensing is based on optical measurement of refractive index changes associated with the binding of analyte molecules from a liquid sample to recepting molecules immobilized on the metal surface of SPR sensor. The change in the effective index of the surface plasmon due to the capture of analyte can be expressed as

$$\Delta n_{\mathrm{eff}} = K \Delta \Gamma,$$

where K is a proportionality constant and $\Delta\Gamma$ is the corresponding surface concentration of the ligand. High-performance SPR sensors may be able to resolve changes in the surface concentration as small as $0.1\,{}^{\mathrm{pg}}/_{\mathrm{mm}^2}$ [17].

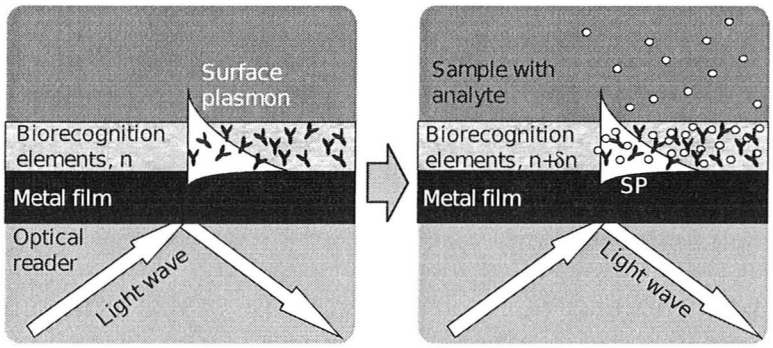

Figure 1.13: Principle of operation of SPR affinity biosensors [17]

The SPR measurement method is very popular for biomolecular-interaction analysis due to its ability to monitor molecular binding in real-time without labeling. It has also been applied for glucose measurements. Despite its ability to precisely measure the index of refraction of glucose solution and correlate changes to glucose concentration, application of SPR for complex biological fluids relies on a specific recognition element. There has been an attempt to use the high specificity of glucose oxidase with industry-class Biacore 3000 instrument. Despite its sensitivity to the fluids' refractive indices, it was unable to detect glucose-GOx binding versus control solutions of nonbinding compounds. This experiment demonstrates the difficulty to observe the binding of a small analyte molecule (180 Da) to a large target enzyme (160 kDa). Although the application of micro-cavity SPR sensors with the diameter on the order of 1 micron seems promising for glucose detection [18].

The main issues to use SPR techniques for continuous glucose monitoring are high cost, complexity and large size of optical instrumentation required for efficient conversion of light into plasmons and their characterization. In addition, the size of classical planar SPR sensors is relatively large, on the order of 1 mm^2. Reduction of the sensor surface is limited due to negative effects on SPR sensitivity.

1.6.4 Cantilevers

Cantilever sensors have been demonstrated to detect with high sensitivity various surface processes, including conformational changes of proteins, ligand-receptor and antigen-antibody interactions, hybridization of DNA, adsorption of ultrasmall masses, etc. Such detectors are miniature and have much smaller surface area ($< 0.05\,mm^2$) than surface plasmon resonance ($\sim mm^2$) and quartz crystal microbalance ($\sim cm^2$) biosensors. Moreover, in contrast to these technologies, the sensitivity and efficiency of microcantilever transducers increases with size reduction. Cantilever devices can be mass-produced and integrated into versatile sensor arrays using conventional fabrication technologies adopted from semiconductor industry.

Cantilever sensing platform seems to be ideal for creation of miniature implantable devices based on non-enzymatic recognition. This transduction paradigm is described in detail in Chapter 2.

1.7 Conclusion

In this work, three different molecular recognition systems are examined in combination with the perspective microcantilever sensing platform.

Glucose oxidase has been chosen as the most studied and commonly used protein with high affinity and specificity for glucose (Chapter 5). In contrast to other glucose binding proteins, it is commercially available with high purity and at relatively low cost.

Two types of synthetic receptors, boronic acids and molecular imprinted polymers, have been also tested (Chapters 6 and 7 respectively) as very promising molecular probes for glucose measurement systems because of their high chemical and thermal stability. In addition, these artificial recognizing agents can be rationally designed and tailored to specific requirements. However, due to the limited scope of the project the tested formulations were derived from literature as is.

2 Microcantilever-based sensors

A cantilever is a long suspended beam, clamped at one side and free to move on the other side. In the field of MEMS, it is the simplest and most basic structure, but it has been demonstrated that microcantilevers could be used both as actuators and as a sensor.

It has recently become clear that cantilever transducers offer an opportunity for the development and mass production of extremely sensitive, low cost sensors for real time sensing of many chemical and biochemical species. In this chapter, transduction principles, readout techniques, and sensing applications related to microcantilever sensors are reviewed.

2.1 Cantilevers in scanned probe microscopy

The use of cantilevers to measure forces dates back to the invention of the atomic force microscope (AFM), a type of scanning probe microscopy, in 1986 [19]. At first, it was an extension of scanning tunneling microscope (STM), but soon it took its own part as an indispensable tool for surface researchers.

In the AFM, the sample is scanned by a tip that is mounted on a cantilever beam. While scanning, the force between the tip and the sample is measured by monitoring the deflection of the cantilever. A topographic image of the sample is obtained by plotting the deflection of the cantilever versus its position on the sample. Alternatively, the height position of the translation stage is plotted in tapping mode. This height is controlled by a feedback loop, which maintains a constant force between tip and sample.

The first AFM probe consisted of a thin metal plate and an STM was placed above the plate measuring the deflection. Later, micromachining techniques were applied to fabricate cantilevers in materials commonly used in the microelectronics industry like silicon, silicon oxide and silicon nitride, making it possible to produce small cantilevers with high resonant frequencies and low spring constants. The spring constant of commercial microcantilevers is on the order of $50\text{—}10^{-3}\,\mathrm{N/m}$, which allows the detection of extremely small forces ($10^{-12}\text{—}10^{-9}\,\mathrm{N}$). For comparison, the force to break a single hydrogen bond is on the order of $10^{-12}\,\mathrm{N}$. Atomic resolution with the deflection sensitivity of approximately 1 Å is also achievable.

Recently, it has become possible to detect one molecule interactions by means of cantilevers functionalized with polymer coatings, self-assembled monolayers or target

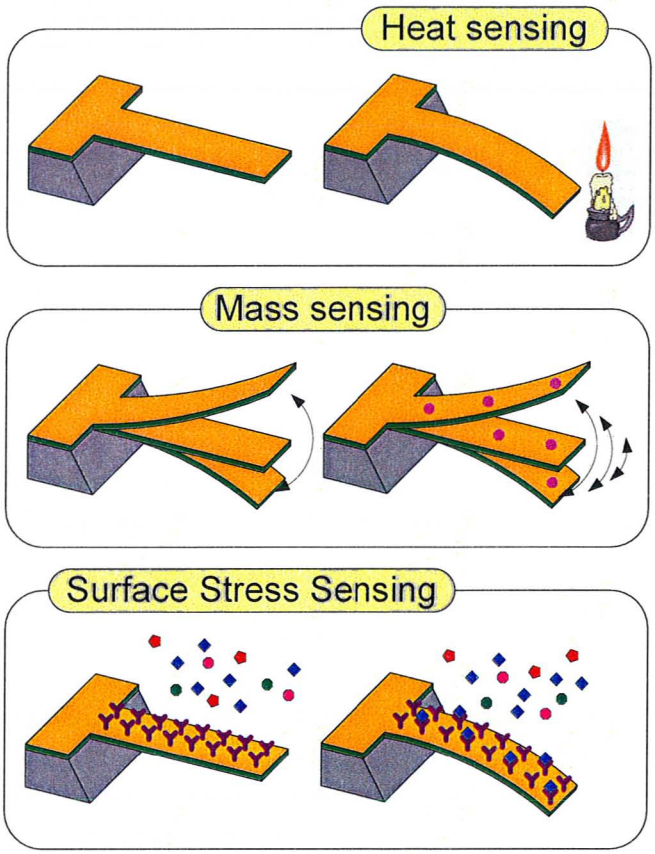

Figure 2.1: Cantilever sensing modes [20]

specific receptors. This showed the potential use of microcantilevers developed for AFM as biochemical sensors. Major advantage of this approach is the possibility of real time and label free measurement of chemical processes at nanoscale.

2.2 Theory of operation

Three general approaches for cantilever sensing are illustrated in Figure 2.1.

2.2.1 Heat sensing

Small amounts of heat generated due to chemical reactions on a cantilever surface or change in surrounding temperature can cause deflection of a bimorph cantilever structure because of the thermal expansion mismatch between two layers with different thermal expansion coefficients. The deflection due to the thermally induced stress,

so-called bimetallic effect, was first calculated by Timoshenko [21]:

$$\delta = \frac{3l^2}{t_1 + t_2} \frac{\left(1 + \frac{t_1}{t_2}\right)^2}{3\left(1 + \frac{t_1}{t_2}\right)^2 + \left(1 + \frac{t_1}{t_2}\frac{E_1}{E_2}\right)\left(\frac{t_1^2}{t_2^2} + \frac{t_2}{t_1}\frac{E_2}{E_1}\right)} (\alpha_1 - \alpha_2) \cdot \Delta T, \tag{2.1}$$

where ΔT is the change of temperature, l is the length of the cantilever, t_1, t_2 are thicknesses, E_1, E_2 are Young's modulus and α_1, α_2 are coefficients of thermal expansion (CTE) of both layers. This equation is based on the small deflection approximation.

As result, in response to thermal stress, a cantilever takes a circular bending profile similar to bending due to surface stress (see Section 2.2.3).

Bimaterial cantilevers are the basis of a variety of physical and chemical sensors including ultrasensitive temperature detectors and uncooled infrared detectors.

2.2.2 Dynamic mode

Dynamic mode refers to the measurement of the change in the resonant frequency due to mass adsorption on the cantilever or change in viscosity of surrounding medium.

The mechanical properties of cantilevers are characterized by the spring constant and the resonance frequency. The *spring constant* is the ratio between a force F applied at the free end of the beam and a resulting deflection δ. For a rectangular shaped cantilever with length l, width w and thickness t it is given by

$$k = \frac{F}{\delta} = \frac{Ewt^3}{4l^3} \tag{2.2}$$

The *resonance frequency* for the fundamental mode in a damping free medium can be written

$$f = \frac{1}{2\pi}\sqrt{\frac{k}{m^\star}} \tag{2.3}$$

where $m^\star$ is the *effective cantilever mass* that takes into account the shape of the vibration mode of the cantilever. For a rectangular cantilever with (distributed) mass m_c and a concentrated mass at the tip m_t it is given by

$$m^\star = 0.2427 m_c + m_t$$

As can be seen from equation (2.3) change in the mass of the cantilever due to, for example adsorbed molecules, causes the change in the resonance frequency with the relationship approximately described by

$$\frac{\Delta f}{f_0} \approx \frac{1}{2}\frac{\Delta m}{m} \tag{2.4}$$

where f_0 is the initial resonance frequency, Δf is the change in the frequency, Δm and m are the adsorbed mass and initial mass of the cantilever, respectively.

In a viscous medium, it is necessary to take into account the dissipation of the resonator energy due to damping. In this case, the resonance frequency of the cantilever can be expressed as

$$f_{\text{damped}} = \frac{1}{2\sqrt{2}\pi}\sqrt{\frac{k}{m^\star}}\frac{\sqrt{2Q-1}}{Q} \tag{2.5}$$

where Q is the quality factor of the environment.

Measurements of adsorbed mass based on resonance frequency variation are usually done in gaseous environments. In liquids, the frequency resolution is significantly lower because of the peak broadening due to the damping. However, as can be seen from equation (2.5), damping modulation due to adsorption of the analyte on the sensor might be used for sensing in this case.

2.2.3 Static deflection mode

As any chemical reaction, molecular adsorption on a solid surface or a receptor/ligand binding reaction are driven by Gibbs free energy reduction, and such reduction leads to a change in surface stress. *Surface stress* is defined as the amount of reversible work per unit area needed to elastically stretch a pre-existing surface, whereas *surface free energy* is the excess free energy per unit area needed to create a new surface. At the same time, surface stress can by defined as a force per unit length, acting on a line and being in the plane of the surface; for isotropic surfaces the force is perpendicular to the line and the (isotropic) surface stress σ is the half-sum of the diagonal components of the surface stress tensor [22, 23]. As result, there are two equivalent choices for its unit: $^{\text{N}}/_{\text{m}}$ (force per unit length) and $^{\text{J}}/_{\text{m}^2}$ (energy per surface). *Tensile* stress is considered positive, whereas for *compressive* its value is negative. The plane stress in a liquid surface is known as the *surface tension*.

Using the Shuttleworth equation [22, 24], the surface stress σ and surface free energy γ can be interrelated by:

$$\sigma = \gamma + \frac{\partial\gamma}{\partial\varepsilon} \tag{2.6}$$

where ε is the surface strain defined as the ratio of change in surface area $\partial\varepsilon = {}^{\partial A}/_{A}$. The second term relates to the change of material properties at the interface due to elastic deformation. For gases and liquids, it is equal to zero, whereas for solids ${}^{\partial\gamma}/_{\partial\varepsilon}$ is not zero due do the fact that surface atomic structure is modified during deformation. However, this term is usually small and for small deformations assumed to be zero.

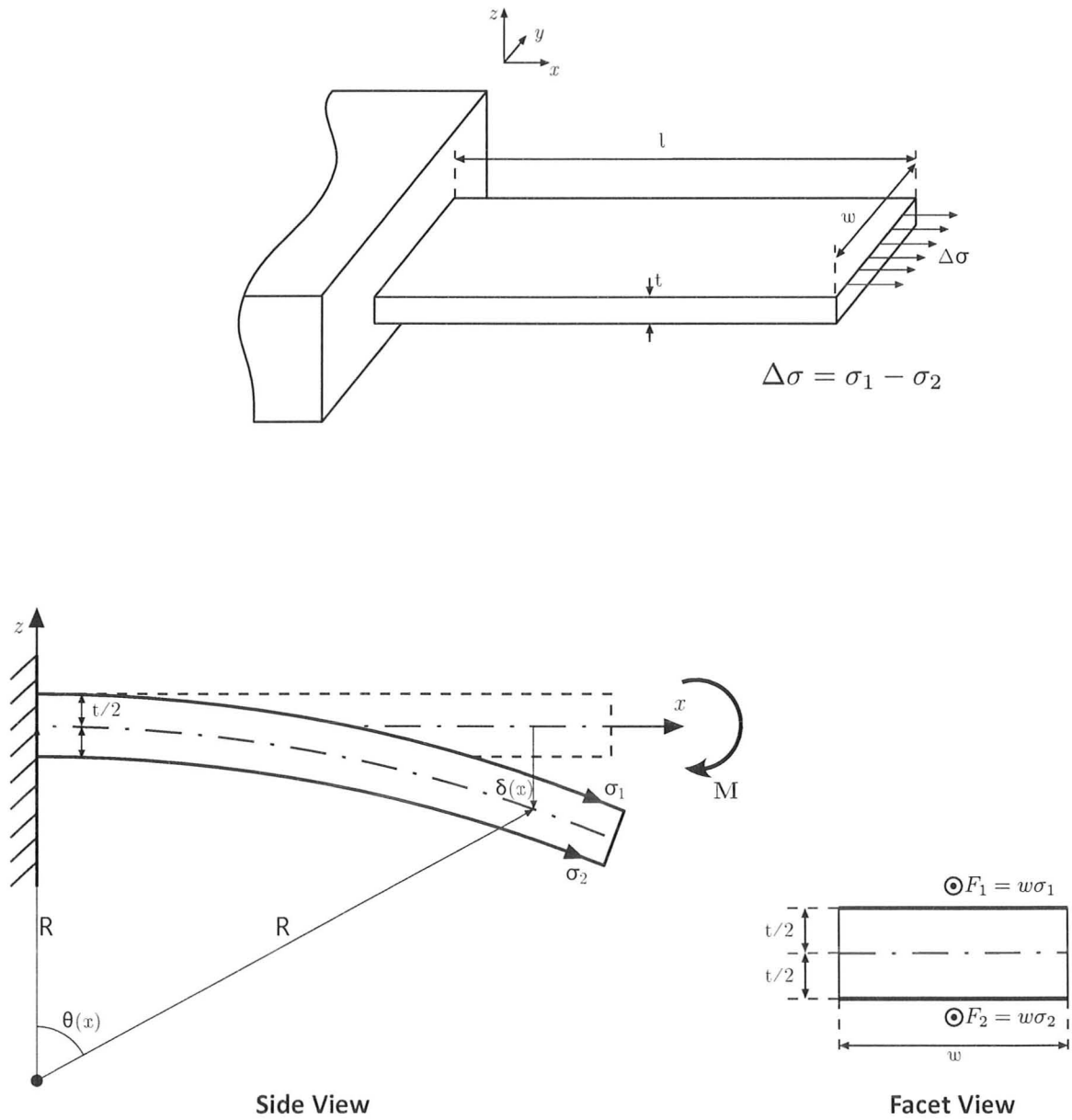

Figure 2.2: Diagram of cantilever bending due to surface stress loading

While this surface stress produces no observable macroscopic change on the surface of a bulk solid, the induced surface strain is sufficient to bend a cantilever if the adsorption is confined to only one surface of the beam. Usually, the effect of the **surface stress is modeled as a concentrated bending moment** applied at the cantilever beam's free end [25–27] with axial loading neglected [25]. The model is illustrated in Figure 2.2 for a cantilever with a rectangular uniform cross-section. The beam's material is assumed isotropic and homogeneous. Its centroid axis defines x-axis and is the neutral axis under the condition of no axial loading. The beam bends about the y-axis. The origin of the coordinate system is at the centroid of the clamped edge. The applied surface stress is assumed homogeneous and isotropic in nature.

As can been seen from Figure 2.2 (*facet view*), due to differential surface stress, there are in-plane forces working around y-axis on the facet edges and producing bending moment M perpendicular to the plane of the drawing

$$M = \frac{wt}{2}\Delta\sigma, \tag{2.7}$$

where $\Delta\sigma$ is the difference between the surface stresses of a top and a bottom side of the cantilever:

$$\Delta\sigma = \sigma_1 - \sigma_2.$$

The transverse (in the z direction) displacement of the centroid axis from its unloaded position is defined as $\delta(x)$. In the **thin beam model**, the transverse strain is zero, as result the profile of the beam surface is also given by $\delta(x)$. The deflection is assumed small and can be calculated from the Euler–Bernoulli beam equation, which relates the curvature of the beam to the bending moment at each section of the beam:

$$\frac{\partial^2}{\partial x^2}\delta(x) \simeq \frac{1}{R} = \frac{M}{E^\star I}, \tag{2.8}$$

where R is the radius of the beam's curvature, $E^\star$ is the elastic modulus of the beam and I is the area moment of inertia. The second moment of area for a rectangular cross-section A with respect to the centroidal axis is

$$I = \int_A z^2 dA = \frac{wt^3}{12}. \tag{2.9}$$

A direct result of equations (2.7) and (2.8) is that the cantilever under differential surface stress takes a **circular** shape with curvature $1/R$ constant over its length. This relationship was originally derived by Stony [28] and in the modified form is given by

$$\frac{1}{R} = \frac{6}{E^\star t^2}\Delta\sigma. \tag{2.10}$$

Comparing to original Stoney's equation developed for uniaxial stress, this form

considers isotropic surface stress that is the case for thin films and the film-substrate interfaces. As result the bi-axial modulus $E^\star$ is used instead of Young's (uniaxial) modulus E. These moduli are interrelated through Poisson's ratio ν by the following expression:

$$E^\star = \frac{E}{1-\nu}. \tag{2.11}$$

The bending profile is obtained from equation (2.8) by using integration and boundary conditions for the clamped end (at $x = 0$) given as

$$\delta|_{x=0} = 0, \tag{2.12}$$

$$\left.\frac{\partial\delta}{\partial x}\right|_{x=0} = 0. \tag{2.13}$$

The first integration of equation (2.8) gives the slope of the deflection, approximately equal to the deflection angle θ (the small angle approximation), and the second integration produces the displacement δ as follows:

$$\theta(x) \simeq \frac{\partial}{\partial x}\delta(x) = \frac{Mx}{E^\star I}, \tag{2.14}$$

$$\delta(x) = \frac{Mx^2}{2E^\star I} = \frac{\theta(x)}{2}x. \tag{2.15}$$

The maximum deflection angle $\theta_{\max}$ and the maximum deflection $\delta_{\max}$ at the free end of the cantilever are given by the following

$$\theta_{\max} = \frac{6(1-\nu)l}{Et^2}\Delta\sigma = \frac{2\delta_{\max}}{l}, \tag{2.16}$$

$$\delta_{\max} = \frac{3(1-\nu)l^2}{Et^2}\Delta\sigma. \tag{2.17}$$

Equations (2.16) and (2.17) can be written as

$$\theta(a) = \theta_{\max}a, \tag{2.18}$$

$$\delta(a) = \delta_{\max}a^2, \tag{2.19}$$

where a is the normalized position ($0 \leq a \leq 1$) along the length direction of the cantilever:

$$a = \frac{x}{l}.$$

The functional dependency of the deflection angle and displacement on the dimensionless position a along the cantilever length is given in Figure 2.3. As result, the cantilever under differential surface stress has a circular profile with linearly

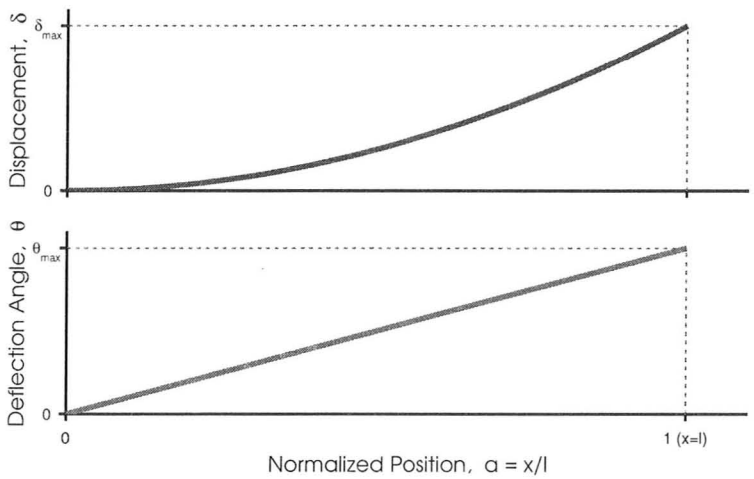

Figure 2.3: Deflection angle and displacement of a rectangular cantilever under differential surface stress

varying angle and constant curvature.

This mechanical response to the chemical interaction occurring at the surface is exploited in design of enormous amount of chemical and biochemical sensors. To achieve this, a microcantilever is modified on one side with a receptor that exhibits affinity for the analyte of interest. Specific interactions between the analyte and the recognition element induce a surface stress and deflection of the cantilever in nano- or even micrometer range. As can been seen from equations (2.16) and (2.17), transduction efficiency of such a sensor increases when the stiffness of the cantilever is reduced. Therefore, longer and/or thinner cantilevers with smaller spring constants are desired to obtain higher sensitivity.

2.3 Readout techniques

In the original AFM setup, deflection of a cantilever was measured by means of STM probe. Since those times a number of readout techniques have been developed. Most commonly used methods are briefly described in the following sections.

Optical

The most extensively used measurement methods of cantilever deflection are optical, which include optical beam deflection (or optical lever method) and interferometry.

In the optical beam deflection technique, a laser beam is focused on the free end of the cantilever. A beam reflected from the cantilever surface is tracked by a position sensitive detector (PSD). When the cantilever bends due to an analyte-surface interaction, the reflected light spot moves on the PSD surface. Its shift is measured and

correlated with the slope of the cantilever. Linear response, simplicity, and reliability are major advantages of the optical lever method.

In contrast to optical beam deflection method, the interferometry method provides a direct and absolute measurement of the cantilever displacement. The detection method is based on the interference of a reference laser beam with the one reflected from the cantilever surface. The main drawback of interferometry is complexity and high cost of its optical setup.

Usually the interferometry is considered superior to optical lever in terms of sensitivity. However, fundamental limits of resolution are the same for both techniques in noise-limited case [29].

Optical readout methods are suitable only for operation in low opacity, low turbidity media. Its application for *in vivo* sensors seems impossible due to issues with miniaturization of such a complex optical design.

Piezoresistive

A piezoresistive material changes its resistance when put under strain. The relative resistance change for a piezoresistor is given by

$$\frac{\Delta R}{R} = K_{\perp}\,\varepsilon_{\perp} + K_{\parallel}\,\varepsilon_{\parallel} \tag{2.20}$$

where ε is strain and K is the gauge factor of the material. The subscripts $\perp$ and $\parallel$ denote longitudinal and transversal components with respect to the direction of the current flowing in the resistor.

Piezoresistive readout technique is based on silicon cantilevers with highly doped regions that change electrical resistivity under stress arising from beam bending. Piezoresistive detection, compared to the optical methods, has several advantages:

- Direct electronic measurement of deflection;
- No need for expensive and complex optical setups;
- Possible operation in opaque liquid solutions;
- Ease of integration with readout electronics;
- Highly parallel operation of cantilever arrays for high-throughput imaging and multi-analyte sensing [30].

Piezoresistive probes are versatile and sensitive detectors that allow imaging even with atomic resolutions [31]. Recently piezoresistive cantilevers have become commercially available from a few vendors. For example, *Cantion* produces cantilever sensing platforms that can operate both in dynamic and static modes in liquids. However, piezoresistive probes have not received widespread adoption due to much

more complicated fabrication process. Applied operational voltage required to make measurements can also be an issue because of possible heating of the cantilever and local region. Usage of such devices in conductive liquids, for example for *in vivo* sensing, requires robust electrical insulation of piezoresistors that still is a technical challenge. In addition, piezoresistive probes are in general more expensive than conventional monolithic ones.

Piezoelectric

The advantage of the piezoelectric technique is the possibility of self-sensing and self-actuation due to the bidirectional piezoelectric effects. However, the piezoelectric readout is inefficient when slowly changing cantilever deflections need to be measured. Therefore, in a cantilever sensor it is mainly used for resonance frequency change detection instead of static deflection detection.

2.4 Applications

The cantilever sensors developed for AFM have been applied and shown capable of measuring other physical quantities than the force interactions from the AFM measurements. These include the measurement of temperature changes causing the cantilever to bend because of the bimorph effect, the measurement of mass changes obtained through the change in resonant frequency of a vibrating cantilever, and surface stress changes typically measured via the static deflection.

One of commercial applications of this technology is a micromachined humidity sensor manufactured by Hygrometrix. Water vapor interaction with the thin film polymer coating on cantilevers induces the strain in built-in piezoresistors. An integral temperature sensor is used for correction of temperature dependence resulting in a highly accurate and robust detector resistant to nearly all the failure modes affecting capacitive and resistive type humidity sensors.

Another promising example is a microcantilever sensor coated with a thiol self assembled monolayer or polymers for gas phase explosive detection at the 10-30 part per trillion lever of concentration.

A hybridization of complementary oligonucleotides immobilized on a cantilever surface was performed recently with detection of a single base pair mismatch between two 12-mer oligonucleotides [32]. The mathematical model was developed by linking the beam deflection to changes in configurational entropy and intermolecular energetics induced by molecular interactions.

Compared with more conventional sensors, cantilever sensors offer improved dynamic response, greatly reduced size, high precision, and increased reliability. Array sensors sensitive to multiple analytes could be mass manufactured at low cost using

microfabrication technology derived from the integrated circuit industry. This opens possibility for creation of complex sensing platforms like an electronic nose.

2.5 Conclusion

Cantilever-based surface stress sensing is a universal platform for studying reactions because it is driven by free energy reduction that is common for all chemical reactions. As result, it can be used as transducer for any glucose receptor presented in Chapter 1, that is not possible to achieve with any other measurement method. Moreover, the static cantilever bending measurement is ideal for liquid-based applications where frequency-based sensors suffer from significant viscous damping.

Surface stress measurement by means of commercial microcantilevers makes the basis of all glucose sensors studied in the thesis.

3 Immobilization techniques

This chapter describes immobilization steps common for all three sensor types used in the work.

3.1 Basic concepts of immobilization

The operation of microcantilever sensors in static deflection mode requires difference in surface stress between two sides. Therefore, a cantilever has to be modified in such a way that one of its sides exhibits strong affinity for the intended analyte, glucose, whereas the opposite side is relatively passive.

As a first step, usually a thin layer of a noble metal such as gold or titanium is deposited on a cantilever to allow the use of functionalization chemistry specific to only one side. The commercial cantilevers employed in the project have a thin gold coating sputtered on the top surface of silicon chips. As result, one surface is inert due to gold and the other is silicon susceptible to different modification approaches. In reality, silicon has a very thin layer of native silicon dioxide with thickness on the order of 1 nm.

For selective response to the analyte of interest (glucose) a sensor needs to have an attached receptor. For long-term application, such attachment should be robust and hydrolytically stable to withstand operation in aqueous solutions.

Sensitive coatings for microcantilever sensors could be divided in two broad categories based on the phase where ligand-receptor interaction happens:

- For a **thin layer** coating chemical reactions happen on the surface producing surface stress. Transduction efficiency is increased with decrease of the thickness of the layer.

- In a **thick** analyte-permeable coating, the interaction happens in the bulk of the layer causing swelling and inducing bulk stress. Examples of such coatings are hydrogels and polymers. The response of the sensor usually increases with the thickness of the layer. On the other hand, reaction time suffers due to slow diffusion of analyte inside the coating. Moreover, reversibility and recovery of sensors could be an issue, especially for application *in vivo*, because some molecules of analyte or surrounding medium can be trapped inside.

The immobilization process was optimized to produce thin coatings to increase transduction efficiency and decrease response time.

Immobilization methods

There are a few common approaches for immobilization of a ligand onto a solid support:

Physical adsorption is the simplest method based on non-specific adsorption of a reagent on the surface due to electrostatic, van der Waals forces or hydrophobic interactions. In general, such technique does not allow directional immobilization and the attachment is very weak. Moreover, biomolecules such as proteins can irreversibly change their conformation due to hydrophobic interaction with the support losing their activity.

Cross-linking is extension of physiosorbtion approach to enhance its stability and strength. A support is simply immersed in solution of a protein in presence of a cross-linker, for example, glutaraldehyde. Initial adsorption is followed by covalent cross-linking of molecules of protein producing robust network of macromolecules. This method has a widespread use due to its simplicity. However, it is not applicable to immobilization of small molecules and there are concerns of its reproducibility. In addition, it is very hard to apply in such a way that the coating is created on only one side of a cantilever. The actively developed method to avoid this obstacle is ink-jet printing of solution onto the surface.

Entrapment. Recognition molecules can be **entrapped in matrix**, for example a polymer or a gel. It makes possible to keep the receptors in optimum environment and configuration, at the same time, enhancing response due to very high immobilization density.

This type of coating is commonly used for fabrication of glucose sensors based on enzymatic electrodes, because the hydrogels restrict the access of interfering substances and act as a diffusion barrier for glucose. However, for micromechanical devices the resulting thick coating has significant drawbacks discussed previously.

Covalent coupling to a support is most preferable method because it results in a strong bond between the surface and the receptor. The careful choice of chemistry allows to make coupling preferential to either side of a cantilever.

It has been reported that covalent immobilization may improve the long-term performance of enzymes due to stabilization of three-dimensional conformation of the protein. In addition, leaching of the reagent is prevented.

The immobilization procedure (Figure 3.1 on page 42) consists of the following steps that are described in detail in the subsequent sections:

1. Cleaning in piranha solution and surface activation in a concentrated solution of sodium hydroxide to remove organic and inorganic contaminates and enhance concentration silanol groups on the silicon surface.

2. Silanization with aminopropyltriethoxy silane (APTES) for amine derivatization ($-NH_2$) of the silicon side.

3. Succinylation to convert amino groups ($-NH_2$) into carboxyl groups ($-COOH$). This step is done only for immobilization of APBA that has only amino group for coupling.

4. Covalent coupling of a receptor by means of coupling reagents EDC/NHS.

3.2 Overview of self-assembled monolayers

Self-assembled monolayers (SAMs) are highly ordered and oriented molecular assemblies formed by the adsorption of an active surfactant on a solid surface. The driving forces for the spontaneous organization of the 2D structure are chemical bond formation of molecules with the surface and inter- or intramolecular interactions [33]. In contrast to film deposition technologies, such as spin coating, molecular beam epitaxy (MBE), and chemical vapor deposition (CVD), the self-assembling approach allows to easily control the thickness in (sub)nanometer range and engineer surface properties incorporating a wide range of functional groups both in the alkyl chain and at the chain terminal. At the same time, technological process is very simple being a short-time immersion in solution or exposure to vapors of an active reagent. These factors determine widespread use of SAMs in fabrication of DNA chips, chemical and biochemical sensors. Moreover, due to their dense and highly stable structure, SAMs are applied for hydrophobisity/hydrophilisity surface modulation, corrosion and wear prevention, friction reduction, etc. Also, silane reagents are commonly used in microelectronics industry as adhesion promoters.

For cantilever sensors, it is very important for the SAM layer to have high quality, uniformity, and packing density. Since cantilever bending is due to surface stress change, a rigid self-assembled monolayer would produce a stronger cantilever deflection as compared to a loosely packed SAM.

There two types of self-assembled techniques commonly used for fabrication of biodevices distinguished by their underlying chemistry and target substrates as thiols for gold and silver surfaces and silanes for hydroxyl rich supports.

Thiol self-assembled monolayers

Organosulfur compounds have a strong affinity to transition metal surfaces such as gold, silver, copper, GaAs and InP. The most studied are alkanethiols (R–SH) and dialkyl disulfides (R–S–S–R) on Au(111) surfaces. The spontaneous adsorption results in formation of monolayers with two-dimensional semicrystalline structure. The driving force is a coordinative bond between gold and sulfur atoms, that forms Au(I)

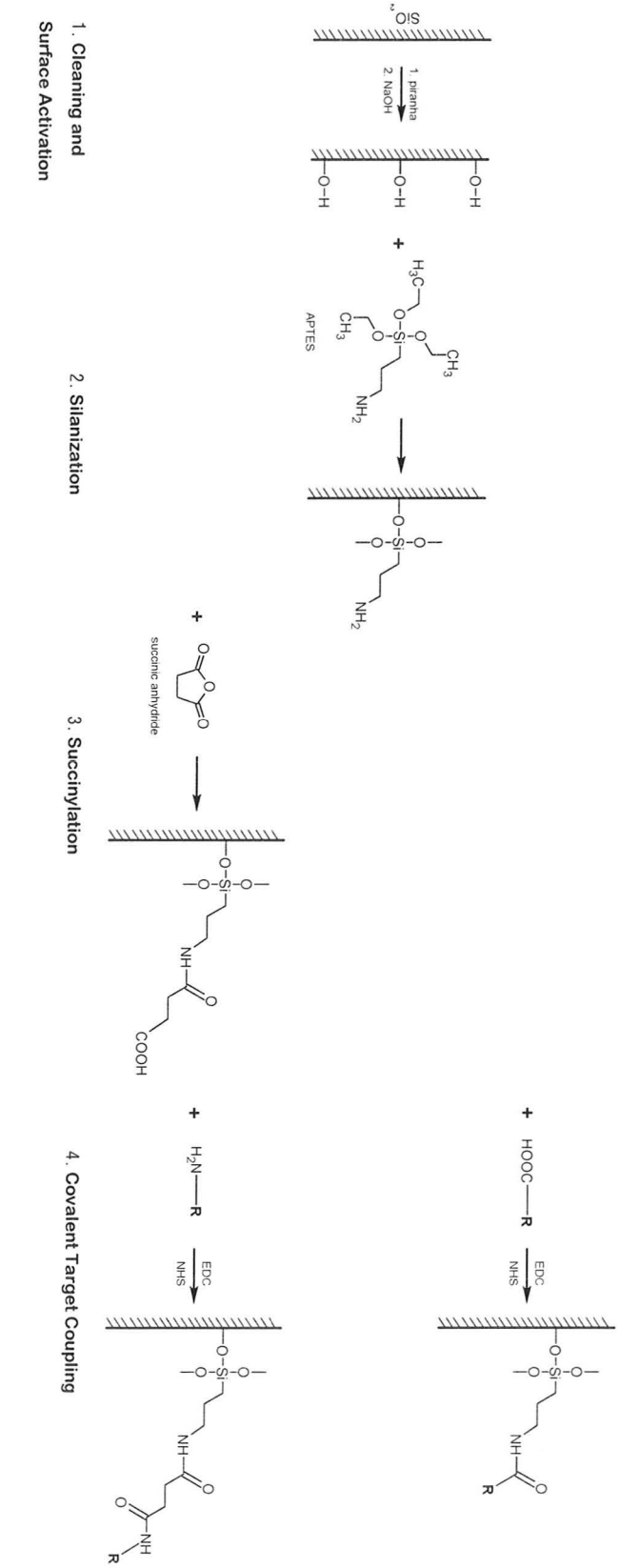

Figure 3.1: Immobilization scheme

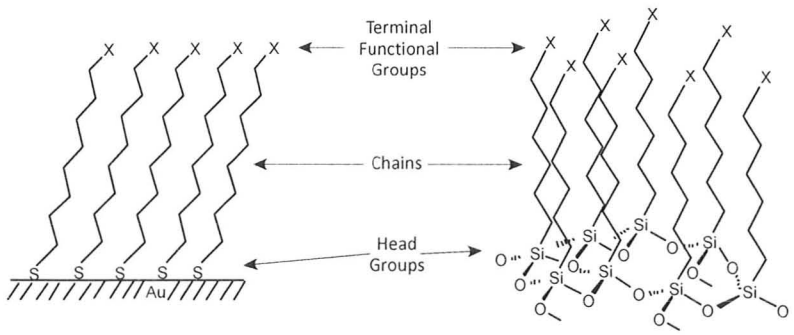

Figure 3.2: Thiol (left) and silane (right) self-assembled monolayers

thiolate molecule (RS–Au). The bonding of the thiolate group to the gold surface is very strong with bond strength of $40\,^{\mathrm{kcal}}/_{\mathrm{mol}}$. At the same time, thiolates keep their ability to migrate on the surface that is essential for formation of a dense monolayer and healing of defects. Chain-chain interactions (van der Waals, dipole-dipole forces) induce surface crystallization process of hydrocarbon chains to assume hexagonal close packing.

Thiols allow formation of SAMs with high quality and excellent reproducibility in a simple immersion procedure. However, their long-term stability is questionable. For example, Flynn *et al.* [34] reported the loss of monolayer integrity over 35 days in aqueous solution due to oxidation of thiolate headgroups to sulfinates and sulfinites, followed by desorption into the surrounding medium. In addition, due to significant mobility of thiolates, an adsorbed layer could be partially washed out by strong nonpolar solvents. Interestingly, free gold atoms were observed in a solution of thiols suggesting an undergoing etching process by organosulfur compounds [33].

Utilization of thiol monolayers for fabrication of robust sensors is further complicated because an underlying metal surface has to be atomically flat and of particular crystallographic orientation. The most inert metal, gold has usually a polycrystalline structure with poorly controllable grain size, when deposited by commonly used sputtering process on microfabrication relevant materials, silicon and silicon nitride. As result, quality of SAMs on such surfaces is of a big concern.

Silane self-assembled monolayers

Silanes with hydrolytically unstable bonds such as alkylchlorosilanes (with Si–Cl bond) and alkylalkoxysilanes (with $\mathrm{Si{-}OC_nH_{2n+1}}$ bond) are prone to condensation on hydroxylated surfaces of silicon dioxide and metal oxides forming a layer of polysiloxane, which is covalently bound to the support. Surfaces of clean silicon dioxide or silica can have up to $5\,\mathrm{nm}^{-2}$ silanol groups (–Si–OH) capable of chemically reacting with the silane molecules producing 2D network of molecules interconnected via Si–O–Si bonds that are very strong and hydrolytically stable. In addition, exposed functional

groups at the chain terminal can significantly alter surface properties and might be anchoring points for immobilization.

The main advantage of silanes over thiols for preparation of self-assembled monolayers is formation of strong **covalent** bonds both between molecules and with solid support. Excellent mechanical properties of such layers have been revealed with AFM and tribometers, and find its practical application for mechanical enforcement of fiber-polymer composites. Moreover, these bond are not prone to hydrolytic attack in aqueous solutions or oxidation due to atmospheric oxygen. Silane coatings are also stable in mild alkaline or acidic solutions and in a wide range of solvents. Remarkable long-term stability of sensors based on silane chemistry has been reported in literature [35, 36].

3.3 Silanization

Based on careful comparison of silane and thiol self-assembled monolayers, aminopropyltriethoxy silane (APTES) was chosen as a reagent for cantilever modification in this work. It rapidly forms a coating on the silicon side of devices leaving gold layer intact. Gold does not have a stable surface oxide under normal conditions, thus silanes cannot form permanent chemical bonding to the Au surface and its surface can be easily cleaned from the physically and chemically adsorbed molecules [33]. Amine groups of APTES enable a wide range of conjugation reactions.

Reproducible high-quality monolayers of silanes, especially aminosilane derivatives, are very difficult to achieve. The silanization process strongly depends on reaction conditions, including presence of water, solvent, concentration, temperature and duration of reaction, surface cleaning and post-treatment (washing and baking). Probably the most significant factor is the amount of water in solution and/or on the surface. While incomplete monolayers are formed in the absence of water, excess water usually results in adverse polymerization in solution and polysiloxane deposition on the surface producing a thick and rough coating with numerous agglomerates. In most cases, this results in poor performance of devices.

Detailed literature analysis reveals high variability of quality, structure and thickness of silane films, even for similar reaction conditions. There have been a few attempts to correlate different factors affecting result. For example, in Figure 3.3 the reaction condition matrix with superimposed AFM images of APTES films illustrates dependency of film morphology on such process parameters as reaction temperature, solution concentration and reaction time [37].

The main reasons of such process variability of silane SAMs comparing to thiol-based SAMs are self-polymerization in solution phase and restricted mobility of individual molecules on surface due to covalent bonding. As result, the assembly cannot reach organized equilibrium structure. In contrast, thiol molecules interact only non-covalently and even coordination with gold atoms is relatively weak and mobile.

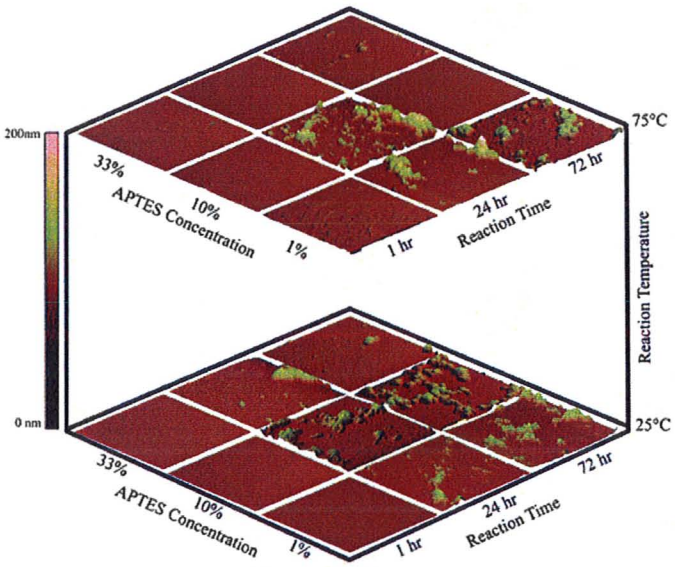

Figure 3.3: Three-by-three matrix of AFM scans of APTES films prepared under different conditions [37].

It allows for thiols to reach equilibrium highly ordered quasi-crystalline structure. In addition, thiols lack ability to cross-link and thus, thickness is limited only to a monolayer [33].

Figure 3.4 schematically illustrates parallel reactions occurring during treatment of a silicon dioxide surface with aminopropyltriethoxy silane (APTES):

- Rapid hydrolysis of ethoxy groups of silane by water produces ethanol and trisilanols ($R{-}Si(OH)_3$). On other hand, $Si{-}C$ bond is hydrolytically stable and is not cleaved.

- Adsorption of silane molecules on a surface. It is more efficient for aminosilanes at neutral pH, because amine groups of the silane are protonated (positively charged) and surface silanols are negatively charged.

- Slow condensation of hydroxyl groups of silane with themselves (in solution) or with silanols on the support.

These complicated processes result in deposition of silane molecules that could be classified in two categories:

- Chemisorbed molecules that are either covalently linked to the support or strongly polymerized with surrounding molecules in the layer. Such bonds are very strong and resulting coating is very stable and robust to many chemical treatments;

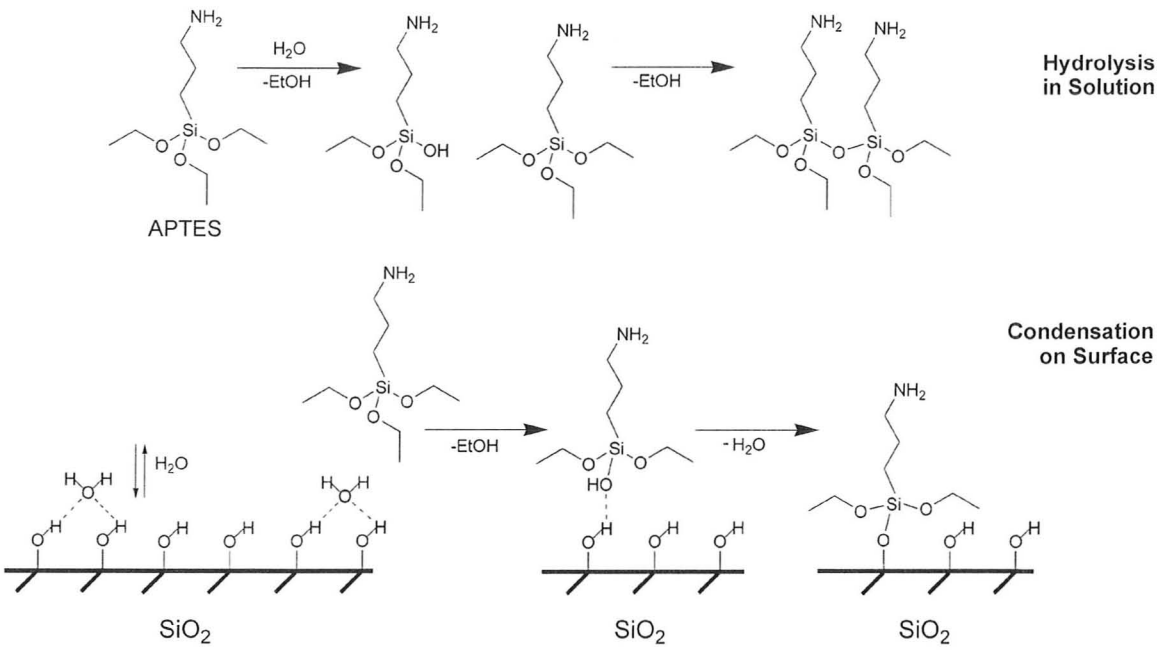

Figure 3.4: Scheme of APTES silanization reaction [37]

- Physically adsorbed molecules that have weak connection to the SAM and the support by means of van der Waals interaction, ionic bonds or incomplete condensation. Such molecules can be removed by extensive washing in solvents or by ultrasonication.

As it has been reported in [38], extensive rinsing in methanol and water is effective enough to remove all weakly bounded physisorbed molecules to obtain a smooth and reproducible coating surface.

A common approach to deal with influence of water on quality and thickness of SAMs is to use anhydrous aprotic solvents, for instance toluene. However, the outcome depends on extent and thoroughness of solvent dehydration and considerably complicates the process. Therefore, it was decided to use aqueous solutions of low silane concentration. As has been reported when the silane and the resulting reactive silanol are diluted, the polymers resulting from condensation are of lower molecular weight. At sufficiently low silanol concentrations, low molecular weight oligomers and even monomers are favored allowing formation of a monolayer.

Protocol

Silanization protocol is based mostly on the work of Metwalli *et al.* [38]. The formation of a high quality monolayer was reported.

1. A mixture of concentrated sulfuric acid and 30% hydrogen peroxide in ratio 3:1 is prepared for piranha etch.
2. Cantilever chips are immersed in the cleaning solution for 30 min.
3. The devices are washed in pure water for 5 min two times.
4. For surface activation, the devices are soaked in 2.5 M NaOH solution overnight.
5. The devices are washed in pure water for 5 min two times and then in methanol for 10 min.
6. Silanization of the cantilevers is performed by immersion in 1% (v/v) APTES aqueous solutions for 15 min.
7. Rinse 2 times in methanol for 5 min and then in water for 10 min manually agitating.
8. Dry under nitrogen stream.
9. Bake on hot plate at 110°C for 30 min.

3.4 Introduction of carboxyl groups

For immobilization of molecules with amine anchoring groups (for example, APBA) it is preferable to use a carboxilated solid support. Succinic anhydride is efficient agent for introduction of carboxyl functions on amine terminated APTES film. The introduction of carboxyls also affects the overall charge characteristics of surface. The modification of amine residues by acylation with anhydrides changes surface charge from the positive charge of the protonated amine to the negative charge of the carboxylic acid. As result, it facilitates adsorption and coupling of positively charged species [39].

Succinic anhydride is a result of the intramolecular dehydration of two carboxylic acid groups of succinic acid. Carbonyl groups of the anhydride are highly reactive toward nucleophiles, especially amines producing a very strong amide bond. Upon succinylation reaction the ring structure of the anhydride opens, one of carbonyl groups participates in amide linkage and the other becomes a terminal carboxylic acid (Figure 3.5).

In aqueous solutions, the major side reaction of succinylation is hydrolysis of the anhydride. Addition of one molecule of water yields succinic acid. Therefore, an excess of the anhydride in the reaction medium is needed. The optimum pH of the solution is between 6.0 and 9.0. Acidification of the reaction solution should be prevented by periodic addition of NaOH.

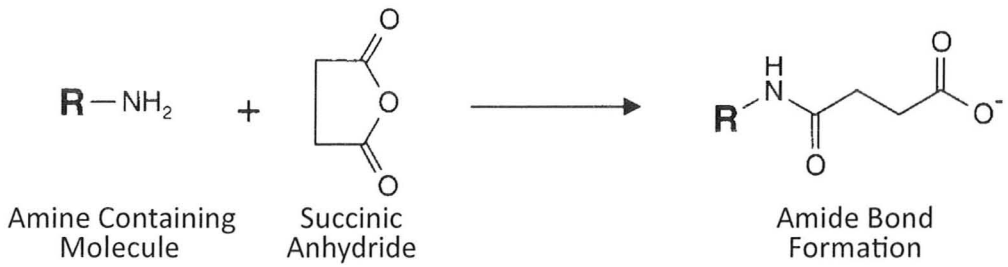

Figure 3.5: Reaction of succinic anhydride with primary amine groups [39]

Protocol

1. Dissolve 0.2 g of succinic anhydride in 10 ml of 0.1 M Phosphate Buffer Saline pH 7 to obtain concentration of 0.2 M.
2. Immerse cantilever chips into the solution.
3. Maintain pH in 7 – 8 range by periodic addition of 1 N NaOH.
4. Add more succinic anhydride every 15 min.
5. React for 2 h with continuous shaking at room temperature.
6. Rinse with pure water and then methanol in order to remove reactants and by-products.

3.5 Target conjugation

Carbodiimides are the most popular type of zero-length crosslinkers that mediate the formation of covalent amide linkages (−CO−NH−) between carboxylates (−COOH) and primary amines ($-NH_2$) without addition of any intervening linker or spacer. The condensation reaction is very efficient and occurs under mild conditions, as result carbodiimides are commonly used for conjugation of wide range of molecules, including proteins and nucleotides.

For the immobilization process there has been chosen a water-soluble carbodiimide, 1-ethyl-3-(3-dimethylaminopropyl)carbodiimide hydrochloride (EDC). It particularly serves for coupling of proteins, including glucose oxidase, because most biomolecues are soluble in aqueous solutions and not only the crosslinking agent itself able to dissolve in the reaction medium, but the by-product of the reaction, an isourea, is also water-soluble. Unreacted reagents and by-products can be easily removed by washing in a buffer solution.

The reaction involves formation of highly reactive o-acylisourea intermediates through carbodiimide activation of carboxylic acids. This active species then can

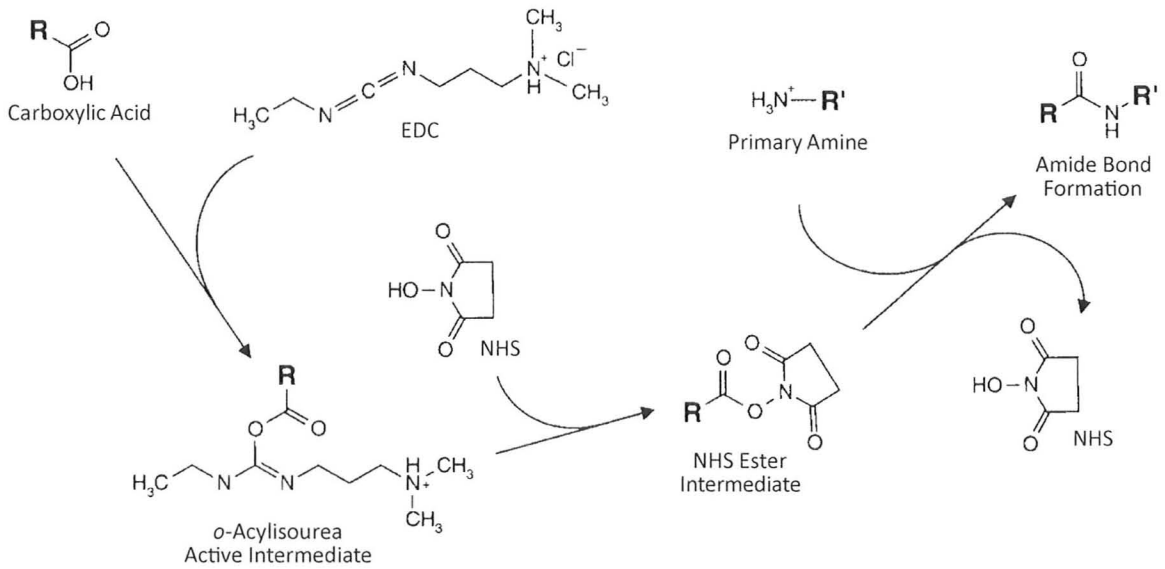

Figure 3.6: EDC/NHS mediated coupling reaction of carboxyls and amines [39]

react with a nucleophile such as a primary amine to form an strong amide bond. Unfortunately, this reactive ester complex is slow to react with amines and can hydrolyze in aqueous solutions, regenerating the carboxylate group. If the target amine does not find the active carboxylate before it hydrolyzes, the desired coupling cannot occur. In addition, EDC itself is very unstable in presence of water. Therefore it is a common practice to use EDC together with N-hydroxysulfosuccinimide (NHS) forming a more stable active intermediate, NHS ester, which ultimately reacts with the attacking amine, creating the final product identical to that obtained using EDC alone. Even low concentrations of NHS can significantly increase the yield of amide bond formation. The overall mechanism of coupling is illustrated in Figure 3.6.

The carbodiimide coupling effectively occurs between pH 4.5 and 7.5. As the reaction progresses, the medium becomes more alkaline. To help keep pH constant, buffered solutions are conveniently used because the pH does not have to be constantly monitored. A phosphate buffer pH 7 at 0.1 M is probably the most preferable, because at lower pH the amines are protonated and therefore less reactive.

Protocol

The reaction protocol is based on [39, 40].

1. Dissolve 0.144 g of EDC and 0.052 g of NHS in 10 ml of 0.1 M Phosphate Buffer Saline pH 7 to obtain 75 mM EDC and 45 mM NHS in the result.

2. Target small molecules (APBA or ACVA) are dissolved at concentration of 50 mM. For proteins (glucose oxidase) the concentration is 2 mg/ml.

3. The pH is maintained constant between 7 and 8 by addition of HCl or NaOH.
4. The cantilever chips are soaked in the reaction solution for 2 h with continuous stirring or shaking.
5. Soak in fresh PBS for 15 – 30 min and then rinse with pure water.

Reagents

All chemicals were used as received without futher purification.

Deionized water was obtained from a Barnstead NANOpure purification system that uses ion exchange and filtration steps to achieve finale resistivity of 18.2 MΩ-cm.

Some chemical reactions are pH sensitive and require pH to be kept in particular range. It can be achieved by manual periodic monitoring of the pH or with help of a pH stat. However, the most convenient method is a buffer solution that has a natural ability to resist to changes of the pH when a small amount of strong acid or base is added to the solution. Buffer solutions are aqueous solutions consisting of a mixture of a weak acid and its conjugate base or a weak base and its conjugate acid. For pH 7 – 8, a sodium phosphate buffer (PBS) is commonly used.

0.1 M sodium phosphate buffer pH 7.0 was prepared as follows:

1. Sodium Phosphate Monobasic, monohydrate ($NaH_2PO_4 \cdot H_2O$) 1.19 g.
2. Sodium Phosphate Dibasic, anhydrous (Na_2HPO_4) 2.32 g.
3. Dissolve the salts in 200 ml of deionized water.
4. Adjust the pH to 7.0 with 1 N HCl or 1 N NaOH.
5. Bring to the final volume of 250 ml.

4 Experimental setup

4.1 Cantilevers

Microfabrication of cantilevers is very time-consuming process, therefore it was decided to use commercially available cantilevers produced for atomic force microscopes. As consequence of Stoney's equation (2.17), to achieve highest displacement sensitivity, it is preferable to use cantilevers of larger length and smaller thickness. Based on these factors, rectangular tipless cantilevers *Arrow TL2Au* from *NanoWorld* were chosen (500 μm long, 100 μm wide and 1 μm thick). The spring constant is 0.03 $^{N}/_{m}$, making them one of the "softest" cantilevers available on market. On other hand, fairly large dimensions make focusing laser beam on an apex more convenient, which is highly beneficial for optical design.

The cantilevers were fabricated in the form of chips made from monolithic crystalline silicon with two rectangular beams having a triangular free end. The cantilevers have a pitch of 250 μm. Initially it was planned to use one of two cantilevers as a reference in order to increase measurement accuracy and subtract environmental factors. However, it was rejected due to the tremendous difficulty to individually carry out chemical reactions on such microscopic objects. Moreover, by the time a chip is installed in the holder, usually one of the cantilevers are either damaged or broken.

Single-crystal silicon has properties that makes it one of the best materials for micromechanical devices. To begin with, it is inert to a wide range of solvents, acids and basis, which is essential for chemical sensors. Additionally it is mechanically robust and easy to micromachine. Silicon nitride is another material commonly used for fabrication of AFM tips. However, silicon allows to create stress-free cantilevers with much more reproducible characteristics. For this reason, non-contact and tapping mode cantilevers are usually made of silicon.

The extremely high softness of the cantilevers makes them very fragile to manipulate. As an example, initially during chemical fuctionalization operations, the surface tension of the solution, in which the cantilevers were immersed, would easily damage them resulting in a high breakage rate. To circumvent this problem, special Teflon holders were fabricated, which allowed for the slow introduction of the chips into the solutions with the cantilevers pointing vertically upwards thereby avoiding the stress due to surface tension. The holder as well allows for the manipulation of 4 cantilevers simultaneously. However, damage of cantilevers still occurs during installation in the fluid cell.

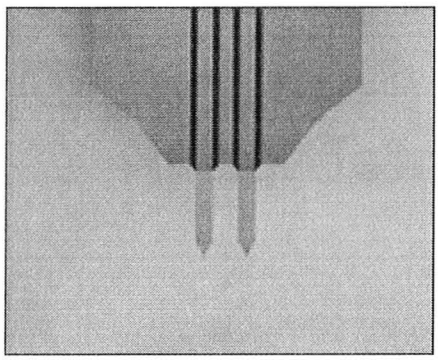

Figure 4.1: Cantilever chip [41]

Table 4.1: Nominal parameters of cantilevers

Parameter	Nominal Value
Thickness, t	1.0 μm
Width, w (rectangular part)	100 μm
Length, l	500 μm
Pitch	250 μm
Force Constant, k	0.03 N/m
Resonance Frequency	6 kHz

The top side of the sensors has 5 nm titanium and 30 nm gold coating. As a common practice, a thin layer of titanium is used to facilitate adhesion of gold to silicon surface. The coating is intended to increase laser beam reflection and eliminate light interference inside cantilevers for optical setups of AFM equipment. It is claimed by the manufacturer to improve signal strength by a factor of 2.3.

For the project, such coating is essential to make surfaces of a cantilever unequal for further chemical derivation. Gold is chemically inert and is not prone to silane attachment. Solvents and water washes are enough to remove physiosorbed molecules leaving receptors only on the silicon side.

On other hand, the coating introduces bimetallic effect to cantilevers due to difference in thermal expansion coefficients of silicon and gold. The thermo-mechanical sensitivity of the probes can be estimated from Timoshenko's equation (2.1) as

$$S_T = \frac{\delta}{\Delta T} = (\alpha_1 - \alpha_2) \cdot \frac{3l^2}{t_1 + t_2} \frac{\left(1 + \frac{t_1}{t_2}\right)^2}{3\left(1 + \frac{t_1}{t_2}\right)^2 + \left(1 + \frac{t_1}{t_2}\frac{E_1}{E_2}\right)\left(\frac{t_1^2}{t_2^2} + \frac{t_2}{t_1}\frac{E_2}{E_1}\right)} = 126.5\,\frac{\text{nm}}{\text{K}}, \tag{4.1}$$

Table 4.2: Material properties of the cantilevers from *NanoWorld* [42]

	Young's modulus, E (GPa)	Poisson ratio, ν	CTE, α ($10^{-6}\,\mathrm{K}^{-1}$)
Silicon	156	0.23	2.6
Gold	78	0.42	14.2

where $l = 500\,\mu\mathrm{m}$ is the length of cantilevers, $t_1 = 30\,\mathrm{nm}$ and $t_2 = 1\,\mu\mathrm{m}$ are thicknesses of the gold layer and silicon substrate, respectively (titanium layer is neglected due to its thickness being much smaller than the thickness of gold). Material properties of gold and silicon, are listed in Table 4.2 and based on Snow *et al.* [42].

Cantilever deflection of 127 nm due to 1 K temperature increase would correspond to surface stress of $0.034\,\mathrm{N/m}$, which has the same order of magnitude as most surface chemical reactions ($0.01 - 0.1\,\mathrm{N/m}$). Such high sensitivity of cantilevers makes them very susceptible to environmental factors, thus requiring continuous control of temperature during experiments. This control of temperature was achieved via a heating stage described in Section 4.2. For comparison, temperature fluctuations of air in the lab were measured to be around 0.4 K during 4 hours as illustrated in Figure 4.2.

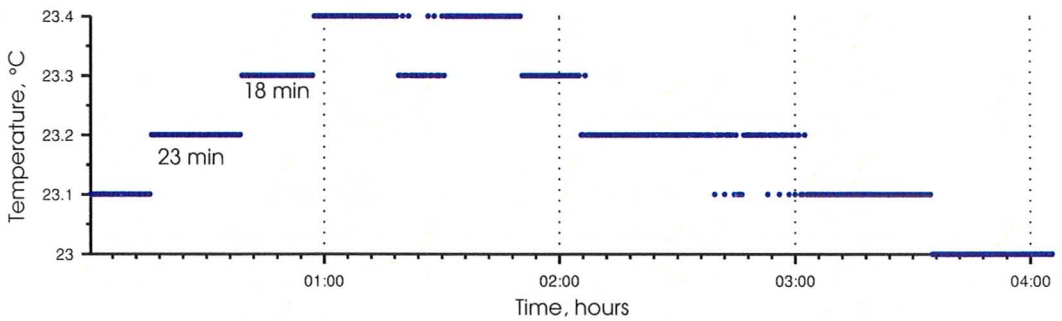

Figure 4.2: Temperature log of the stage without temperature control

4.2 Environmental control

A cantilever chip is placed in the inclined groove on the bottom side of a fluid cell (FC) and is held in by a spring-loaded gold-coated wire clip (Figure 4.3). The fluid cell is a commercial accessory manufactured by *Veeco* for AFMs. It is machined from a monolithic piece of BK7 glass that gives superb chemical inertness and outstanding optical performance. The unit has an anti-reflection coating to increase transmission and decrease false laser reflections. The cell has two fluid ports that are connected by means of tubes to a syringe with a solution of interest and a waste container. An

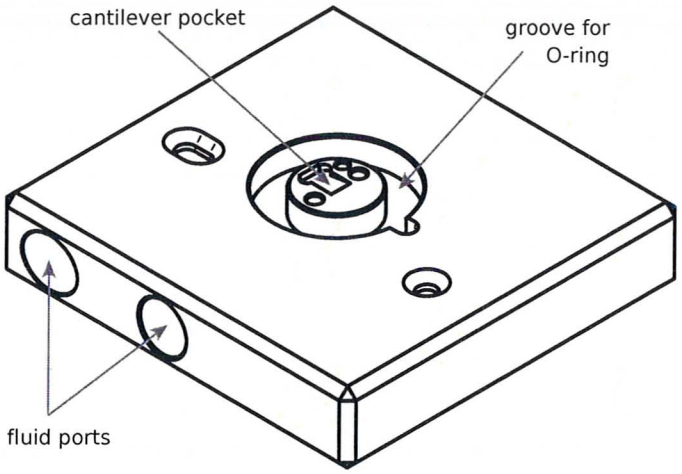

Figure 4.3: Drawing of the fluid cell (bottom side view) [43]

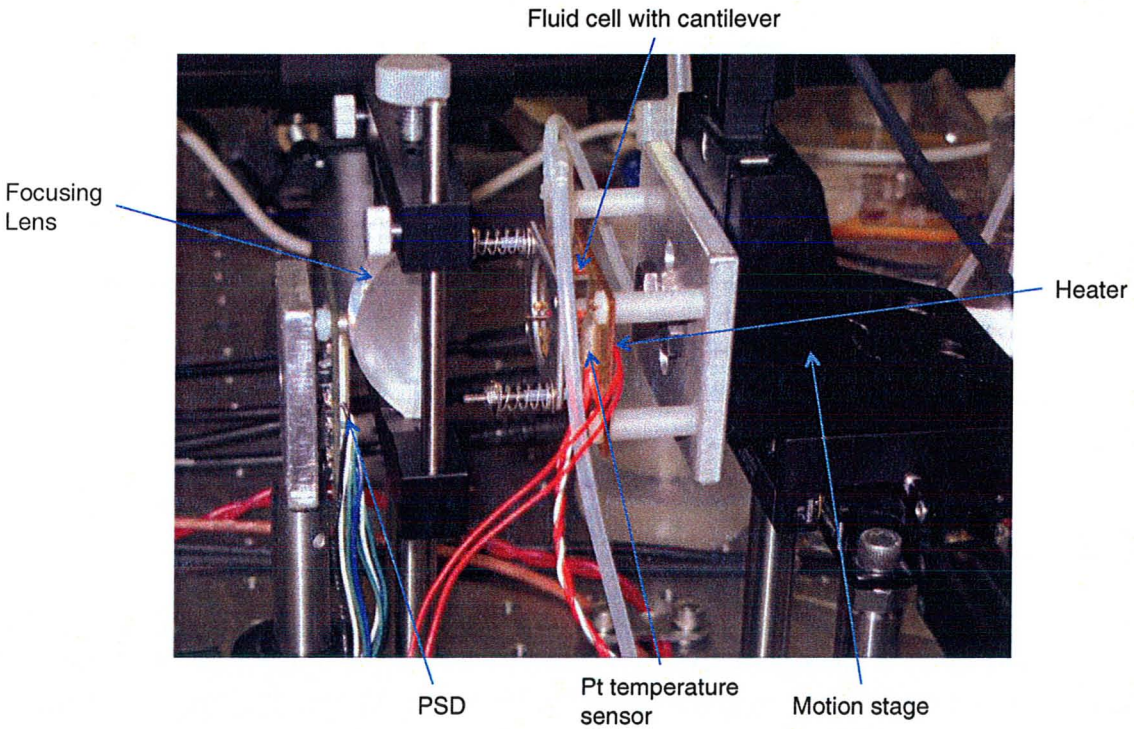

Figure 4.4: Photo of the experimental setup

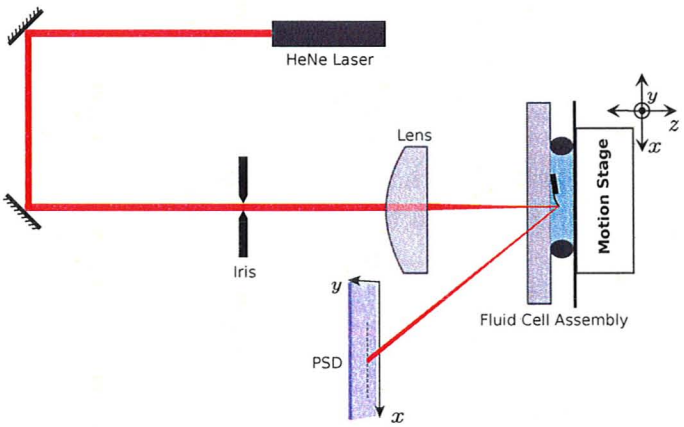

Figure 4.5: Scheme of the optical setup

approximate 50 µl cavity with liquid is enclosed within a silicone O-ring that sits in a circular groove. It has been lightly coated with vacuum grease Apiezon to form a fluid and air-tight seal. The total inner volume of the FC including the channels is less than 300 µl and the volume of tubing is approximately 1.1 ml.

The fluid cell is mounted on a copper plate that has high thermal conductivity. It is protected from oxidation in air and liquids by gold coating. On the same side of the plate beside the cell (as close to the cantilever as possible) a platinum thermoresistor is fixed for temperature measurement. The opposite side is covered with a thin thermofoil heater from *Minco*. Both the thermosensor and the heater are connected to a closed-loop PID temperature controller *Omega CYC321* that allows to keep temperature stable at specified setpoints within ±0.1°C. The main goal of the system design is to minimize thermal resistances and heat capacities of all components in order to increase its temperature responsiveness and accuracy.

The whole assembly is mounted on a 3 axes translational stage (see Figure 4.4). Movement in X and Y directions is performed by motorized linear actuators (*Newport CMA-25CCCL*) connected to a motion controller *Newport ESP300*. The location of the stage and its motion are programmed by a computer. The position in Z direction is manipulated manually with a microshifter.

4.3 Optical setup

The optical setup is based on optical lever method commonly used to measure angular rotations and small bending deflections. It was chosen due to its simplicity and high sensitivity. Detailed analysis [29] shows that such configuration can achieve performance comparable to much more complicated interferometric techniques.

A Helium-Neon laser *JDS 1107P* emits coherent light with wavelength of 632.8 nm and nominal power of 0.8 mW. The produced beam is focused by an aspheric

lens onto a cantilever placed in a fluid cell. Due to the inclined groove in the cantilever holder, the chip is fixed at angle of 10° with respect to the incident beam. As a result, reflected light is directed towards a bidirectional position sensitive photodetector (PSD). Its output voltage is linearly related to position of the light spot on its surface. Bending of a cantilever leads to a change in the beam reflection angle causing the displacement of the the light spot on the PSD. Two mirrors and an iris are used for beam alignment.

Each component of the setup is described in detail in the following sections.

4.3.1 Laser beam focusing

Laser radiation is usually assumed to have an ideal Gaussian intensity profile in a plane perpendicular to direction of propagation. According to specification from the manufacturer, *JDS*, the HeNe laser used in the experiments emits at least 95% of its power in the form of the fundamental TEM_{00} mode. Therefore the beam can be considered as a Gaussian beam.

For a Gaussian beam in free space, the complex electric field amplitude is given by

$$E(r,z) = E_0 \frac{w_0}{w(z)} \exp\left[-\frac{r^2}{w^2(z)}\right] \exp\left[-ikz - ik\frac{r^2}{2R(z)} + i\zeta(z)\right], \tag{4.2}$$

where r is the radial distance from the center axis of the beam, z is the axial distance from the beam waist, $k = \frac{2\pi}{\lambda}$ is the wavenumber, λ is the wavelength, $\zeta(z)$ is the phase retardation, $R(z)$ is the radius of curvature of the wavefront, $w(z)$ is the beam width, defined as the radius at which the field amplitude drops to $1/e$ of its axial value, and $w_0 = w(0)$ is the waist size.

The waist of a Gaussian beam is the place along the beam axis, where its width $w(z)$ takes the minimum value w_0 and the wavefront becomes planar. Further evolution of beam parameters with propagation in free space, is described by the following equations:

$$R(z) = z\left[1 + \left(\frac{z_\mathrm{R}}{z}\right)^2\right], \tag{4.3}$$

$$w(z) = w_0\sqrt{1 + \left(\frac{z}{z_\mathrm{R}}\right)^2}, \tag{4.4}$$

where z_R is called the Rayleigh range. It relates to the distance over which a Gaussian beam can be collimated before it spreads significantly due to diffraction. In particular, the Rayleigh range is the distance that the beam travels from the waist before the beam diameter increases by $\sqrt{2}$. The relationship between the beam waist and the Rayleigh range is given by

$$z_\mathrm{R} = \frac{\pi w_0^2}{\lambda}. \tag{4.5}$$

As can be seen from equation (4.4), far away from the waist, when $|z| \gg z_R$, the beam radius $w(z)$ has an asymptote making the angle θ with the beam axis. The so-called divergence is given by

$$\theta \simeq \tan\theta = \frac{\lambda}{\pi w_0}. \tag{4.6}$$

A consequence of this equation is that beams with smaller waist sizes diverge much more quickly.

The light intensity distribution is

$$I(r,z) = \frac{c\epsilon_0}{2}|E|^2 = I_0(z)\exp\left[-\frac{2r^2}{w^2(z)}\right], \tag{4.7}$$

where $I_0 = I(0,z)$ is the peak intensity at the center of the beam. At beam radius $w(z)$, the intensity drops by e^2 times reaching 13.5% of the peak value.

Integration of equation (4.7) gives power P that passes through a circle of radius r in the transverse plane at position z:

$$P(r,z) = P_0\left\{1-\exp\left[-\frac{2r^2}{w^2(z)}\right]\right\}, \tag{4.8}$$

where

$$P_0 = \frac{1}{2}\pi I_0 w^2 \tag{4.9}$$

is the total power of the beam.

Consequently, a circle of radius $r = w(z)$ contains only 86.5% of the beam power. However, a circular aperture of radius

$$r = \pi/2 \cdot w(z). \tag{4.10}$$

encloses 99% of the total optical power.

According to the specification, the HeNe laser produces a beam with a diameter of 0.48 mm at the laser aperture. From the laser aperture the beam travels 65 cm. In this path the beam encounters the following optical instruments: alignment mirrors, iris and attenuator. This increases the spot size to 1.1 mm as measured in Section 4.3.2. This number significantly exceeds the size of the cantilevers (500μm × 100μm). Therefore, it is necessary to use a lens to focus the light to a spot less than 64 μm in diameter to collect 99% of the optical power (4.10).

One of characteristic properties of Gaussian optics is that after reflection by a mirror or refraction by a lens, a Gaussian beam is transformed into another Gaussian beam with a different set of parameters. Self [44] has derived transformation equations for a thin lens by assuming that the waist of the input beam represents the object,

and the waist of the output beam represents the image. Analogous to the well-known thin lens formula, for a Gaussian beam we get:

$$\frac{1}{s + z_R^2/(s-f)} + \frac{1}{s'} = \frac{1}{f}, \tag{4.11}$$

where s is the object distance, s' is the image distance, and f is the focal length of the lens. Then, the magnification is given by

$$m = \left|\frac{s'}{s}\right| = \frac{1}{\sqrt{(1 - s/f)^2 + (z_R/f)^2}}. \tag{4.12}$$

The size of the image waist is calculated from $w_0' = m w_0$.

Depth of focus is usually defined as the range in the image space over which the focused beam diameter does not increase more than $\sqrt{2}$ times, therefore it is related to a Rayleigh range:

$$DOF = 2z_R'. \tag{4.13}$$

The choice of a lens for the setup is constrained by a few factors. First, it should be able to focus to a spot of at least 64 µm in diameter. Second, a low bound on the focal length is set by the need to allow for free propagation of the beam reflected from the cantilever to the detector and is also set by the increase in divergence due to a tighter focus given by equation (4.6). As result, an aspheric plano-convex lens *Melles Griot 01LAG011* was chosen with nominal focal length of 42.0 mm. Based on equation (4.11) the distance to the waist of the focused beam is $s' = 44$ mm and the radius of the light spot is $w_0' = 15$ µm. An aspheric design of the lens significantly reduces spherical aberration up to the sixth order and allows focusing close to diffraction limited performance. To achieve the highest optical performance the aspheric surface of the lens was directed towards the incident beam.

However, the claimed tolerance of the focal length is ±2.9 mm, which significantly exceeds the calculated depth of focus, 2.2 mm. Thus it was essential to measure the position and the size of the focus spot. The experiment is described in Section 4.3.2.

4.3.2 Knife edge measurements

As evident from equations (4.2)–(4.5), a Gaussian beam is completely defined by its wavelength λ and the waist radius w_0. It is therefore possible to fully characterize a Gaussian beam by determining the size and location of the beam waist. There are a few techniques to measure these parameters [45–47] with the knife edge method being the most popular due to its simplicity and high accuracy for micron range beams [48, 49]. In this technique a "knife edge" moves (along axis X) perpendicular

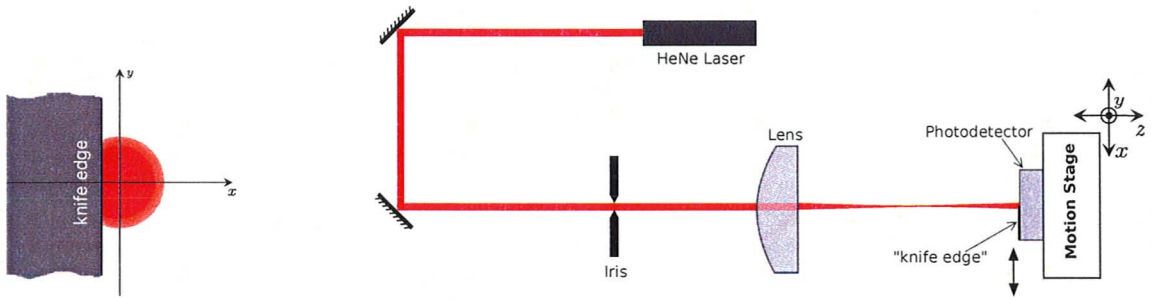

(a) Principle (b) Scheme of the optical setup

Figure 4.6: Knife-edge technique

to the direction of propagation of the laser beam, and the total transmitted power is measured as a function of the knife-edge position.

Integration of equation (4.8) gives the power transmitted by half-plane obstacle as a function of the axial and radial positions x and z:

$$P(x,z) = \int_{x}^{\infty}\int_{-\infty}^{\infty} I(r,z)\,dxdy = \int_{x}^{\infty}\int_{-\infty}^{\infty} I_0 \exp\left[-\frac{2\left((x-x_0)^2+(y-y_0)^2\right)}{w^2(z)}\right] = \\ = \frac{P_0}{2}\left\{1-\operatorname{erf}\left[\frac{\sqrt{2}\,(x-x_0)}{w(z)}\right]\right\}, \tag{4.14}$$

where (x_0, y_0) is the center axis of the beam.

Technically, knife edge experiments were conducted with a power meter *Newport 1815-C* mounted on a motorized computer-controlled stage moving in X and Z directions. A thin foil with a very sharp edge was attached to the surface of the detector as "a knife edge". Therefore the photodetector and the "knife edge" were shifted as a whole, which significantly simplified the experiment design. The optical setup is illustrated in Figure 4.6b. Scans were performed at step sizes of 1 µm in the transverse direction and 1 mm in the longitudinal direction thereby measuring the beam profile at various positions along the beam propagation axis.

Measurements were done both for a laser beam before the lens and for a focused beam after the lens. Figure 4.7b demonstrates a plot of the normalized transmitted power $P(x)/P_0$ versus the knife edge displacement x at distance $z = 35$ mm from the back surface of the lens, near the focus point. Baseline power level due to stray light was subtracted and data were fitted with the function defined by (4.14) using nonlinear least square method. The calculated normalized intensity profile with Gaussian distribution is supperimposed for comparison.

Calculated values of the beam width are plotted in Figure 4.8 as a function of the beam propagation distance from the lens. The lack of points between $z = 25 - 30$ mm is due to the limited travel range of the translation stage and the need to reposition

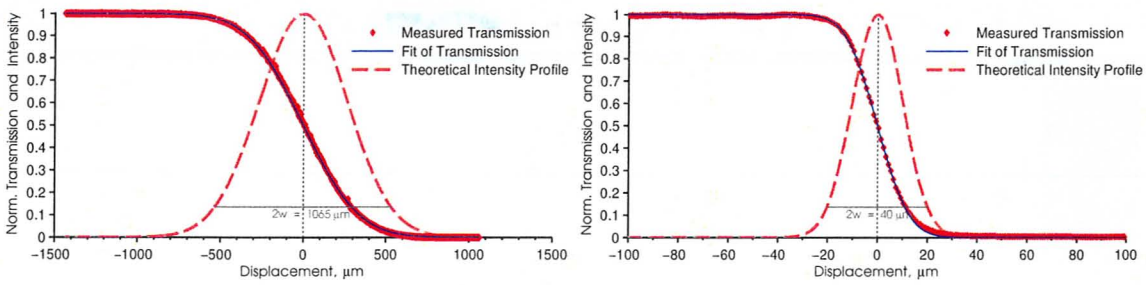

(a) Before Lens (b) After Lens near the focus

Figure 4.7: Knife-edge scans of the beam

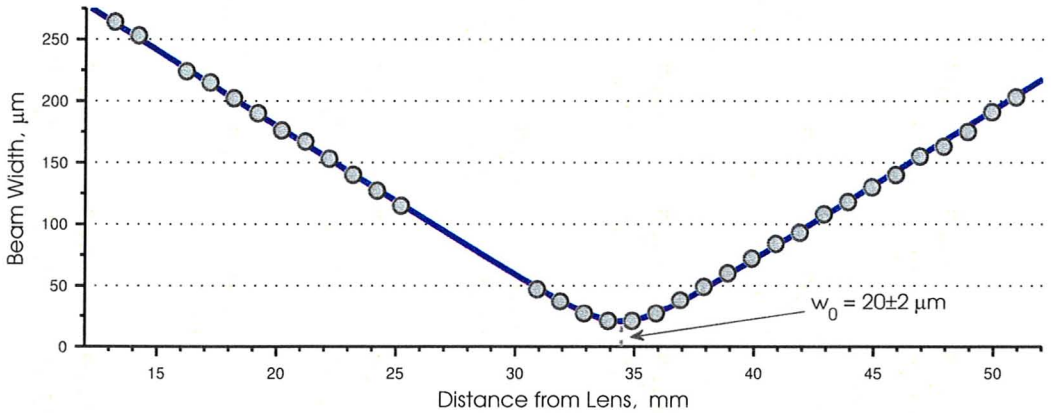

Figure 4.8: Beam width measurements

it. The beam waist size is determined by fitting data with equation (4.4), which determines evolution of beam size with propagation. As result, the focus spot size is found to be $w_0' = 20 \pm 2\,\mu m$. The deviation from theoretical value of 15 µm can be explained by misalignment of the lens and its fabrication tolerance. However, the obtained focus spot is significantly smaller than the width of cantilever (100 µm) justifying the optical design. The position of the beam waist is also determined and used in following experiments.

4.3.3 Position Sensitive Detector (PSD)

A position sensitive detector (PSD) is an optical sensor that measures intensity and position of a light spot on its surface in one or two-dimensions. There are two widely used types of such devices:

Segmented (split) detectors consist of two or four active areas separated by a small gap as shown in Figure 4.9a. When a symmetrical light spot is equally incident on all the halves (quadrants), the device generates equal currents and the spot

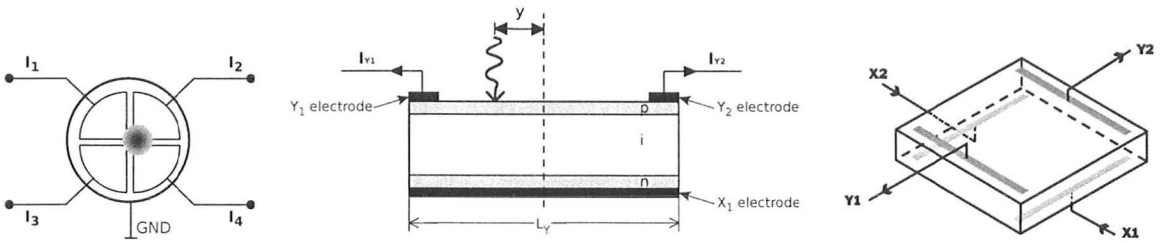

(a) Segmented PSD (b) Lateral effect (c) Duolateral PSD

Figure 4.9: Position Sensitive Detectors

is said to be located on the device's electrical center. As the spot is translated across the active area, the current output for each segment can be used to calculate the position of the spot.
This type of detectors has very high sensitivity and permits measurement of absolute position of a beam due to its intrinsic reference point that is the electrical center. Thus such devices are commonly used in nulling and beam centering applications where the goal is to maintain optical alignment by keeping a balanced or null signal.
On other hand, this design is prone to light distribution variation within the spot giving low performance for non-circular spots or irregular illumination. Moreover such devices are prone to stray light and usually have very limited measurement range that is constrained by the width of the gap and the beam spot size.

Lateral-Effect (continuous) detectors are based on lateral photoelectric effect of p-i-n photodiodes (Figure 4.9b) providing an analog output directly proportional to the position of a light spot on the sensor active area.
An advantage of such devices over split detectors is that accurate position information is obtained independently of intensity profile, symmetry or size of the light spot. Moreover, working area can be significantly increased reaching up to 20 mm and more in each dimension allowing displacement measurements over long ranges with high resolution and outstanding position linearity. The main disadvantage is that continuous detectors do not have any distinctive physical feature that could be a reference point and therefore, they are suitable only for relative measurement of a beam position.

As outlined in Section 4.3, to achieve high sensitivity of cantilever deflection it is desired to have long distance between the cantilever and the PSD. On the other hand, the tightly focused laser light rapidly spreads out after the focus point decreasing resolution capability of the photodetector. Therefore the tracking sensor is required to have large working area, to be insensitive to variation of light intensity in a beam spot

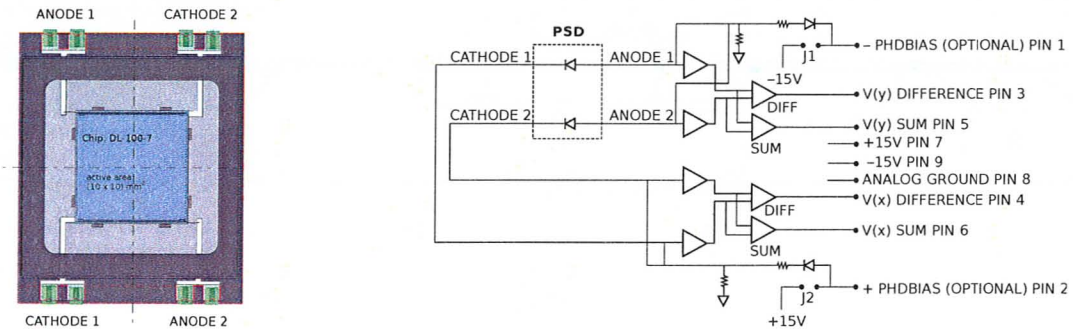

(a) Detector (b) On-board electrical circuit

Figure 4.10: Duolateral two-dimensional PSD from *Pacific Silicon Sensors* [50]

and to be immune to diffraction artifacts. As result, a duolateral two-dimensional PSD (*Pacific Silicon Sensors DL100-7PCBA3*) was selected with square active area of 10 mm × 10 mm (Figure 4.10a).

The sensor consists of n-type silicon substrate with two resistive layers separated by a p-n junction as illustrated in Figures 4.9b and 4.9c. The front side has a p-type resistive layer with two contacts at opposite ends. The back side has an n-type resistive layer with two contacts at opposite ends placed orthogonally to the contacts on the front side. Incident light generates a photocurrent that flows from the incident point through the resistive layers to the electrodes. The resistivity of the doped layers is uniform so the current at each electrode is inversely proportional to the distance between the light spot and electrode due to current division effect:

$$\begin{aligned} I_{Y1} &= \frac{\frac{L_Y}{2}+y}{L_Y} I_0 \,, \\ I_{Y2} &= \frac{\frac{L_Y}{2}-y}{L_Y} I_0 \,, \end{aligned}$$

where I_0 is the total photogenerated current proportional to light intensity and L_Y is the distance between Y electrodes. The currents flowing through the device are seen as two input currents and two output currents. The distribution of the output currents (at top electrodes) relates to the light position in Y dimension, and the distribution of the input currents (at bottom electrodes) relates the position in X dimension. Rearrangement of these equations and the similar equations for X electrodes gives the coordinates of the beam spot measured from the center of the detector

$$x = \frac{L_X}{2} \cdot \frac{I_{X1} - I_{X2}}{I_{X1} + I_{X2}} = \frac{L_X}{2} \cdot \frac{I_X^{diff}}{I_X^{sum}} \,, \tag{4.15}$$

$$y = \frac{L_Y}{2} \cdot \frac{I_{Y1} - I_{Y2}}{I_{Y1} + I_{Y2}} = \frac{L_Y}{2} \cdot \frac{I_Y^{diff}}{I_Y^{sum}} \,. \tag{4.16}$$

As a result, the measured position of the beam is independent of the light intensity. Moreover, due to high linearity of the device, output currents are directly proportional to the position of the "centroid of optical power density". Therefore, the ratios of output signals do not depend on the size of the light spot or on the angle between the surface of the sensor and the incident beam as this factors do not affect relative intensity distribution within the spot. The only effect is the change of resolution and signal-to-noise ratio. Moreover, in contrast to segmented PSDs, the operation of the lateral sensor in relative measurements is not perturbed by stray light as long as ambient light conditions stay unchanged.

The sensor used in the experiments is mounted by the manufacturer on a printed circuit board with built-in transimpedance amplifiers that convert currents into voltages (Figure 4.10b). Therefore, beam tracking is conducted trough measurement of difference and summation voltages:

$$x = \frac{L}{2} \cdot \frac{V_X^{diff}}{V_X^{sum}}, \tag{4.17}$$

$$y = \frac{L}{2} \cdot \frac{V_Y^{diff}}{V_Y^{sum}}. \tag{4.18}$$

At the same time outputs V_X^{sum} and V_Y^{sum} can be used to measure the power of the incident beam. When the centroid of light spot falls on the active area of the sensor, normalized voltage signals can take values only in the range from -1 to $+1$.

4.3.4 PSD calibration

Equations (4.19)–(4.20) could be rewritten in more general form:

$$x = k_x \cdot \frac{V_X^{diff}}{V_X^{sum}} = k_x X^{ratio}, \tag{4.19}$$

$$y = k_y \cdot \frac{V_Y^{diff}}{V_Y^{sum}} = k_y Y^{ratio}, \tag{4.20}$$

where k_x and k_y are scaling factors that define conversion from the normalized output voltages X^{ratio} and Y^{ratio} into real coordinates. Ideally,

$$k_x = k_y = \frac{L}{2} = 5\,\text{mm}. \tag{4.21}$$

Operation of an ideal PSD is described by equations (4.19)–(4.21) but real devices exhibit position non-linearity and intensity dependence. These factors have been investigated in calibration experiments with an optical setup depicted in Figure 4.11.

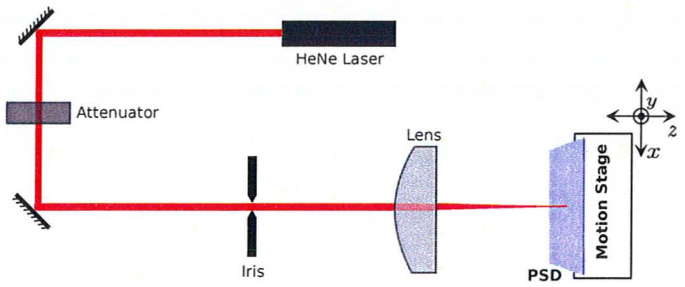

Figure 4.11: Optical setup for PSD calibration

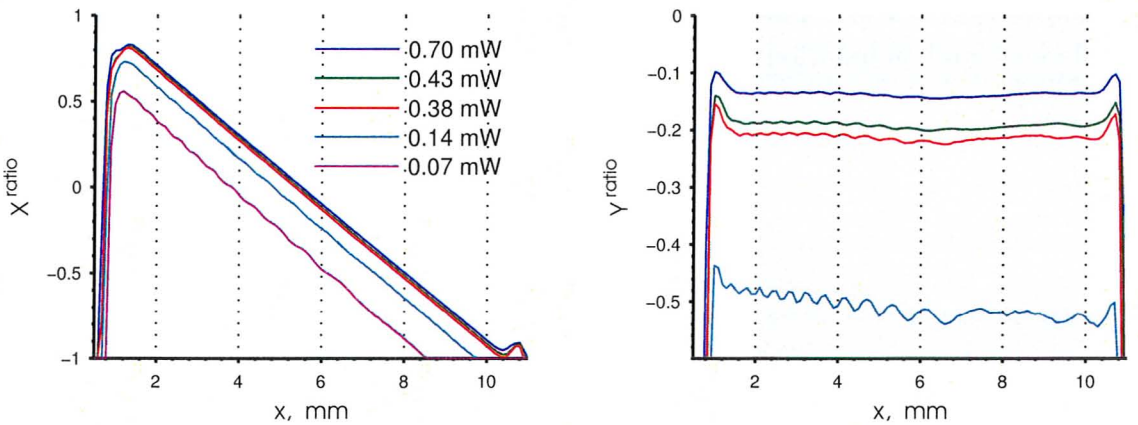

(a) X output (b) Y output

Figure 4.12: Normalized PSD output voltages versus horizontal position x at different power levels. All scans were done at the same vertical position y in the middle of the PSD.

Basically, the laser beam is directed at right angle onto the sensor mounted on the motion stage. The PSD is scanned in X and Y direction in steps of 0.1 mm and 1 mm respectively, covering the whole active area. The beam is defocused to investigate the efficiency of the device to a diverging beam with a substantially large light spot. The distance between the detectors and the lens is manually adjusted with a microshifter. A variable optical attenuator was used to control light intensity and investigate its effect on the operation of the sensor.

Figure 4.12 represents series of X scans across the PSD at varying light power levels. The vertical position is in the middle of PSD The diameter of the beam spot is around 350 µm. Both X^{ratio} and Y^{ratio} have strong dependence on the intensity of light. Below some power level (~ 0.3 mW) the sensor responds in a nonlinear fashion with strong fluctuations and significant decrease in working range. For high enough power, the operation is approximately linear with inverse displacement sensitivity over

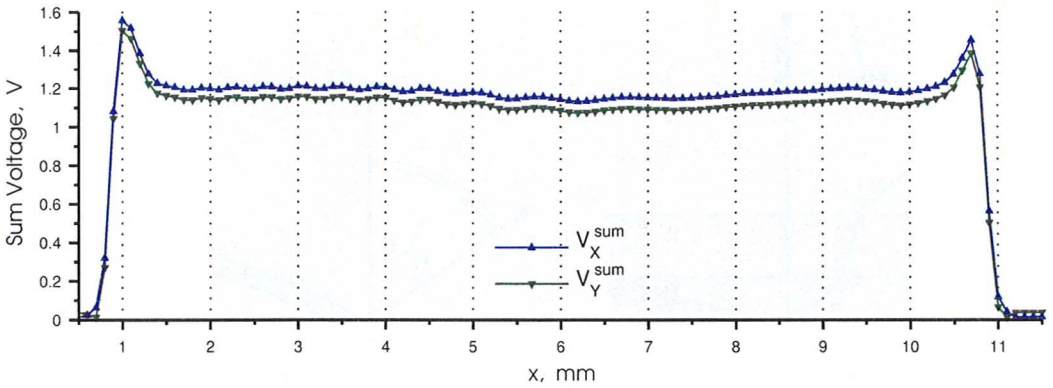

Figure 4.13: Summation PSD output voltages versus horizontal position x at power $P = 0.43\,\text{mW}$. The scan was done in the middle of PSD.

the center area (8 mm) being

$$k_x^{-1} = 0.200 \pm 0.0025\,\text{mm}^{-1}$$

that matches expected value (4.21). The error of $\pm 1.3\%$ is comparable to the specified linearity of 1% of the full scale. As a result, the laser was used at its maximum power to achieve the best possible performance from the detector. There operation of the sensor was limited to 8 mm × 8 mm central area of the device surface to avoid nonlinearities near the edges.

Figure 4.13 shows summation voltages at X and Y channels for X scan taken at light power $P = 0.430\,\text{mW}$. All other conditions are the same as in Figure 4.12. The plot clearly shows moderate voltage offset of 0.06 V between V_X^{sum} and V_Y^{sum}. The variation of voltages is approximately $\pm 2\%$. Therefore, summation outputs can be used for rough indication of light power level.

4.3.5 Optical analysis

The diagram of light propagation in the experimental optical-lever system is illustrated in Figure 4.14. The fluid cell is aligned in such a way that its surface is perpendicular to an incident laser beam thus the light propagates forward without refraction. It should be noted that discontinuities of refractive index at air–glass and glass–liquid interfaces induce the position shift of the focus but do not change the spot size [51]. After loading of a new cantilever chip in the fluid cell, the position of the stage is readjusted to bring the focus on the cantilever's apex as described in Section 4.5.2. Therefore, in the range equal to depth of focus, the beam can be assumed collimated with a plane wavefront. Moreover, due to the width of a cantilever covering area of the focus spot with at least 99% of the beam power, diffraction effects could be neglected.

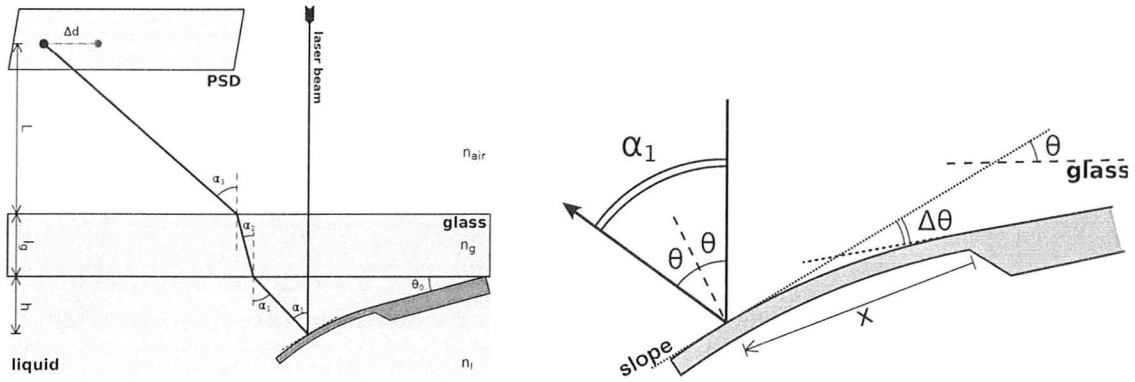

(a) (b)

Figure 4.14: Schematic illustration of the optical system

The following conditions allow the light beam to be treated as bundle of rays with the center ray along the beam axis:

- the PSD is placed in the far-field (far from the waist of the beam), but still in the paraxial region;
- in linear mode of operation, the PSD tracks indeed the centroid of the beam spot on its surface, as result the light distribution in the spot is not significant for position determination.

The following analysis of the optical system is based on principles of geometric optics, validity of which is based on the aforementioned factors.

Due to design of the fluid cell, cantilever chip has fixed tilt angle $\theta_0 = 10° = 0.175\,\text{rad}$.

As shown in Sections 2.2.1 and 2.2.3, a cantilever undergoing bending due to bimetallic effect or surface stress has a circular deflection profile. Let us denote the slope of the cantilever at the center of the Gaussian spot as $\Delta\theta$ and its relative location in respect to the base of the cantilever chip as $a = x/l$ $(0 \leq a \leq 1)$. Thus, the angle between the cantilever surface and the plane perpendicular to Z axis is

$$\theta = \theta_0 + \Delta\theta. \tag{4.22}$$

Here we can assume $\Delta\theta$ as a small quantity ($\theta_0 \gg \Delta\theta$ - small deflection approximation) because in most cantilever sensors deflection is in nanometer range and is much smaller than beam's length. For example, even for 10 K temperature change, deflection angle for the project's cantilevers is estimated to be $\Delta\theta \simeq 0.005\,\text{rad}$, more than an order of magnitude smaller than the tilt angle $\theta_0 = 0.175\,\text{rad}$. As result, the shift of the spot on the cantilever and vertical displacement of the beam can be neglected.

As shown in Figure 4.14b, the beam reflection angle is

$$\alpha_1 = 2\theta.$$

In the glass and air the beam angles with respect to the normal are obtained from Snell's law

$$\sin\alpha_2 = \frac{n_l}{n_g}\sin\alpha_1, \tag{4.23}$$

$$\sin\alpha_3 = n_l \sin\alpha_1, \tag{4.24}$$

where indexes of refraction at 632.8 nm are $n_l = 1.333$ for water and $n_g = 1.515$ for BK7 glass [52], the material of the fluid cell.

The PSD is aligned perpendicular to Z axis. The position of the light spot on its surface is given by the sum of lateral shifts of the optical path in each medium

$$d = L\tan\alpha_3 + l_g\tan\alpha_2 + h\tan\alpha_1 \simeq L\tan\alpha_3 + l_g\tan\alpha_2, \tag{4.25}$$

where $L = 48 \pm 0.5$ mm is distance between the fluid cell and the sensor, $l_g = 5.6$ mm is the thickness of the glass and $h \sim 0.5$ mm is the distance from the cantilever apex to the glass surface. The third term is less than 1% of the sum value, thus the optical path in liquid can be neglected. On the other hand the second term accounts for around 10% of the beam deflection, therefore it should be considered despite common practice in literature to neglect it.

Usually small angle assumption is taken

$$\tan\alpha \approx \sin\alpha \approx \alpha. \tag{4.26}$$

As result

$$\alpha_2 = \frac{n_l}{n_g}\alpha_1, \tag{4.27}$$

$$\alpha_3 = n_l\alpha_1, \tag{4.28}$$

$$d \approx L\alpha_3 + l_g\alpha_2 = \left(L + \frac{l_g}{n_g}\right) n_l\alpha_1. \tag{4.29}$$

The displacement of the beam spot on the PSD Δd due to the deflection $\Delta\theta$ of cantilever is then

$$\Delta d = d\left(\theta = \theta_0 + \Delta\theta\right) - d\left(\theta = \theta_0\right) = 2n_l\Delta\theta\left(L + \frac{l_g}{n_g}\right), \tag{4.30}$$

and the angular sensitivity is

$$S_\theta = \frac{\Delta d}{\Delta\theta} = 2n_l\left(L + \frac{l_g}{n_g}\right). \tag{4.31}$$

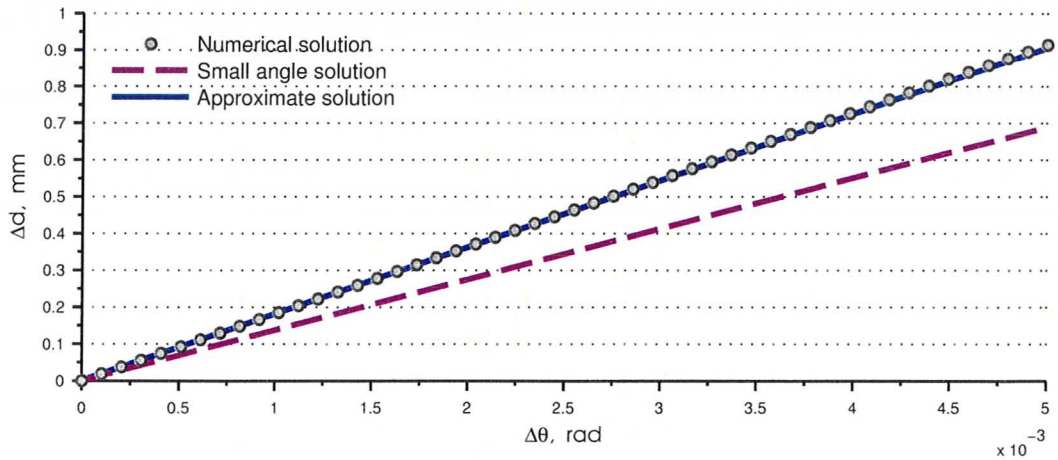

Figure 4.15: Comparison of solutions for the optical-lever system

However comparison (Figure 4.15) between this small angle approximation solution (dashed curve) and numerical solution of equations (4.23)–(4.25) reveals 24% error. The reason for this discrepancy is due to relatively large initial angle making the small angle approximation invalid. For example, deviation between $\tan\alpha_3$ and α_3 is almost 10%.

The exact form of equation (4.25) in terms of reflection angle α_1 is

$$d = L \cdot \mathcal{F}_{n_l}(\alpha_1) + l_g \cdot \mathcal{F}_{\frac{n_l}{n_g}}(\alpha_1), \tag{4.32}$$

where

$$\mathcal{F}_\eta(\alpha) = \tan(\arcsin(\eta \sin\alpha)) = \frac{\eta \sin\alpha}{\sqrt{1-\eta^2\sin^2\alpha}}. \tag{4.33}$$

Taking into account small deflection assumption, we can write equation (4.32) as a first-order Taylor series in the form

$$f(x) = f(x_0) + f'(x_0)(x - x_0) + \cdots$$

As a result, the beam displacement is approximately

$$\Delta d \simeq 2\Delta\theta \left[L \cdot \mathcal{F}'_{n_l}(2\theta_0) + l_g \cdot \mathcal{F}'_{\frac{n_l}{n_g}}(2\theta_0) \right], \tag{4.34}$$

where

$$\mathcal{F}'_\eta(\alpha) = \frac{\partial}{\partial\alpha}\mathcal{F}_\eta(\alpha) = \frac{\eta\cos\alpha}{(1-\eta^2\sin^2\alpha)^{3/2}}. \tag{4.35}$$

Comparison of (4.34) with numerical solution of (4.25) gives error less than 0.5% as illustrated in Figure 4.15. The angular deflection sensitivity is

$$S_\theta = \frac{\Delta d}{\Delta \theta} = 181.2 \frac{\text{mm}}{\text{rad}}. \tag{4.36}$$

As derived in Section 2.2.3, the deflection angle $\Delta\theta(a)$ along the cantilever is related to the displacement of the free end by

$$\delta_{\max} = \frac{l}{2a}\theta,$$

then the displacement sensitivity S_δ is given by

$$S_\delta = \frac{\Delta d}{\Delta \delta_{\max}} = \frac{2a}{l} S_\theta = 725 \cdot a. \tag{4.37}$$

This dimensionless factor determines "amplification" properties of the optical-lever setup to translate nanometer-scale displacements of the cantilever into millimeter-range displacements of the beam spot on the PSD.

In general, due to the tilt an effective length $l_{\text{eff}} = l\cos\theta_0$ should be used instead of the cantilever length l . In our case, this correction is small (1.5%) and is neglected.

The conversion factor to the surface stress is derived with the help of equation (2.16) as

$$S_\sigma = \frac{\Delta d}{\Delta \sigma} = \frac{6(1-\nu)}{Et^2} al\, S_\theta = a \cdot 2.68 \times 10^{-3} \frac{\text{m}^2}{\text{N}}. \tag{4.38}$$

Cantilevers are installed in such a manner that the gold side faces towards the incident light beam. As result, positive values of the deflection signal Δd are related to the gold side bending away. It corresponds either to thermal stress due to temperature increase (gold expansion) or to tension surface stress on the receptor-functionalized silicon side of cantilevers.

In AFM systems, a deflection sensitivity is usually calibrated by pressing a cantilever against a substrate. Then the resulting deflection signal is compared to displacement of a piezo scanner. In contrast, for cantilever sensors there is no robust technique for calibration. The lack of any "standard" that could produce reproducible and accurately measured surface stress is a fundamental limitation of such sensors. The temperature induced stress is a commonly used approach for calibration but its precision is very limited because of dependence on material properties of the cantilever and heat conductance of the system. Another method is to use a fiber-optic interferometer or a confocal microscope to relate output signal with absolute cantilever deflection, however this approach is technically challenging, expensive and time consuming. The simplest method to calibrate the angular sensitivity of the

optical lever system would be to use a custom-built cantilever holder with a few reflective facets at different angles to the incident laser beam forming *in situ* angle references.

4.4 Electronics and software

The 4 voltage outputs of the position sensitive detector are connected through a programmable signal switcher *WaveTek 604* to two digital multimeters *HP 3478A*. The use of the switcher allows to multiplex channels and to measure voltages for both X and Y coordinates sequentially. The overall acquisition rate is 2 dual-axis measurements per second. Such configuration gives an ability to use limited number of high resolution multimeters with 5 digits precision that is essential for accurate beam tracking.

All measurement equipment, the switcher and the motion controller *Newport ESP300* are computer controlled via the standard industrial bus *IEEE-488 (GPIB)*. Data acquisition and positioning of the motion stage are computer controlled using *LabVIEW*. The following data analysis is conducted in *MATLAB*. Due to high interactiveness of data interpretation process, a few dedicated GUI programs have been developed in *MATLAB*.

The experimental workflow consists of two major types of measurements:

1. Two-dimensional scanning (*profiling*) of a cantilever chip surface (see Section 4.5.1). A program developed in *LabVIEW*, so-called a virtual instrument (VI), controls translation of the motion stage with the fixed sensor chip in two directions, X and Y, simultaneously acquiring information from the PSD. The obtained data are then analysed in a *MATLAB* program (illustrated in Figure 4.16) to determine the apex of the cantilever and its relative position a.

2. In deflection experiments, a *LabVIEW* program acquires the voltage signals from the PSD and writes the data in a file. The following timeseries and statistical analyses are performed in a dedicated *MATLAB* program (illustrated in Figure 4.17).

4.5 Experiments

All experiments described in this section and the following chapters were conducted either in deionized water or in glucose solutions. All solutions were prepared in pure water without any salts to avoid salt deposits in the fluid cell and to eliminate dependence of results on ionic strength of the medium. In this respect, most molecular interactions are the strongest at zero ionic strength. Except for short infusions of

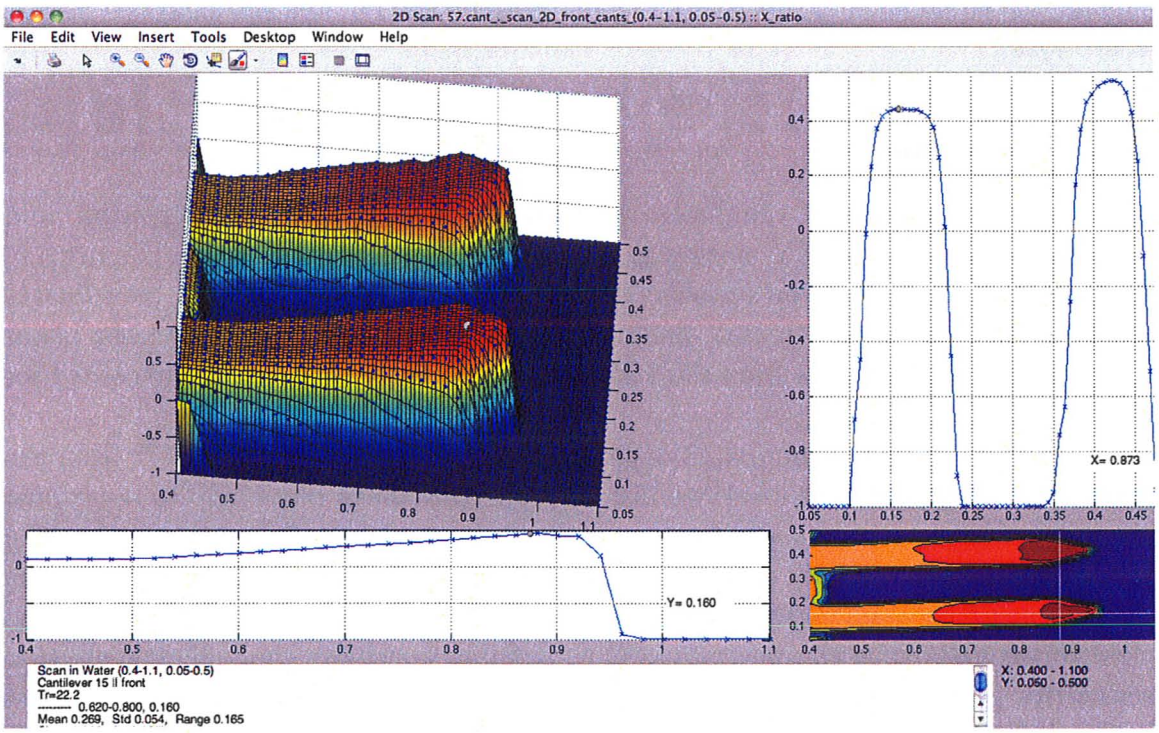

Figure 4.16: MATLAB program for analysis of 2D scans

Figure 4.17: MATLAB program for timeseries analysis of deflection data

liquids, the tubes were clamped and the liquid inside the FC was stationary — "static conditions".

4.5.1 2D scanning

The large working area of the duolateral PSD (at least 8 mm in each direction) and computer control of the XY motion stage allow to use the optical setup (Figure 4.5) for *profiling* of a cantilever surface. A dedicated *LabVIEW* program coordinates movement of the mount in two directions scanning the surface by the laser beam. The voltage measurements from the PSD are acquired at each point and recorded for further analysis.

As an example, Figure 4.18 depicts normalized voltage signal X^{ratio} from the PSD obtained at different locations during a 2D scan. Such plots help to determine the apex of the cantilevers and the best position for focusing of the laser beam. The relative location of the light spot on the cantilever is denoted as $a = x/l$, where x is the distance from the base of the cantilever chip. In general, it is preferable to focus as close to the end of the cantilever ($a = 1$) as possible to achieve the highest deflection sensitivity. However, due to the finite size of the light beam the range of a is limited by $a = 0.9$. Higher values lead to losses of the reflected beam intensity and diffraction artifacts. In the case illustrated in Figure 4.18, the beam was focused at $a = 0.88$. The uncertainty of a determination is about 4%, limited by the focus spot width ($w_0 \approx 20\,\mu m$).

It should be noted, that plots such as in Figure 4.18 does not depict the real profile of the surface. Instead, they illustrate slope at different locations of the surface, because optical lever technique does not directly measure displacements, but angles. However, the profile (in units of length) may be obtained by integration of the slope function.

4.5.2 Knife edge measurements *in situ*

As it has been mentioned in Section 4.3.4, the PSD may be used for coarse estimation of light intensity. Therefore, the optical lever setup has been applied for knife edge measurements similar to experiments in Section 4.3.2 using either an edge of a sensor chip or a cantilever itself as "knife-edge". In the latter case, summation voltage V_X^{sum} or V_Y^{sum} from the photodetector is recorded as the cantilever is moved along the direction parallel to the width of the cantilever. Then the data are fitted with the transmission function from equation (4.14). Figure 4.19 illustrates results of such an experiment. It should be noted that calculated width of the beam spot can be used only for estimation. The inaccuracy results from nonlinearity of the PSD, stray light reflections inside the fluid cell and diffraction at the cantilever edge that leads to significant beam divergence and incomplete light capture by the detector. However, it

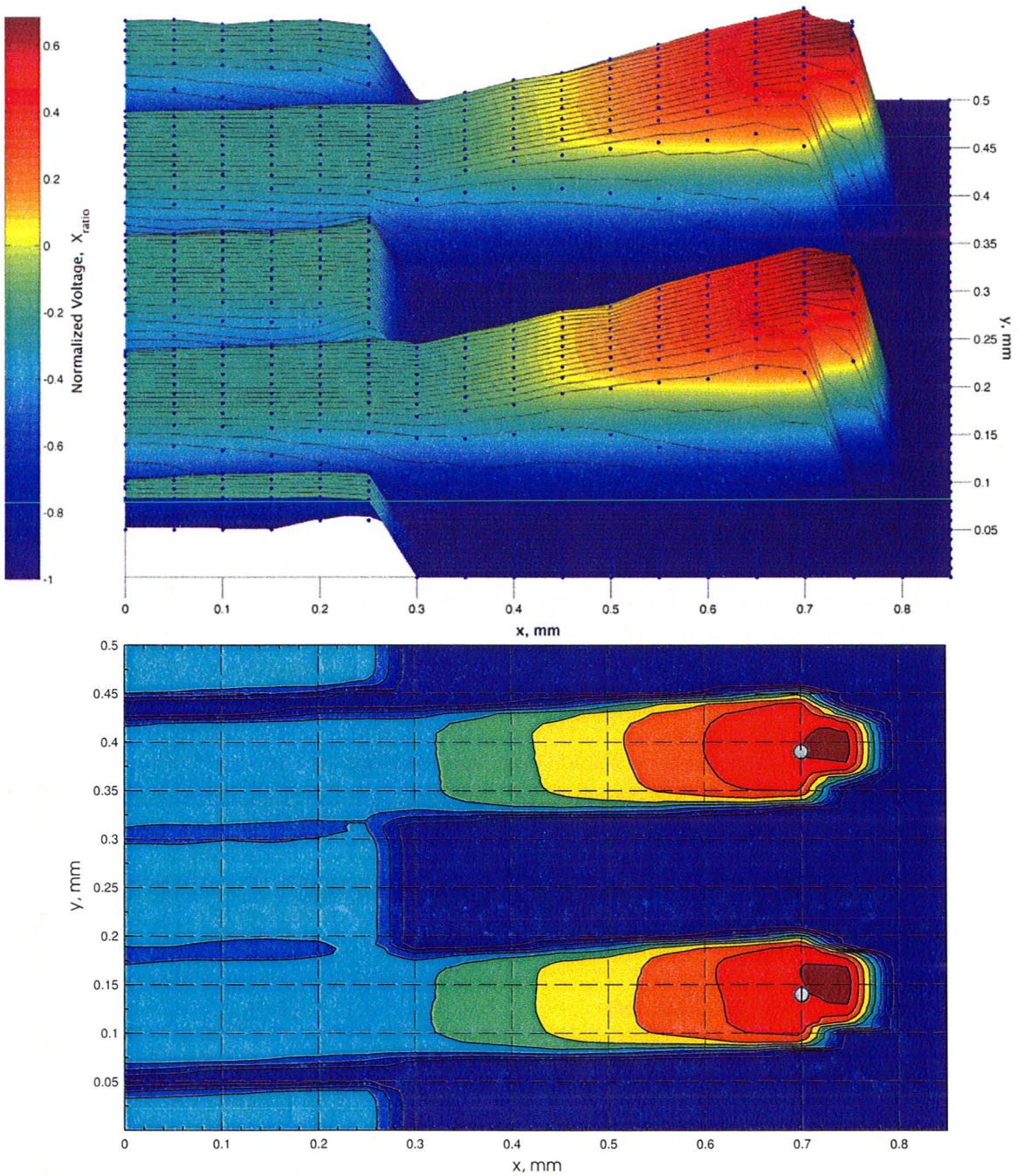

Figure 4.18: Surface and contour plots of laser beam displacement signal X^{ratio} from the PSD obtained during a 2D scan of a cantilever chip. The plots depict surface slope variation at different points. The positions of the focus spots are marked, $a = 0.88$.

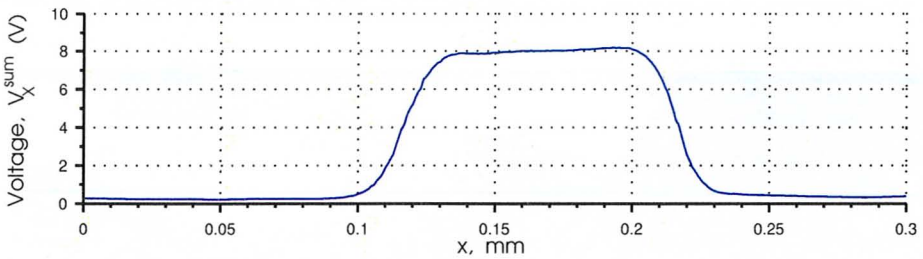

(a) Summation voltage V_X^{sum} from the PSD

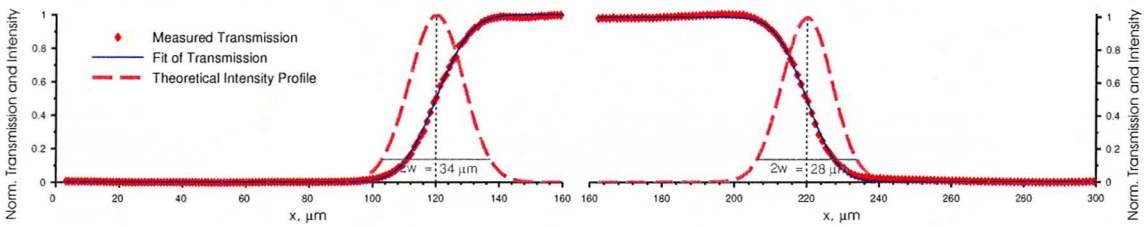

(b) Results of fitting the transmission function (4.14)

Figure 4.19: Knife-edge measurement *in situ* across a cantilever

could be certainly concluded from Figure 4.19a, that the beam spot is considerably smaller than the width of the cantilever.

Knife edge experiments *in situ* — using the optical setup designed for deflection measurements — have twofold benefit:

- After installation of a new sensor chip, estimations of the size of the beam spot on the cantilever surface can be used to determine if the cantilever is in focus. As needed, re-adjustments could be made to bring it in focus.
- The edges of the cantilever and the sensor chip could be precisely located for proper focus placement.

4.5.3 Noise and resolution

Noise in normalized voltage X^{ratio} signal from the PSD was determined by focusing the laser beam on a cantilever chip body and recording the signal for an extended period of time (Figure 4.20). The scale of the plot is chosen to be comparable to a deflection signal for 1 K temperature rise (see Section 4.5.4). As it can be seen, substantial noise is present with rather frequent outliers and standard deviation of about 0.001. It should be noted that noise distribution is not normal and its kurtosis is large (10 – 15).

Noisiness of the detector defines the ultimate limit on resolution and detection limit of the experimental setup. To achieve satisfactory results, time-averaging of the acquired deflection signal is required. Using averaging over 5 min, the 95%

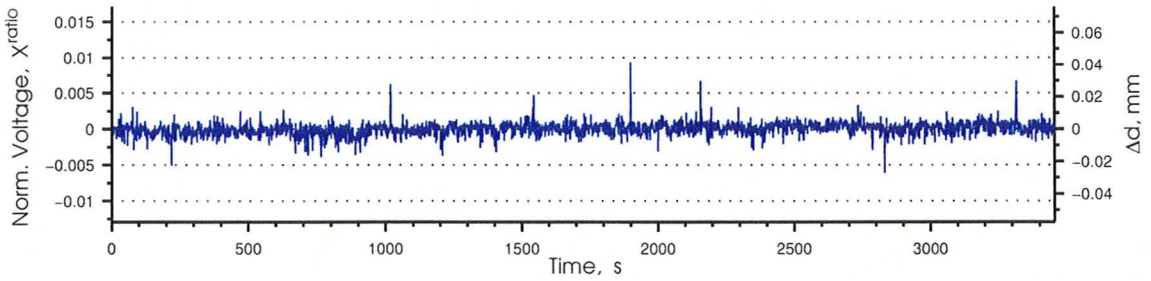

Figure 4.20: Noise evaluation in the PSD signal X^{ratio} measured at the cantilever base for 1 hour.

bootstrap confidence interval of the normalized voltage measurements was estimated to be ± 0.0001, corresponding to PSD tracking resolution of 1 μm. It corresponds to cantilever deflection resolution of approximately 1.5 nm.

4.5.4 Temperature sensitivity

The top side of the silicon cantilevers is coated with gold, as result the cantilevers are very sensitive to temperature changes due to bimetallic effect.

Figure 4.21 illustrates deflection of a cantilever in water subject to different temperature setpoints 1 K apart defined by the temperature controller. The thermal sensitivity was measured to be 209 nm/K. However, the theoretical deflection for the bimorph beam was calculated to be 127 nm/K. The discrepancy could be explained by manufacturing tolerances, particularly large for the value of cantilever thickness. Indeed, the vendor claims nominal thickness of the cantilever substrate to be 1 μm with tolerance range of $0.5 - 2.5$ μm. Hence, the real thermal sensitivity may lie anywhere in the range of $21 - 490$ nm/K. Unfortunately, precise measurement of cantilever thickness using even high-resolution SEM is challenging and calibration of cantilever properties is complicated by extreme fragility of the probes.

Figure 4.22 demonstrates deflection response of the same cantilever as in Figures 4.21 subject to two cycles of 1 K temperature rises and drops in water. The signs of poor reversibility are noticeable, because despite the return of the temperature to the original level, the deflection does not reach the original values.

The time required to obtain moderately stable deflection level in response to 1 K temperature increase is around 3 – 4 min. For 1 K temperature drop, stabilization time is 5 – 6 min.

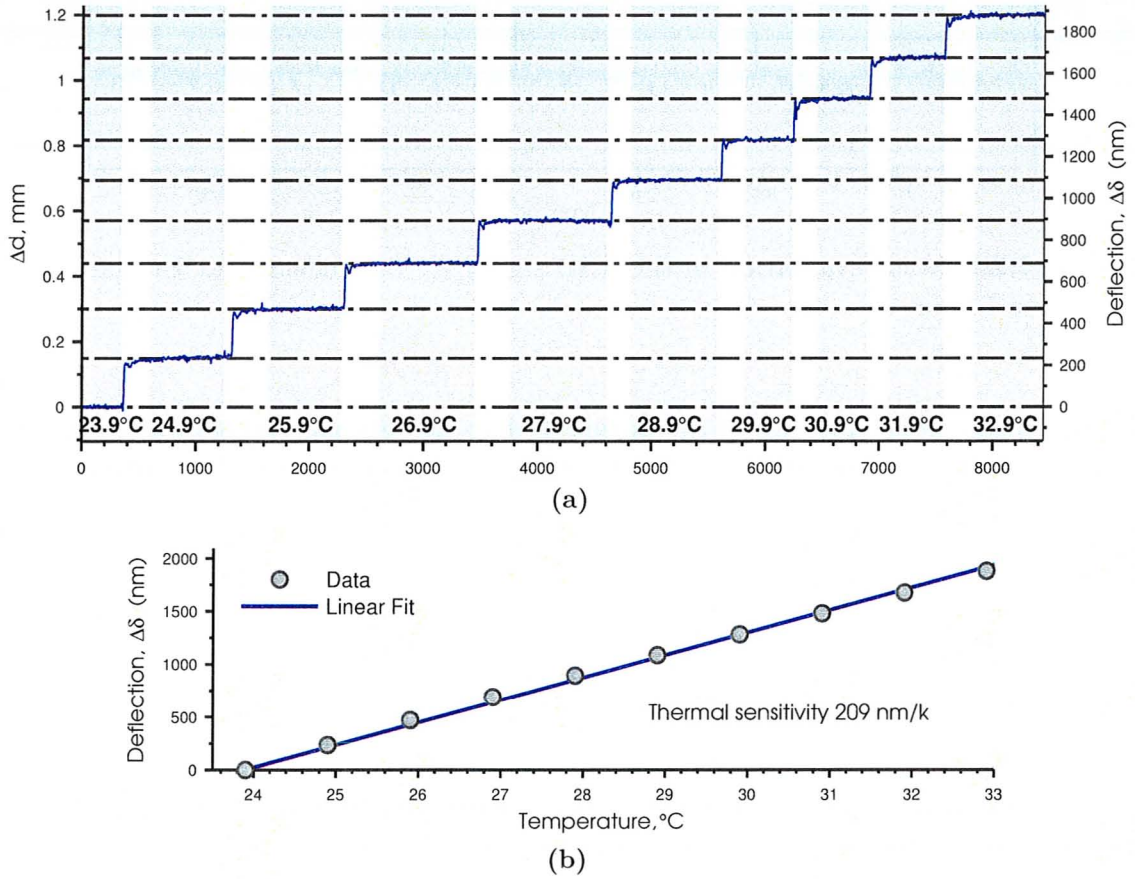

Figure 4.21: Cantilever deflection response to temperature

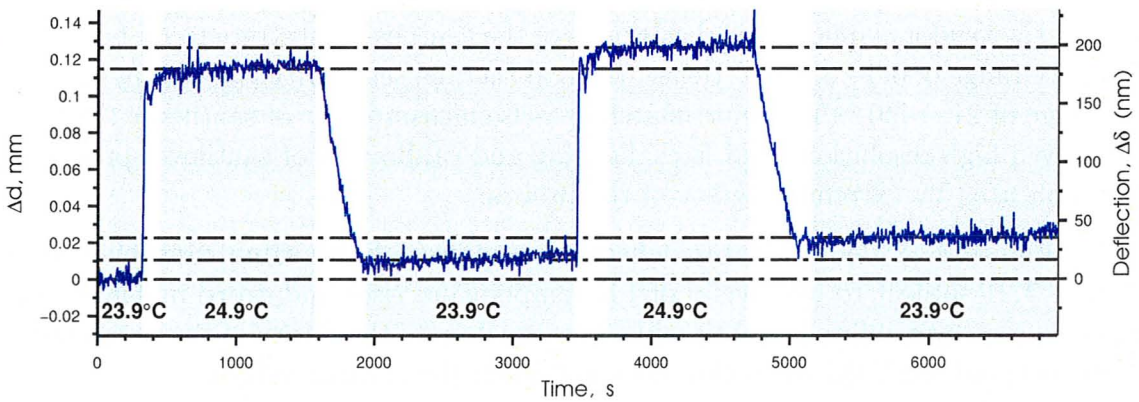

Figure 4.22: Cantilever deflection response to temperature cycles

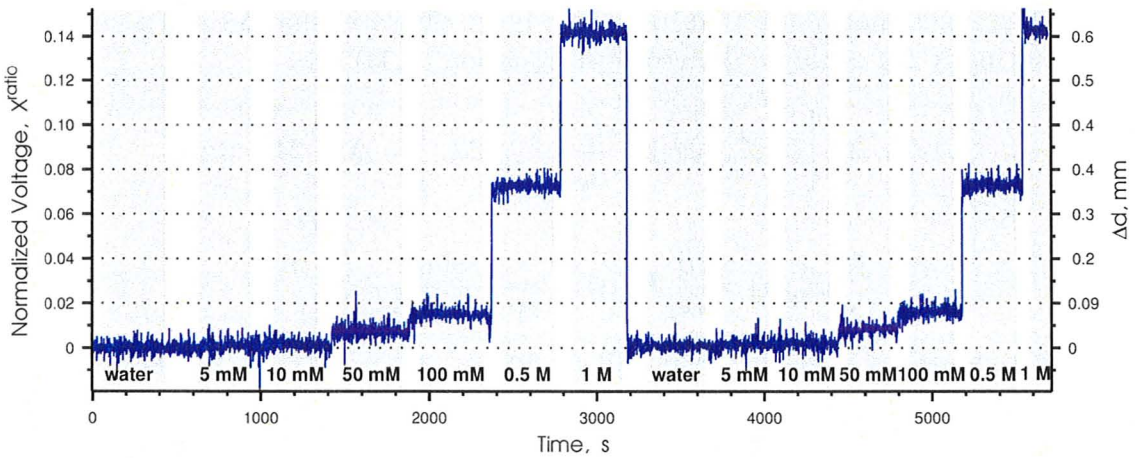

(a)

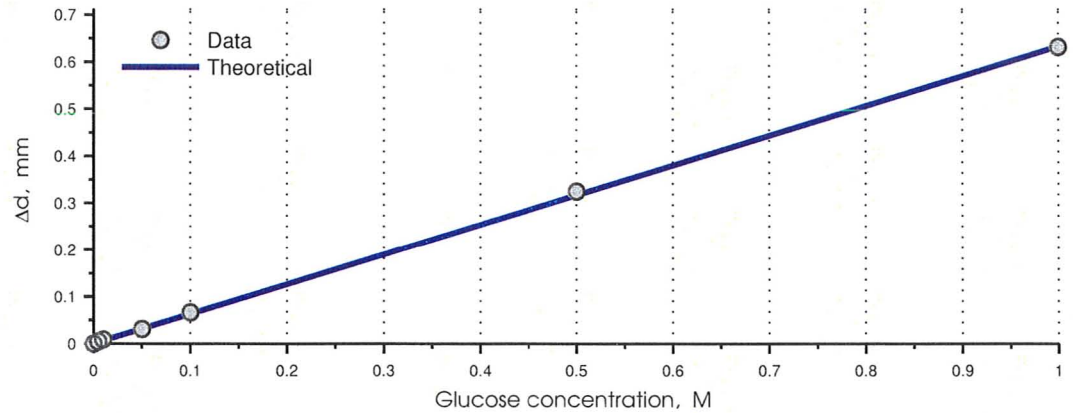

(b)

Figure 4.23: Calibration of response to refraction index variations of glucose solutions (measured at the base of a cantilever chip)

4.5.5 Refraction index variation

Glucose concentration affects refractive index of the aqueous solution. For relatively small concentrations, the dependence is linear and may be related by [52]:

$$\Delta n = 0.0254\,[\text{Glucose}] \tag{4.39}$$

where [Glucose] denotes glucose concentration in moles per liter (M).

These variations of the refractive index can have profound effects on the optical lever setup. For example, in 100 mM glucose solution the index of refraction is increased by $\Delta n = 0.0025$ comparing to pure water. This would result in displacement signal of 67 µm corresponding to apparent deflection of about 105 nm.

The functional connection between a beam displacement Δd and a change of refractive index Δn could be derived from equation (4.32) as:

$$\Delta d \simeq \Delta n \left[L \cdot \widetilde{\mathcal{F}}_{n_l}(2\theta_0) + \frac{l_g}{n_g} \cdot \widetilde{\mathcal{F}}_{\frac{n_l}{n_g}}(2\theta_0) \right] = \Delta n \cdot 24.7\,\text{mm}, \tag{4.40}$$

where

$$\widetilde{\mathcal{F}}_{\eta}(\alpha) = \frac{\partial}{\partial \eta}\mathcal{F}_{\eta}(\alpha) = \frac{\sin\alpha}{\left(1 - \eta^2 \sin^2\alpha\right)^{3/2}}.$$

Combining equations (4.39) and (4.40) we obtain relationship between the beam displacement and glucose concentration

$$\Delta d \simeq [\text{Glucose}] \cdot 0.628\,\tfrac{\text{mm}}{\text{M}}. \tag{4.41}$$

The influence of glucose concentration on the displacement signal was determined experimentally by filling the fluid cell with solutions of glucose at different concentrations: 5 mM, 10 mM, 50 mM, 100 mM, 0.5 M, 1 M. The laser beam was focused on the stationary part (base) of a cantilever chip and the displacement Δd of the reflected beam was measured by the PSD (Figure 4.23a). The difference between the experimental data and the theoretical prediction given by equation (4.41) is around 3% as illustrated in Figure 4.23b.

In the following experiments with glucose solutions, the deflection results were compensated by subtracting the correction factor determined using equation (4.41).

4.5.6 Drift analysis

Drift has been identified as a major problem in the cantilever deflection experiments. Figure 4.24 illustrates an observed drift pattern for a cantilever immersed in water. The occurrence and strength of the phenomenon seem unpredictable. Drift rate can be as high as 250 nm/h. In some cases, deflection signal is stable up to 3 hours but sometimes it is impossible to achieve a moderately stable level at all. The cause of the problem has not been identified yet. However, the drift cannot be explained by temperature instability, because the closed-loop temperature control system has resolution of 0.1 K that may lead only to deflection fluctuations less than 20 nm.

Drift is a commonly observed issue with cantilever sensing of surface stress [53–56]. There are a few typical approaches to deal with this issue that can be pointed out:

- A cantilever is equilibrated in solution for a long time (from a few hours to up to a couple of days) in the hope that the system would eventually reach the equilibrium state [53, 55]. Unfortunately, it has been impossible to conduct experiment for longer than 5 hours, because of gradual air bubble formation in

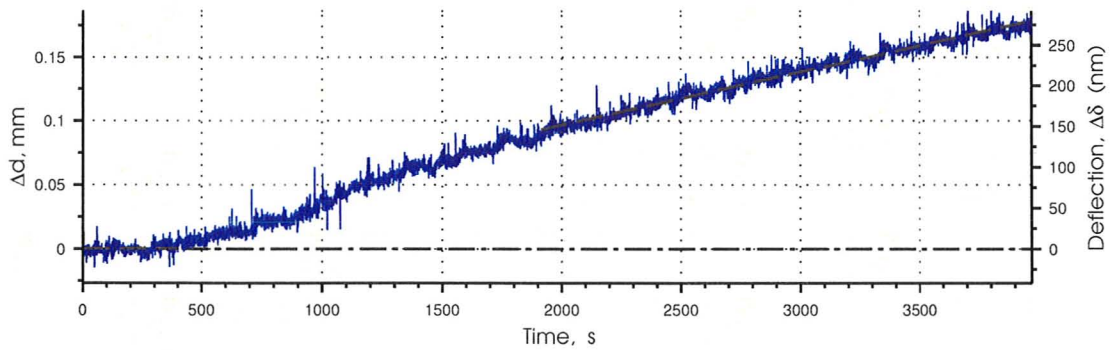

Figure 4.24: Time-stability experiment demonstrating drift of cantilever deflection signal with rate of 250 $^{nm}/_{h}$

the fluid cell. Despite degassing of liquids by ultrasonication, clamping the tubes and greasing the joints and the FC, this problem has not been resolved.

- Drift trend is determined and subtracted from data [53, 54]. Practically, drift slope is not constant over time and usually changes after liquid infusions.

- The most preferable approach is to use at least two identical cantilevers, where one of them — working — has a coating sensitive to the target, while the second one — reference — is either bare or passivated and is not specifically sensitive [32]. As result, the differential deflection signal should be more immune to drift artifacts. This method requires more sophisticated read-out setup to simultaneously detect deflection of several beams. In addition, completely independent functionalization of cantilevers on the same chip is still a great challenge. Moreover, it has been reported that even a differential signal for identical cantilevers can drift in unpredictable manner.

As result of drift issues, duration of experiments was very limited and the true equilibrium values of cantilever deflection were not possible to measure. Therefore, the experimental strategy was to do each measurement for some period of time, usually for 30 min, and afterwards to replace the solution for the next measurement. In most cases, repeatability was poor and it was impossible to collect measurement statistics to make definitive conclusions.

4.5.7 Cantilever deflection in response to solution exchange

Replacement of measurement solution in the fluid cell was performed manually by means of a syringe connected through silicone tubing to the FC. The total volume of the FC and the tubing is approximately 1.5 ml, therefore an injection volume was set to 5 ml to ensure complete solution replacement.

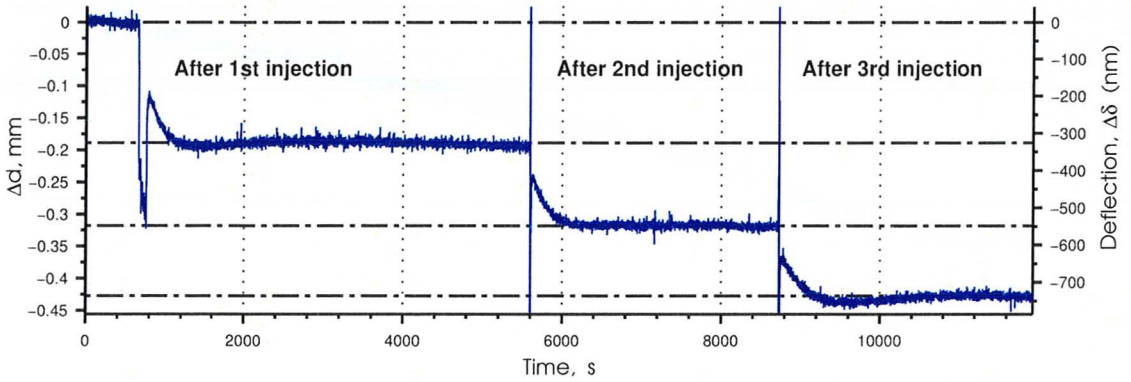

Figure 4.25: Cantilever deflection in response to a series of water injections. The original solution is pure water and the temperature is kept constant at 27.0°C.

Figure 4.25 shows the general deflection pattern in response to a solution injection. In this particular case, the fluid cell was originally filled with pure water and at some moment 5 ml of pure water was pumped through the system. Because the temperature of the mount is always set somewhat higher than the room temperature, there is an initial downward deflection. When the temperature stabilizes, the deflection increases but does not attain the original level. In Figure 4.25 the difference is $200 - 300$ nm. This phenomenon significantly compromises reliability and repeatability of measurements of cantilever response to glucose solutions. Therefore, before the start of glucose infusions, the system was subjected to a few injections of pure water to establish deflection pattern and determine a correction factor for subsequent measurements in glucose solutions. At the end, the system was washed with pure water again.

4.5.8 Conclusion

Time-stability experiments reveal serious drift and repeatability problems that make reliable measurements of surface stress very difficult to achieve. The use of measurement scheme with a reference cantilever and redesign of the fluid cell seem necessary.

Temperature cycling and solution exchange experiments demonstrate that a deflection signal does not reach the original level after a perturbation. Surprisingly, despite "static" conditions (tight temperature controll and no steady flow of the fluid) cantilevers seem to be not in equilibrium state. In this respect, a commonly used *continuous flow-through* experimental configuration, when a liquid is constantly circulated through the system at a low flow rate, may be beneficial [56]. The state of such as system is determined by the external influence, and as result may exhibit more stable behavior.

5 Sensor based on Glucose Oxidase

5.1 Overview

Glucose oxidase (β-D-glucose:oxygen 1-oxidoreductase; Enzyme Commision (EC) Number 1.1.3.4) is an enzyme isolated from a range of different fungal organisms, mainly from the genus *Aspergillus* and *Penicillium*, of which *A. niger* is the most commonly utilized for the commercial production of the enzyme. It catalyzes the oxidation of β-D-glucose at C1 position to D-glucono-δ-lactone, by utilizing molecular oxygen as an electron acceptor with simultaneous production of hydrogen peroxide:

$$\beta\text{-D-glucose} + O_2 + H_2O \xrightarrow{\text{GOx}} \text{D-glucono-1,5-lactone} + H_2O_2 \quad + 19\,{}^{\text{kcal}}/_{\text{mol}}$$

Glucose oxidase (GOx) is highly specific for the β-anomer of D-glucose, while the activity to α-anomer and other carbohydrates is significantly smaller. For example, the β-anomer reacts about 150 times as fast (at 20°C) as the α-anomer of D-glucose [3]. The optimum pH range for GOx from the commonly used source *A. niger* is 3.5 – 6.5, while at neutral pH 7.0 the activity is only 60% of the maximum. The Michaelis constant K_M is 33 mM (GOx from *A. niger*) [5] that is appropriate for glucose sensing in the physiological range.

Due to its remarkable selectivity for glucose, stability and high activity over wide range of temperatures and pH, glucose oxidase is the most commercially successful analytical reagent for the determination of glucose. Its application in conventional glucose meters based on electrochemical transduction is reviewed in Section 1.5.2, whereas this chapter describes the use of GOx with static cantilever sensors.

Microcantilever sensors coated with proteins have been described by a number of researchers. For example, a very sensitive detector for Ca^{2+} ions with the detection limit of 10^{-7} M was created by immobilization of Calmodulin (CaM) [57]. Upon binding of Ca^{2+} to CaM, the protein undergoes large conformational changes and becomes more elongated. This consequently leads to compressive surface stress on the order of $0.1\,{}^{\text{N}}/_{\text{m}}$ and cantilever deflection. This experiment suggested that the conformational changes of proteins might be used to develop highly sensitive cantilever biosensors for use in label-free, protein-analyte screening applications.

Ligand-induced reversible conformational transformations are essential for function of most proteins. For example, biological receptors like CaM or GGBP mediate signaling processes through conformational changes and consequent interactions with their protein targets, thereby affecting many different cellular functions. In similar

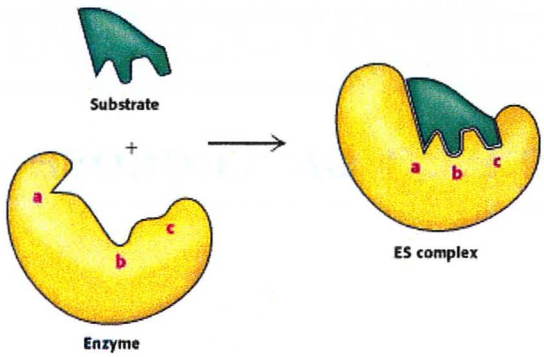

Figure 5.1: Induced fit model of enzyme-substrate binding [58]

fashion, mechanism of the enzyme-substrate interaction is described by *induced fit* model (Figure 5.1). According to this model, the initial interaction between enzyme and substrate is relatively weak, but this weak interaction rapidly induces conformational changes in the enzyme making the shape of the active site complementary to the substrate and strengthening the binding [3]. It is expected that these enzyme conformational changes can result in a surface stress change that can be detected from the consequent bending response of the cantilever.

This idea has been applied by two research groups to create glucose cantilever sensors based on glucose oxidase [54–56, 59, 60]. For instance, Subramanian *et al.* [54] observed deflection of 4 nm at 30 mM glucose using 100 μm long silicon V-cantilevers. At the same time, response to mannose was much smaller. It was determined that the cantilever deflection was not due to thermal energy released in the enzyme-catalyzed reaction.

Pei *et al.* [55] reported deflections on the order of 250 nm for 20 mM glucose solutions using 350 μm long soft silicon cantilevers. The bending was towards GOx-treated side corresponding to tension surface stress, and the magnitude of the deflection was dependent on glucose concentration over a large range (0.2 – 20 mM). Control experiments with fructose and mannose showed no response.

Both Subramanian *et al.* [54] and Pei *et al.* [55] immobilized glucose oxidase by glutaraldehyde cross-linking. The repeatability and stability of such a coating is very questionable because glutaraldehyde is known to self-polymerize and to form a rather labile linkage. It is also doubtful that the coating was formed on only one cantilever side (gold).

In contrast, Yan *et al.* [56, 59, 60] used a novel deposition approach, layer-by-layer nanoassembly, which allows formation of nanometer-scale organized films on any surface through alternate adsorption of oppositely charged components, such as polyions (charged polymers) and enzymes. In this case, glucose oxidase was trapped inside a multilayer structure with total thickness of 30 nm. Yan *et al.* [56] observed cantilever bending proportional to the concentrations of glucose with surface stress

of approximately 0.05 $^{N}/_{m}$ for 10 mM glucose concentration. In contrast to the other reports, the surface stress was compressive. The kinetic and thermodynamic analysis showed that the conformational changes in GOx and probably reduction of pH due to gluconic acid production were the origin of the cantilever deflection. Interestingly, the bending responses were similar in the presence or absence of oxygen. In addition, the sensors were tested with L-glucose that is known to complex with glucose oxidase, but without being oxidized. As expected, the cantilevers responded to L-glucose. However, the bending profiles were different in response to L- or D-glucose, indicating that the bending response to D-glucose was not purely conformational, but also involved some other mechanism.

The surface modification method proposed by Yan *et al.* [56, 59, 60] seems to be complicated and time-consuming. Moreover, this technique produces a multilayer coating held together by ionic forces, as result its stability in physiological liquids with ionic strength of 0.15 M is questionable. In addition, the reported deflection response to glucose is rather moderate.

In this thesis, another method of glucose oxidase immobilization on cantilevers is proposed. In contrast to the reviewed reports, it results in an enzyme monolayer covalently attached to the silicon surface of cantilevers. In addition, it has been applied to immobilization of other types of glucose receptors (see Chapters 6 and 7).

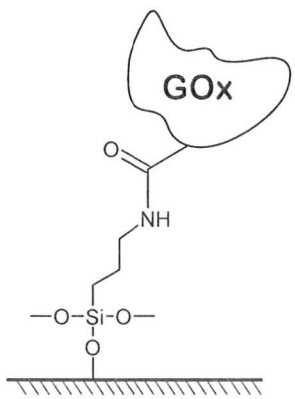

Figure 5.2: Schematic illustration of immobilized glucose oxidase

5.2 Sensor fabrication

Lyophilized powder of Glucose Oxidase (Type X-S, purified from *Aspergillus niger*, 75% purity, 153100 units/g) was purchased from Sigma-Aldrich. The immobilization procedure is described in Chapter 3. The concentration of GOx in the immobilization solution at the final step was 2 mg/ml.

The structure of the immobilized recognition layer is schematically illustrated in Figure 5.2.

5.3 Experimental results

The maximum attained deflection in a 30 min time span was approximately 130 nm. Figure 5.3 demonstrates the best obtained result. In all cases, the direction of the bending corresponded to tensile surface stress. Due to poor experimental repeatability it was impossible to determine the functional dependency of cantilever deflection on glucose concentration and its parameters.

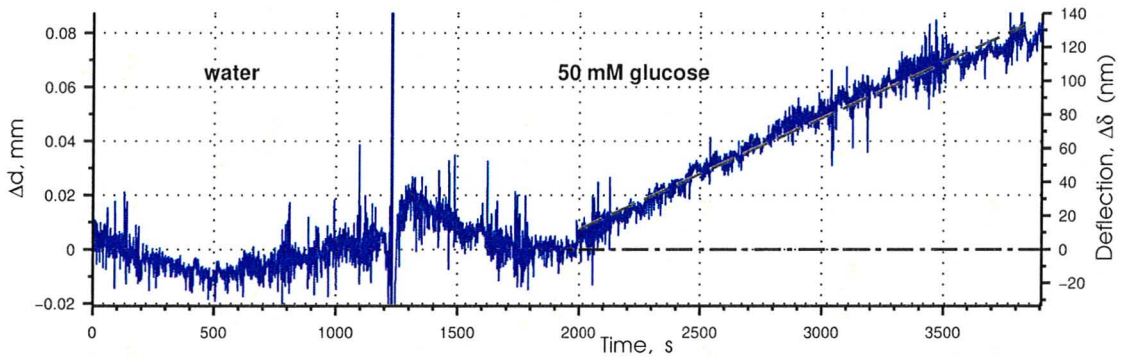

Figure 5.3: Deflection response of GOx sensor to 50 mM glucose solution. The deflection is approximately 130 nm (30 min after glucose injection).

5.4 Discussion

Saturation of cantilever deflection at glucose concentration of 50 mM corresponds quite well with the Michaelis constant of glucose oxidase (33 mM). Another factor may be a limited quantity of available oxygen in the medium that limits reaction rate.

The magnitude and direction of observed cantilever deflection are comparable to values reported in literature [55].

6 Sensor based on aminophenilboronic acid

6.1 Overview

Boronic acids are well known for their unique feature — to form reversible covalent complexes with 1,2- and 1,3-diols (chemical compounds containing two hydroxyl groups). Resulting cyclic boronic esters are stable enough to be even isolated. At the same time, in aqueous solutions boronic acids exist in equilibrium between a neutral form (**1**, Figure 6.1) and a negatively charged form as boronate anions (**2**). Both forms are able to complex with diols, however, boronates typically form more stable esters (**4**) and exhibit much faster kinetics. As result, upon addition of a diol (such as a carbohydrate) in aqueous solution of boronic acid, the chemical equilibrium shifts towards its charged form (**4**) and pH drops by 1 – 3 units — the solution becomes more acidic. For example, the pK_a of phenylboronic acid is ~9, but the phenylboronate esters have pK_a 5 – 7 under the same conditions. It makes the basis of pH — depression method — an analytical technique for investigation of boronic acid–diol interactions. Boronate compounds, immobilized on solid support, have formed the basis of a new field of chromatographic techniques designated for analysis and separation of sugars and glycated proteins, commonly named boronate affinity chromatography.

Figure 6.1 illustrates concurrent processes of ester formation and acid ionization. Because boronic acids and their esters can co-exist in two different ionization states, there are two binding constants: $K_{\mathrm{eq-trig}}$ for the formation of the diol–boronic acid complex (**3**) and $K_{\mathrm{eq-tet}}$ for the formation of the diol–boronate complex (**4**). However, for the purpose of sensor design, the overall binding constant K_{eq} is more suitable (Figure 6.2). Its value depends on pH and composition of a measurement medium.

Similar to other saccharides, hydroxyl groups of glucose molecule are able to reversibly condense with boronic acid, showing potential for the development of a glucose sensor. However, boronic acid–diol complex formation is heavily pH dependent and occurs preferentially when boron is present as the boronate anion. For instance, rate and stability constants increase by around four and five orders of magnitude, respectively, at pHs above the pK_a of the boronic acid. Unfortunately, most boronic acids have relatively high pK_a (in a range from 8 to 10), as result in neutral solutions (pH 7) they are mostly present in the neutral form. Consequently, sensitivity of such sensors under physiological conditions is rather low. There have been extensive

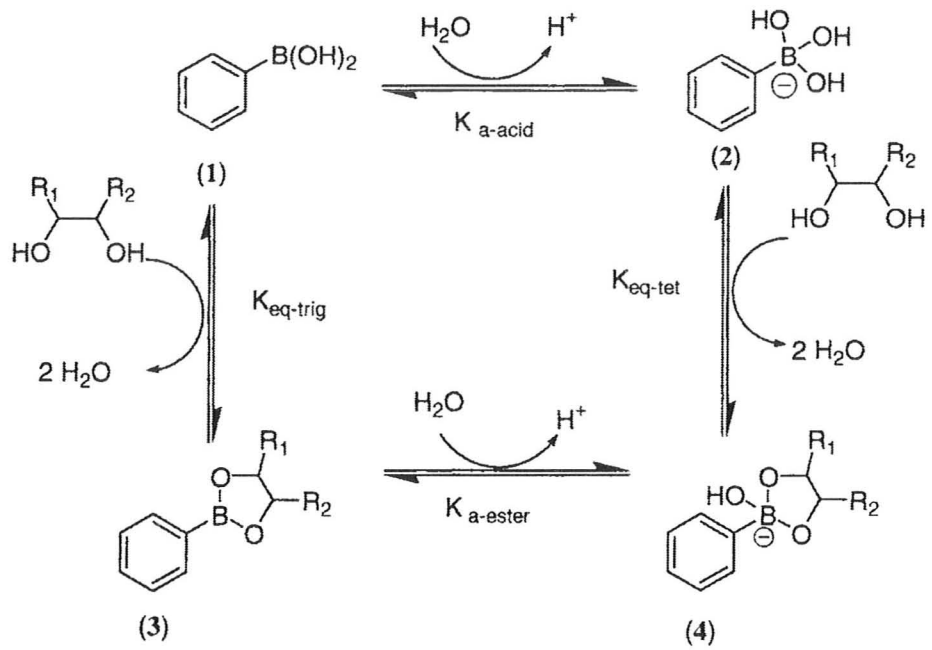

Figure 6.1: Binding process between (phenyl)boronic acid and a diol [61]. It shows the equilibrium between (**1**) the neutral acid, (**2**) the anionic boronate, (**3**) the boronic ester and (**4**) the boronate ester.

research efforts to design boronic acids with pK_a close to 7 for optimal operation in neutral solutions. Recently, a few very promising phenylboronic compounds have been reported using electronegative (electron-withdrawing) substituents at the aromatic ring that stabilize both the transition state and the final anionic product, increasing the stability constant.

Another issue with boronic acids associated glucose sensing is their relatively low selectivity for glucose over other carbohydrates. In this respect, bisboronic acids, consisting of two boronic moieties spatially arranged in a manner optimal for complexation with glucose, look promising. For example, Eggert *et al.* [62] reported a fluorescent bisboronic derivative of anthracene (Figure 6.3) that is very specific to D-glucose and has equilibrium binding constant K_{eq} of 2500 M^{-1} in water at pH 7.4.

Among different compounds 3-aminophenylboronic acid (APBA) has been chosen to test feasibility of using boronic acids with microcantilever transducers. Comparing to other more sophisticated boronic recognition probes, APBA is commercially available. In addition, its amino group ($-NH_2$) makes it very convenient for solid-state immobilization. The pK_a of surface-immobilized APBA-based monolayer is estimated to be around 8.0, lower than in solution (~8.6) [63]. Its glucose esters are expected to have pK_a around 7.

Aminophenylboronic acid has been examined for glucose monitoring by several research groups using different transduction configurations. The most popular signaling

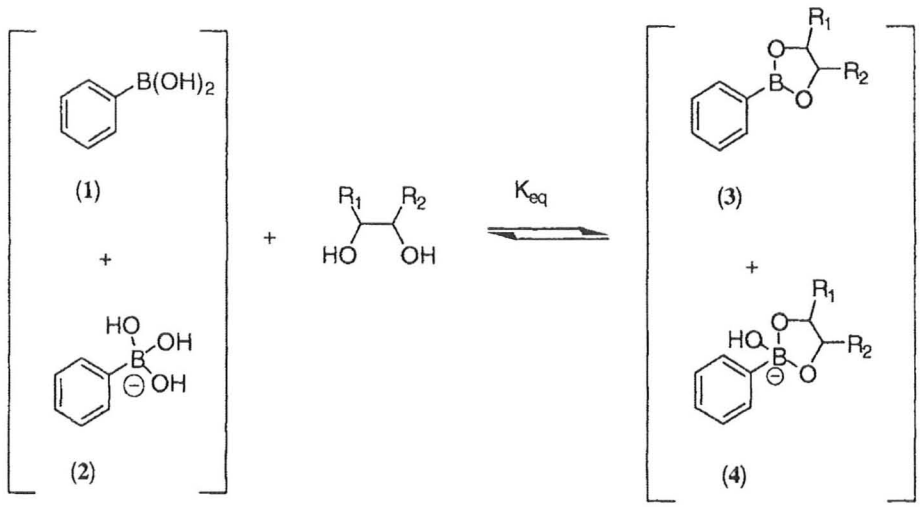

Figure 6.2: Overall binding process between (phenyl)boronic acid and a diol [61]

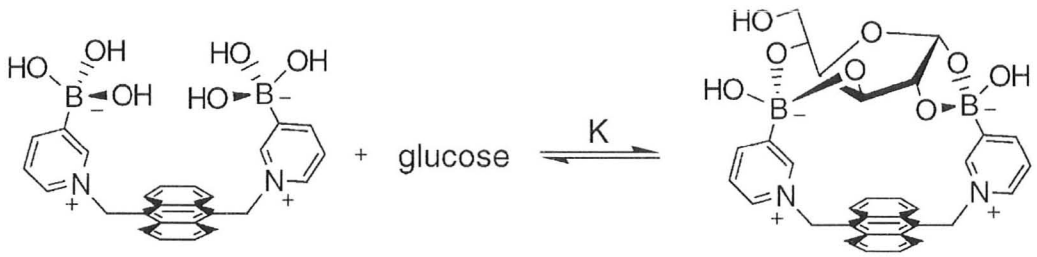

Figure 6.3: Glucose-selective fluorescent bisboronic acid [62]

method is to link boronic acid with a dye or a fluorophore (like anthracene in Figure 6.3) for colorimetric or spectroscopic measurements. However, other transducers have been investigated as well. For instance, Pribyl & Skladal [64] created a direct affinity sensor for saccharides and glycated hemoglobin using a self-assembled monolayer of thiol-coupled APBA on surface of quartz crystal microbalance (QCM) detector. The response to glucose at pH 7.0 was linear for concentrations up to 85 mM with the association constant K_{eq} of $14.4\,M^{-1}$ and the detection limit about 25 mM. At the same time, pH 9.0 was found to be optimal for operation of the QCM sensor with immobilized APBA. It should be noted that sensitivity of QCM method to small molecules (molecular weight of glucose is only $180.16\,g/mol$) is generally low because the signal of QCM sensors is directly proportional to the mass of complex formed on the sensing surface.

Lee *et al.* [65] reported surface plasmon resonance (SPR) spectroscopy of monosaccharides solutions based on a phenylboronic acid monolayer. The measurements were conducted at very low sugar concentrations ($10^{-12} - 10^{-4}$ M) at pH 7.4. The experimental results are quite remarkable, because even at such low concentra-

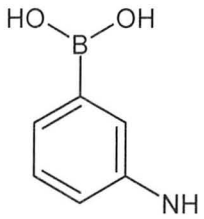

Figure 6.4: Chemical structure of 3-aminophenylboronic acid (APBA)

tions of glucose, there was a gradual change of SPR angle with concentration increase. However, I should notice that it is unclear if control experiments were conducted to rule out the contribution of refractive index changes to the results.

Takahashi & Anzai [63] took another approach and prepared phenylboronic acid–modified electrodes for the voltammetric detection of monosacharides. The operation principle of the sensor is based on increase of the surface density of the anionic charge upon sugar binding. The electrical current exhibited a significant response to glucose even at pH 7.6 with detection range of $3 - 300$ mM. A drop of the monolayer pK_a up to 1.5 units was observed upon ester formation. However, a practical application of such sensors is very problematic because its operation requires presence of soluble redox ions (ferricyanide).

In contrast to the outlined reports, in this work APBA is immobilized through silicon functionalization chemistry that seems more appropriate for construction of robust sensors. It can be speculated that the surface charge, resulting from conversion from neutral phenylboronic acid into anionic phenylboronate ester upon glucose binding, may produce surface stress. This hypothesis is the idea behind combination of sugar recognition by boronic acid with a microcantilever sensor.

6.2 Sensor fabrication

3-Aminophenylboronic acid monohydrate (APBA) was purchased from Sigma-Aldrich. The immobilization procedure is described in Chapter 3. After cantilevers silanization, the surface amino groups ($-NH_2$) were converted into carboxyl groups ($-COOH$) by succinic anhydride treatment. Then molecules of APBA were anchored through its amino group. The concentration of APBA in the immobilization solution was 7.8 mg/ml (50 mM).

The structure of the immobilized recognition layer is schematically illustrated in Figure 6.5.

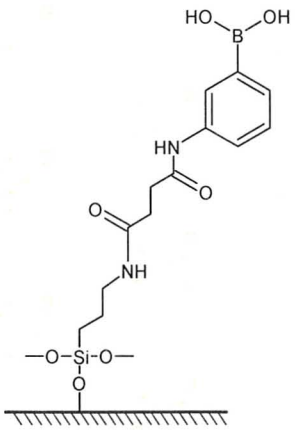

Figure 6.5: Schematic illustration of immobilized aminophenylboronic acid

6.3 Experimental results

The maximum observed cantilever deflection was less than 70 nm. Figure 6.6 illustrates an example of cantilever response to injection of 10 mM glucose solution. The deflection is approximately 50 nm. The direction of the bending corresponded to compressive surface stress. Due to poor experimental repeatability it was impossible to determine the functional dependency of cantilever deflection on glucose concentration and its parameters.

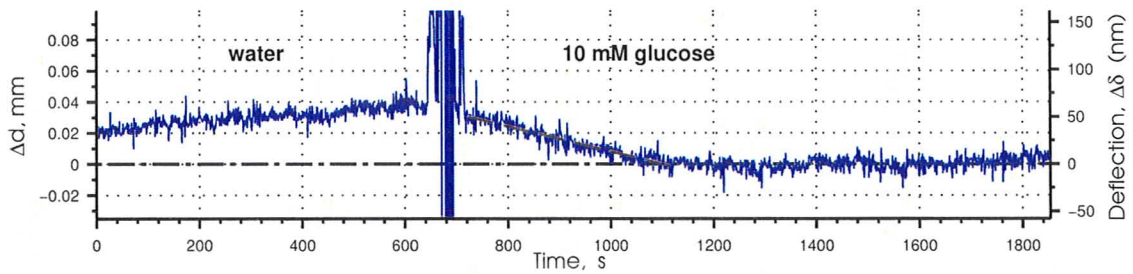

Figure 6.6: Deflection response of APBA sensor to 10 mM glucose solution. The deflection is approximately 50 nm.

6.4 Discussion

The relatively small deflection of cantilevers coated with APBA could be explained by nonoptimal conditions for this boronic acid. As it has been mentioned the pK_a of surface-immobilized APBA-based monolayer is around 8.0, hence at pH 7 only a fraction of molecules are in the boronate form that has high affinity for diols. Therefore, it seems promising to use more sophisticated boronic derivatives with optimized pK_a and glucose selectivity.

7 Sensor based on molecularly imprinted polymer

7.1 Introduction

Molecular imprinting can be defined as process of template-induced formation of specific recognition sites (binding or catalytic) in a material where the template directs the positioning and orientation of the material's structural components by a self-assembling mechanism [66]. Molecular imprinting can be achieved in several materials including inorganic silica and titanium oxide, but polymers are the most popular because of limitless possibilities for composition and mature fabrication and characterization technologies developed for polymers.

Molecularly imprinted polymers (MIPs) are prepared by cross-linking polymerization in the presence of the target compound — *template*. The template molecule is first allowed to form bonds with one or several types of functional monomers in a prearrangement step, and subsequent fixation of these bonds during polymerization and cross-linking leads to the formation of a matrix that contains recognition sites selective for the template. By this procedure, natural binding sites can be mimicked synthetically in a simple but effective way and the resulting molecularly imprinted materials are often characterized by having very high chemical and physical stability. The overall process of template polymerization is illustrated in Figure 7.1 and consist of a few major steps:

- The functional monomers form bonds with the template and arrange in the target-specific manner.

- A polymer network with the recognition sites is formed as result of cross-linking polymerization. Thereby, the position and the spatial conformation of the monomers are fixed in an arrangement complementary to the template.

- The embedded template is extracted from the polymer matrix to make the binding sites available for future rebinding of the analyte.

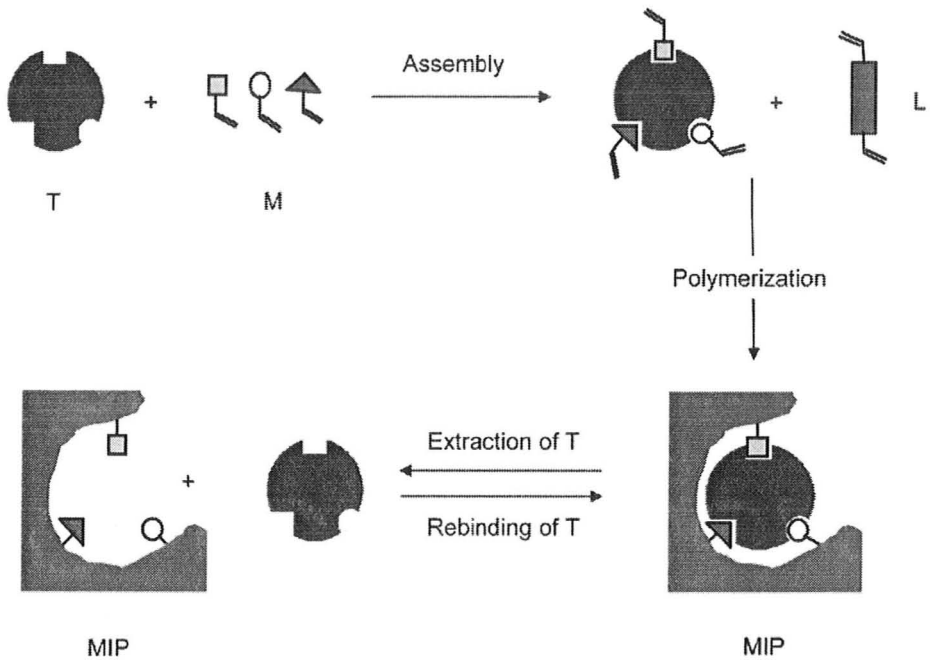

Figure 7.1: The general scheme of noncovalent molecular imprinting [66]. **T** denotes a template, **M**—functional monomers, **L**—a cross-linker.

Template polymerization can be classified in two major types base on the nature of interactions between the template and the monomers:

- The covalent approach is based on formation of reversible covalent bonds between the template and the monomers prior to polymerization. For instance, boronic acids can be used as the functional monomer to form covalently bound stoichiometric complexes with carbohydrates [67, 68]. This method allows to create well-defined recognition sites with high specificity and affinity. However, the template extraction is cumbersome requiring chemical cleavage of the bonds. Therefore, reversibility and repeatability of sensors based on such polymers is very limited.
- In contrast, the noncovalent approach is based on weak noncovalent interactions such as hydrogen bonds and van der Waals forces. This technique is more flexible at expense of a higher degree of heterogeneity in the binding sites and thus less selectivity and strength of recognition.

Molecularly imprinted polymers have been used as antibody mimics in various recognition systems and biomimetic sensors. Compared to biomolecules such as antibodies or enzymes, which can recognize targets with high affinity but have poor chemical stability, polymers offer unmatched robustness under different environmental factors (organic solvents, pH, temperature). Hence, MIPs may be of great utility in construction of implantable sensors including continuous glucose monitoring systems.

Table 7.1: Structural comparison of amino acids with monomers used in the preparation of MIPs [16]

Amino acids	Structure	Monomers	Structure
Aspartic acid (Asp)	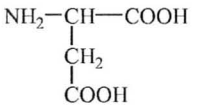	Vinyl acetic acid (VAA)	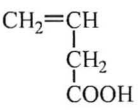
Glutamic acid (Glu)	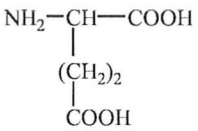	4-Pentenoic acid (PA)	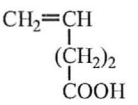
Asparagine (Asn)	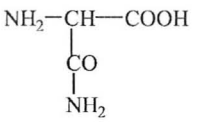	Acrylamide (Aam)	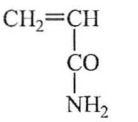
Phenyl alanine (Phe)	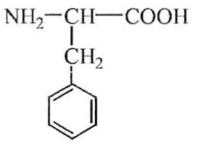	Allyl benzene (AB)	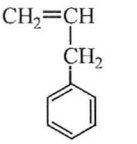

Construction of a noncovalent glucose imprinted polymer has been reported by Seong *et al.* [16] who used the biomimetic approach for the rational design. Table 7.1 lists the amino acids known to form binding sites in five glucose-specific proteins: human glucokinase, D-xylose isomerase, lectins (Lathyrus ochrus isolectin I and Concanavalin A), and glucose/galactose-binding protein (GGBP). Most common asparagine (Asn), aspartic (Asp) and glutamic acids (Glu) define affinity to the monosaccharide through establishment of hydrogen bonds with hydroxyl groups of the glucose molecule. Certain amino acid residues could form multiple hydrogen bonds with different hydroxyl groups of the same glucose molecule. In addition, aromatic rings of phenyl alanine (Phe) or tryptophan may be involved in stacking interaction with glucopyranose ring. However, the latter effect is minor and these amino acids are not essential for glucose binding. The stereochemical analysis indicated that a certain spatial arrangement of the amino acid residues results in glucose-specific binding sites.

Mimicking the natural proteins, Seong *et al.* [16] used the vinyl monomers possessing functional groups similar to the aforementioned amino acids: vinyl acetic acid (VAA), acrylamide (AAm), 4-pentenoicacid (PA), and allylbenzene (AB). Glucose imprinted polymers were synthesized by free radical solution polymerization in dimethyl sulfoxide (DMSO) using glucose as a template and N,N'-methylenebisacrylamide (MBAAm) as a cross-linking agent. Control polymers without glucose imprinting (NIP) were prepared under identical conditions and were used as a reference. It should be noted that glucose imprinting in aqueous phase is hardly possible because water is highly competitive for hydrogen bonds, thus the functional monomers are not able to

prearrange and form associations with glucose molecules. In contrast, DMSO being an aprotic solvent does not display strong hydrogen bonding and at the same time dissolves a wide range of both polar and nonpolar compounds. The synthesized bulk polymers were dried and ground to particles less than 50 μm in diameter. Glucose molecules trapped inside the polymer matrix were extracted by extensive washing with deionized water.

Seong *et al.* [16] examined glucose-binding affinity of synthesized MIPs and NIPs by using an equilibrium dialysis technique that consists in measurement of glucose amount bound to a polymer after equilibration with glucose solution. The highest measured affinity K_d was 1.66 mM, while K_d values of glucose-non-imprinted polymers were in the range of $32.6 - 49.1$ mM. To compare the contribution of each monomer to glucose binding, MIPs having different monomer ratios were synthesized to determine that the strength of interaction with glucose is in the order VAA > AAm > AB > PA. This implies that PA has weaker hydrogen bonding than that of VAA or AAm probably because of its longer side chain that may decrease conformational stability of the binding sites. It is also not surprising that the hydrophobic interaction of AB is weaker than generally stronger hydrogen bonding of VAA or AAm. The amount of cross-linker had a profound effect on polymer properties through stabilization of a polymer network. Highly cross-linked polymers exhibited stronger glucose bonding, while the degree of swelling in water was much less. It should be noted that in general, effective imprinting in polymers requires high degree of cross-linking to stabilize the size and conformation of template–binding sites.

Molecularly imprinted polymers have been used in a number of different sensor configurations, including surface plasmon resonance spectroscopy, quartz crystal microbalance and electrochemical detectors. Surprisingly, to the best of my knowledge there have been no reports on the use of MIPs with microcantilever sensors. One of the objectives of this thesis was to examine glucose-binding properties of the glucose imprinted polymer with surface stress measurement system.

The glucose imprinted polymer designed by Seong *et al.* [16] demonstrated very promising affinity results. However, it was synthesized using solution phase polymerization that produces a polymer in bulk or particle forms suitable only for application in affinity chromatography or extraction columns. In contrast, most types of sensors require a recognition element applied as a thin layer. Furthermore, it is desirable to keep its thickness as small as possible to decrease response time because diffusion constants even for such a small molecule as glucose are very small in highly cross-linked polymers. Therefore, the original bulk polymerization method of Seong *et al.* [16] has been substituted in this work by surface initiated polymerization (SIP). This technique produces an ultrathin polymer film "grafted from" a solid surface with highly controllable thickness. The description of the method is given in the following section.

The imprinted polymer was also synthesized by free radical polymerization for characterization of its bulk properties.

7.2 Surface initiated polymerization

For superior performance of polymer sensors, it is very important to synthesize polymers, strongly attached to surface. In surface initiated polymerization (SIP) or so-called "grafting from" approach polymer chains grow away directly from the surface. It is achieved by application of a polymerization initiator as a self-assembled monolayer on the solid support. As result of initiation and following propagation, generated radicals stay confined to the surface of the substrate and the polymer film forms firmly attached to the substrate through covalent bonds (depending on the type of the underlying self-assembled monolayer). With this technique, very reproducible layers with high graft density and high molecular weight of the tethered chains can be formed. Moreover, the thickness of the polymer film is well controlled by duration of polymerization reaction and can vary from a few nanometers to a micron and more.

In this work, the glucose imprinted polymers were prepared by radical polymerization using initiator azobis(cyanovaleric acid) (ACVA) covalently bound to the silicon side of cantilevers [69]. ACVA is a water-soluble compound with terminal carboxyl groups. Hence, it was possible to use a general immobilization method described in Chapter 3 for a covalent attachment of the initiator to the amino-functionalized support through carbodiimide chemistry. The following polymerization was performed in a solution of monomers (and the template) by thermal initiation.

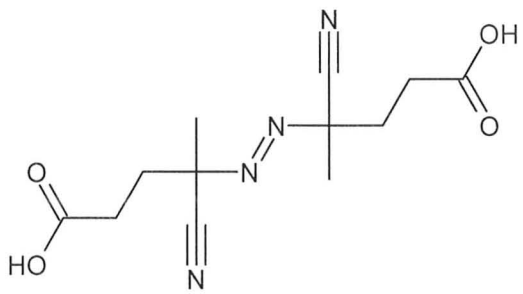

Figure 7.2: Chemical structure of initiator azobis(cyanovaleric acid) (ACVA)

7.3 Polymer fabrication

7.3.1 Bulk polymerization

The polymer formulation was based on polymer P2-4 from [16] with a few modifications. The original initiator azobisisobutyronitrile (AIBN) was substituted by similar water-

Table 7.2: Composition of the glucose imprinted polymers

Formulation	Template[a] D-glucose, (mM)	Functional monomers MAA, (mM)	AAm, (mM)	Cross-linker MBAAm, (mM)	Initiator[b] ACVA, (mM)	Monomer content[c] % (w/v)
"Original" from [16]	2	2	2	60	0.34	0.96%
Modified	100	600	600	130	4.1	11.4%

[a]For imprinted polymers

[b]For bulk polymerization only

[c]The total amount of monomers and cross-linker

soluble 4,4′-azobis(4-cyanovaleric acid) (ACVA) that is suitable for both bulk (solution phase) and surface initiated types of polymerization. The carboxylic functional monomers vinyl acetic acid (VAA) and 4-pentenoic acid (PA) were replaced by more commonly used methacrylic acid (MAA), which carries the carboxyl functional group as well, but its side chain is shorter that should be beneficial for conformational stability of the polymer. The hydrophobic monomer allylbenzene (AB) was not used, because according to Seong *et al.* [16] it was optional for glucose binding.

Table 7.2 lists the compositions of the prepared polymers. "Original" denotes the formulation with the same monomer concentrations as was used by Seong *et al.* [16]. The modified version has higher reagents concentrations with increased total monomer content to improve efficiency of polymerization. At the same time, the molar ratio of cross-linker (MBAAm) to functional monomers was decreased from 15:1 to 1:9 because the amount of the cross-linker determines rigidity of the polymer network and hence swelling behavior. Usually low-crosslinked polymers (like hydrogels) are associated with higher chemomechanical responsiveness and transduction sensitivity than highly-crosslinked counterparts.

Bulk polymer preparation was performed out in a test tube. The monomers, cross-linker, initiator and glucose were dissolved in 10 ml of dimethyl sulfoxide (DMSO). The solution was purged with nitrogen to remove oxygen, which acts as a free radical scavenger. The thermal initiation was carried out by immersing the stopped test tube in a thermostated water bath at 65°C for 3 h. The bulk polymer was cut in cylindrical pieces, washed with DMSO for one day and extensively washed with deionized water for 2 days to remove the template and any unreacted reagents.

Control polymers without glucose imprinting were prepared at the same time under identical conditions.

7.3.2 Sensor fabrication

Immobilization of radical initiator ACVA on the silicon side of cantilevers was carried out using the procedure described in Chapter 3. The concentration of ACVA in the immobilization solution at the final step was 14 mg/ml (50 mM).

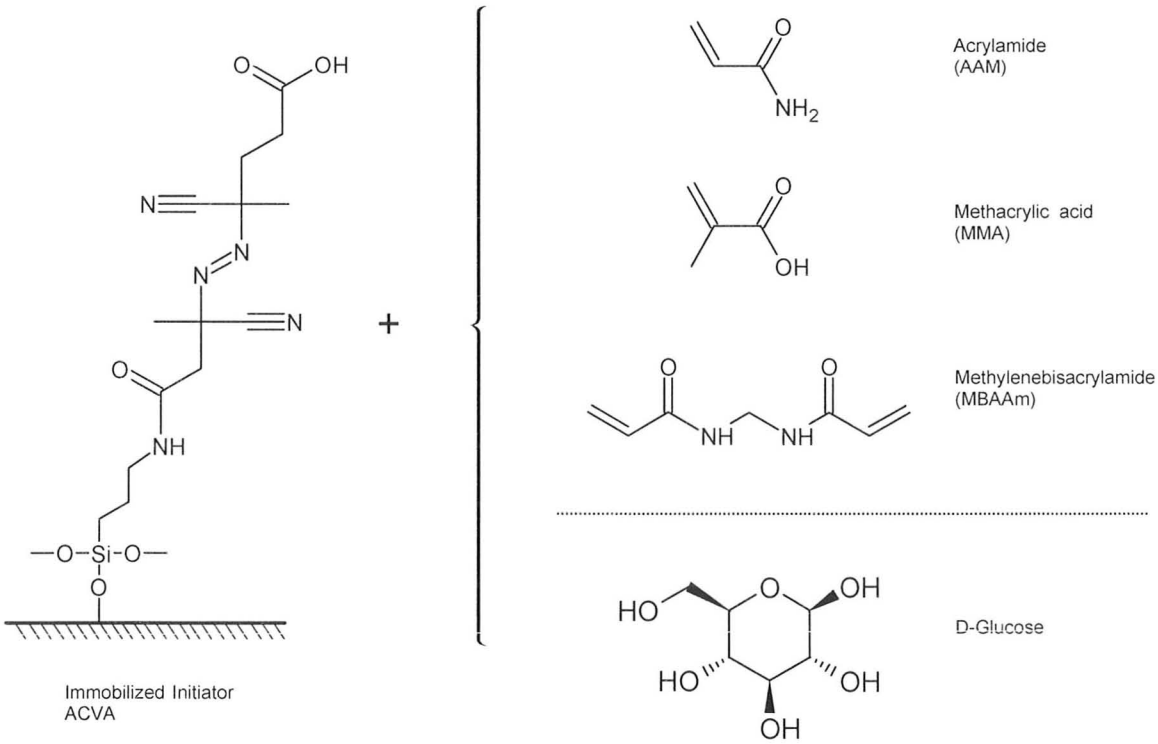

Figure 7.3: Schematic illustration of surface initiated polymerization of glucose imprinted polymer

Prior to polymerization, a solution of the monomers and glucose in DMSO at concentrations listed in Table 7.2 was purged with nitrogen to remove oxygen, which acts as a free radical scavenger. Cantilever chips with the attached initiator were place in a glass vial with the monomer solution and the thermal initiation was carried out in a thermostated water bath at 65°C for 2 h. Then, the chips were washed with DMSO and deionized water for one day to remove the template and any unreacted reagents.

7.4 Experimental results

7.4.1 Cantilever experiments

Cantilevers experiments did not demonstrate any significant bending response.

7.4.2 Characterization of bulk polymers

Surprisingly, polymerization and filtration of the "original" monomer composition, similar to one reported by Seong *et al.* [16], did not result in any observable quantity of a polymer.

In contrast, solution polymerization using the modified formulation resulted in practically complete monomer conversion. Then, swelling behavior was determined by subjecting the polymers to equilibration for 2 days in DMSO, deionized water, 1 M glucose solution and 1 M fructose solution (in water). The swelling ratio (S) was calculated by dividing the weight of the "wet" polymer by that of the dried polymer. The following polymer properties were observed:

- The dry polymer is glassy and highly fragile.
- The polymer in DMSO is translucent and highly swollen with the swelling ratio of 9 – 10.
- The polymer in pure water is opaque and shrunk with the swelling ratio of only 2 – 3. Mechanical integrity and stability are deteriorated.
- The polymer does not demonstrate any noticeable changes upon introduction into concentrated glucose or fructose solutions. The mass increase comparing to its mass in pure water is 10% in both cases.

No difference in imprinted and control polymers was observed.

7.5 Discussion

The zero yield of polymerization using similar conditions ("original" composition) to those reported by Seong *et al.* [16] is very surprising. However, considering very low monomer content (less than 1.5% (w/v) in [16]) a produced polymer should have very low molecular weight and hence its filtration is problematic. Specific binding capabilities in such polymers are highly unlikely.

The polymers synthesized using the modified formulation demonstrated unexpected phase transition behavior in solvents. It was swollen in DMSO, but was shrunk in water despite being composed of the hydrophilic monomers and cross-linker. Hence, the lack of observable glucose affinity can be explained by a significantly disturbed conformation in water comparing to the conformation during imprinting and polymerization. In addition, in a shrunk polymer network glucose diffusion is substantially obstructed.

In light of the conducted experiments, the results claimed by Seong *et al.* [16] look doubtful. Careful examination of the article reveals, for example, that a 10 mg piece of the MIP had a glucose binding capacity of 9 μmol, whereas only 2 μmol of the template was used in polymerization. Moreover, no experiments with other monosaccharides were conducted to determine selectivity for glucose. Therefore, the described glucose binding results were probably because of non-specific glucose absorption. The difference in binding data for "imprinted" and control polymers was

most likely due to higher polymer porosity caused by the presence of glucose during polymerization.

In this respect, the findings made by Fazal & Hansen [70] are remarkable. They determined that glucose specificity of poly(allylamine hydrochloride) hydrogels prepared by Dr Kofinas's group [71, 72] was not because of imprinting effect, but due to the differences in solubilities of closely related sugars in the polymer bulk. They also noticed that far more sugar was bound by the hydrogels than the amount of the template used in their preparation.

Conclusion and Future Outlook

Problems with existing devices based on electrochemistry have encouraged alternative approaches to glucose sensing in recent years. In Chapter 1, several molecular recognition principles and transduction techniques used for sugar detection were reviewed. Three different glucose receptors have been identified for application with very promising microcantilever sensors.

A modular chemical procedure has been designed for covalent modification of silicon surface of cantilevers. It allows "directional" (on only one side) immobilization of a wide class of compounds with amino ($-NH_2$) or carboxyl ($-COOH$) groups by a simple protocol.

The cantilever sensors were tested in aqueous solutions using a custom-built system. The nanoscale deflection was measured by means of an optical lever system with a lateral position sensitive detector for beam tracking. Precision of deflection measurements was around 1.5 nm. However, the performance of the system and repeatability of measurements were seriously compromised by significant drift that could be as high as $250\,^{nm}/_{h}$. The cause of drift phenomena is unclear, but it is probably related to formation of air bubbles inside the fluid cell. It limited duration of experiments and consequently prohibited measurement of the equilibrium state of cantilevers. In addition, only fast processes that induce substantial changes of surface stress can be reliably measured. As result, the use of reference cantilevers to subtract a common drift trend is essential. Such technique has been demonstrated by a few research groups to achieve high sensitivity and reproducibility. However, readout of cantilever arrays requires very sophisticated instrumentation. Moreover, independent chemical modification of microscopic cantilevers is a great challenge.

One type of the cantilever sensors was based on glucose oxidase, an enzyme commonly used for clinical and industrial detection of glucose. The observed noticeable response is comparable to values reported in literature. However, such a sensor is liable to many drawbacks of conventional glucometers — irreversible glucose consumption, dependence on availability of the co-substrate (oxygen) and production of corrosive hydrogen peroxide. In this respect, sensors based on nonreactive glucose binding proteins, such as apo-enzymes, Concanavalin A and genetically engineered glucose/galactose-binding proteins, are promising candidates for future investigations.

The second type of sensors was based on aminophenilboronic acid (APBA). This synthetic compound is able to reversibly complexate molecules of glucose through formation of covalent bonds. Unfortunately, its sensitivity and specificity to glucose under physiological conditions is rather low, which was reaffirmed by moderate response

of APBA-coated cantilevers. However, the performance of such microcantilever detectors can be significantly enhanced by application of sophisticated bisboronic compounds, some of which have been demonstrated to bind glucose with high affinity and selectivity under pH 7.

The third class of sensors was based on molecularly imprinted polymers that formed through non-covalent template polymerization in the presence of glucose. Unfortunately, the cantilevers with the polymer coatings did not show any noticeable response. Bulk polymers with similar composition demonstrated small swelling of the same magnitude to glucose and fructose. As result, glucose imprinting effect is highly unlikely in the synthesized polymers. It should be noted that monosaccharides imprinting through non-covalent interactions for detection in aqueous solutions seems to be hardly possible, because glucose molecules are able to participate only in a few weak non-specific hydrogen bonds and have to **compete** for the bonds with water molecules. Considering heterogeneity and labile structure of polymers, the cavities formed during template polymerization cannot have high stability and complementarity.

This work demonstrates possibility of using highly sensitive cantilever sensors with different classes of receptors for glucose recognition. For a practical application it is necessary to resolve underlying issues with measurement reliability and reproducibility. The performance can be significantly enhanced by careful selection and engineering of a recognition element. Moreover, this transduction platform can be applied to sensing of a great variety of analytes beside glucose using an appropriate receptor.

Bibliography

[1] Edelman, S. V. Importance of glucose control. *Medical Clinics of North America* 1998, *82*, 665–687.

[2] Lodish, H.; Berk, A.; Zipursky, L. S.; Matsudaira, P.; Baltimore, D.; Darnell, J. *Molecular Cell Biology*, 4th edition. W. H. Freeman and Company, 2000.

[3] Raba, J.; Mottola, H. Glucose oxidase as an analytical reagent. *Critical Reviews in Analytical Chemistry* 1995, *25*, 1–42.

[4] Goodsell, D. S. RCSB PDB molecule of the month. doi:10.2210/rcsb_pdb/mom_2006_5 May 2006.

[5] Bankar, S. B.; Bule, M. V.; Singhal, R. S.; Ananthanarayan, L. Glucose oxidase – an overview. *Biotechnology Advances* 2009, *27*, 489–501.

[6] Wang, J. Glucose biosensors: 40 years of advances and challenges. *Electroanalysis* 2001, *13*, 983–988.

[7] Park, S.; Boo, H.; Chung, T. D. Electrochemical non-enzymatic glucose sensors. *Analytica Chimica Acta* 2006, *556*, 46–57.

[8] Wilson, G. S.; Johnson, M. A. In-vivo electrochemistry: What can we learn about living systems? *Chemical Reviews* 2008, *108*, 2462–2481.

[9] Wilson, R.; Turner, A. P. F. Glucose oxidase: an ideal enzyme. *Biosensors and Bioelectronics* 1992, *7*, 165–185.

[10] Staiano, M.; Bazzicalupo, P.; Rossi, M.; D'Auria, S. Glucose biosensors as models for the development of advanced protein-based biosensors. *Molecular Biosystems* 2005, *1*, 354–362.

[11] Chinnayelka, S.; McShane, M. J. Resonance energy transfer nanobiosensors based on affinity binding between apo-enzyme and its substrate. *Biomacromolecules* 2004, *5*, 1657–1661.

[12] Pickup, J. C.; Hussain, F.; Evans, N. D.; Rolinski, O. J.; Birch, D. J. Fluorescence-based glucose sensors. *Biosensors and Bioelectronics* 2005, *20*, 2555–2565.

[13] Zhao, Y.; Li, S.; Davidson, A.; Yang, B.; Wang, Q.; Lin, Q. A MEMS viscometric sensor for continuous glucose monitoring. *Journal of Micromechanics and Microengineering* 2007, *17*, 2528.

[14] Borrok, M. J.; Kiessling, L. L.; Forest, K. T. Conformational changes of glucose/galactose-binding protein illuminated by open, unliganded, and ultra-high-resolution ligand-bound structures. *Protein Science* 2007, *16*, 1032–1041.

[15] Amiss, T. J.; Sherman, D. B.; Nycz, C. M.; Andaluz, S. A.; Pitner, J. B. Engineering and rapid selection of a low-affinity glucose/galactose-binding protein for a glucose biosensor. *Protein Science* 2007, *16*, 2350–2359.

[16] Seong, H.; Lee, H.; Park, K. Glucose binding to molecularly imprinted polymers. *Journal of Biomaterials Science-Polymer Edition* 2002, *13*, 637–649.

[17] Piliarik, M.; Vaisocherova, H.; Homola, J. Surface plasmon resonance biosensing. *Biosensors and Biodetection* 2009, *503*, 65–88.

[18] Amarie, D.; Alileche, A.; Dragnea, B.; Glazier, J. A. Microfluidic devices integrating microcavity surface-plasmon-resonance sensors: Glucose oxidase binding-activity detection. *Analytical Chemistry* 2009, *82*, 343–352.

[19] Binnig, G.; Quate, C. F.; Gerber, C. Atomic force microscope. *Physical Review Letters* 1986, *56*, 930–933.

[20] Lim, S.-H. *Opto-Mechanical Sensor Array for Physicallyl and Chemically Induced Nanoscale Motion Detection.* Ph.D. thesis, University of California, Berkeley 2005.

[21] Timoshenko, S. Analysis of bi-metal thermostats. *J. Opt. Soc. Am.* 1925, *11*, 233–233.

[22] Shuttleworth, R. The surface tension of solids. *Proceedings of the Physical Society. Section A* 1950, *63*, 444–457.

[23] Linford, R. G. The derivation of thermodynamic equations for solid surfaces. *Chemical Reviews* 1978, *78*, 81–95.

[24] Grafov, B. M. The Shuttleworth equation for a finite surface strain. *Journal of Electroanalytical Chemistry* 1999, *471*, 105–108.

[25] Zhang, Y.; Ren, Q.; Zhao, Y.-P. Modelling analysis of surface stress on a rectangular cantilever beam. *Journal of Physics D: Applied Physics* 2004, *37*, 2140.

[26] Miyatani, T.; Fujihira, M. Calibration of surface stress measurements with atomic force microscopy. *Journal of Applied Physics* 1997, *81*, 7099–7115.

[27] Sader, J. E. Surface stress induced deflections of cantilever plates with applications to the atomic force microscope: Rectangular plates. *Journal of Applied Physics* 2001, *89*, 2911–2921.

[28] Stoney, G. G. The tension of metallic films deposited by electrolysis. *Proceedings of the Royal Society of London. Series A* 1909, *82*, 172–175.

[29] Putman, C. A. J.; De Grooth, B. G.; Van Hulst, N. F.; Greve, J. A detailed analysis of the optical beam deflection technique for use in atomic force microscopy. *Journal of Applied Physics* 1992, *72*, 6–12.

[30] Polesel-Maris, J.; Aeschimann, L.; Meister, A.; Ischer, R.; Bernard, E.; Akiyama, T.; Giazzon, M.; Niedermann, P.; Staufer, U.; Pugin, R.; de Rooij, N. F.; Vettiger, P.; Heinzelmann, H. Piezoresistive cantilever array for life sciences applications. *Journal of Physics: Conference Series* 2007, *61*, 955.

[31] Shiraki, I.; Miyatake, Y.; Nagamura, T.; Miki, K. Demonstration of low-temperature atomic force microscope with atomic resolution using piezoresistive cantilevers. *Review of Scientific Instruments* 2006, *77*, 023705.

[32] Fritz, J.; Baller, M. K.; Lang, H. P.; Rothuizen, H.; Vettiger, P.; Meyer, E.; J. Guntherodt, H.; Gerber, C.; Gimzewski, J. K. Translating biomolecular recognition into nanomechanics. *Science* 2000, *288*, 316–318.

[33] Ulman, A. Formation and structure of self-assembled monolayers. *Chemical Reviews* 1996, *96*, 1533–1554.

[34] Flynn, N. T.; Tran, T. N. T.; Cima, M. J.; Langer, R. Long-term stability of self-assembled monolayers in biological media. *Langmuir* 2003, *19*, 10909–10915.

[35] Plueddemann, E. P. *Silane coupling agents*, 2nd edition. Plenum Press, 1991.

[36] Pijanowska, D. G.; Remiszewska, E.; Pederzolli, C.; Lunelli, L.; Vendano, M.; Canteri, R.; Dudzinski, K.; Kruk, J.; Torbicz, W. Surface modification for microreactor fabrication. *Sensors* 2006, *6*, 370–379.

[37] Howarter, J. A.; Youngblood, J. P. Optimization of silica silanization by 3-aminopropyltriethoxysilane. *Langmuir* 2006, *22*, 11142–11147.

[38] Metwalli, E.; Haines, D.; Becker, O.; Conzone, S.; Pantano, C. G. Surface characterizations of mono-, di-, and tri-aminosilane treated glass substrates. *Journal of Colloid and Interface Science* 2006, *298*, 825–831.

[39] Hermanson, G. T. *Bioconjugate techniques.* Academic Press, 1996.

[40] Ghanem, A.; Ghaly, A. Immobilization of glucose oxidase in chitosan gel beads. *Journal of Applied Polymer Science* 2004, *91*, 861–866.

[41] NanoWorld AG. http://www.nanoworld.com/.

[42] Snow, D. E.; Weeks, B. L.; Kim, D. J.; Pitchimani, R.; Hope-Weeks, L. J. Nondestructive experimental determination of bimaterial rectangular cantilever spring constants in water. *Review of Scientific Instruments* 2008, *79*, 083706.

[43] Veeco Probes. http://www.veecoprobes.com/.

[44] Self, S. A. Focusing of spherical Gaussian beams. *Appl. Opt.* 1983, *22*, 658–661.

[45] Cohen, D. K.; Little, B.; Luecke, F. S. Techniques for measuring 1-μm diam Gaussian beams. *Appl. Opt.* 1984, *23*, 637–640.

[46] Sheu, F.-W.; Chang, C.-H. Measurement of the intensity profile of a Gaussian laser beam near its focus using an optical fiber. *American Journal of Physics* 2007, *75*, 956–959.

[47] McCally, R. L. Measurement of Gaussian beam parameters. *Appl. Opt.* 1984, *23*, 2227–2227.

[48] Cannon, B.; Gardner, T. S.; Cohen, D. K. Measurement of 1-μm diam beams. *Appl. Opt.* 1986, *25*, 2981–2983.

[49] Suzaki, Y.; Tachibana, A. Measurement of the μm sized radius of Gaussian laser beam using the scanning knife-edge. *Appl. Opt.* 1975, *14*, 2809–2810.

[50] Pacific Silicon Sensors. http://www.pacific-sensor.com/.

[51] Nemoto, S. Waist shift of a Gaussian beam by plane dielectric interfaces. *Applied Optics* 1988, *27*, 1833–1839.

[52] Lide, D., ed. *CRC Handbook of Chemistry and Physics*, 88th edition. CRC Press, 2007.

[53] Butt, H.-J. A sensitive method to measure changes in the surface stress of solids. *Journal of Colloid and Interface Science* 1996, *180*, 251–260.

[54] Subramanian, A.; Oden, P. I.; Kennel, S. J.; Jacobson, K. B.; Warmack, R. J.; Thundat, T.; Doktycz, M. J. Glucose biosensing using an enzyme-coated microcantilever. *Applied Physics Letters* 2002, *81*, 385–387.

[55] Pei, J.; Tian, F.; Thundat, T. Glucose biosensor based on the microcantilever. *Analytical Chemistry* 2004, *76*, 292–297.

[56] Yan, X.; Xu, X. K.; Ji, H.-F. Glucose oxidase multilayer modified microcantilevers for glucose measurement. *Analytical Chemistry* 2005, *77*, 6197–6204.

[57] Yan, X.; Hill, K.; Gao, H.; Ji, H.-F. Surface stress changes induced by the conformational change of proteins. *Langmuir* 2006, *22*, 11241–11244.

[58] Berg, J. M.; Tymoczko, J. L.; Stryer, L.; Stryer, L. *Biochemistry*, 5th edition. W. H. Freeman and Company, 2002.

[59] Yan, X.; Lvov, Y.; Ji, H.; Singh, A.; Thundat, T. A general microcantilever surface modification method using a multilayer for biospecific recognition. *Organic & Biomolecular Chemistry* 2003, *1*, 460–462.

[60] Yan, X.; Ji, H.-F.; Lvov, Y. Modification of microcantilevers using layer-by-layer nanoassembly film for glucose measurement. *Chemical Physics Letters* 2004, *396*, 34–37.

[61] Kaur, G.; Lin, N.; Fang, H.; Wang, B. Boronic acid-based fluorescence sensors for glucose monitoring. *Glucose Sensing* 2006, pp. 377–397.

[62] Eggert, H.; Frederiksen, J.; Morin, C.; Norrild, J. C. A new glucose-selective fluorescent bisboronic acid. First report of strong α-furanose complexation in aqueous solution at physiological pH. *The Journal of Organic Chemistry* 1999, *64*, 3846–3852.

[63] Takahashi, S.; Anzai, J.-I. Phenylboronic acid monolayer-modified electrodes sensitive to sugars. *Langmuir* 2005, *21*, 5102–5107.

[64] Pribyl, J.; Skladal, P. Quartz crystal biosensor for detection of sugars and glycated hemoglobin. *Analytica Chimica Acta* 2005, *530*, 75–84.

[65] Lee, M.; Kim, T.-I.; Kim, K.-H.; Kim, J.-H.; Choi, M.-S.; Choi, H.-J.; Koh, K. Formation of a self-assembled phenylboronic acid monolayer and its application toward developing a surface plasmon resonance-based monosaccharide sensor. *Analytical Biochemistry* 2002, *310*, 163–170.

[66] Yan, M.; Ramstrom, O. *Molecularly imprinted materials: science and technology.* Marcel Dekker, 2005.

[67] Wulff, G.; Schauhoff, S. Enzyme-analog-built polymers. 27. Racemic resolution of free sugars with macroporous polymers prepared by molecular imprinting. Selectivity dependence on the arrangement of functional groups versus spatial requirements. *The Journal of Organic Chemistry* 1991, *56*, 395–400.

[68] Gao, S.; Wang, W.; Wang, B. Building fluorescent sensors for carbohydrates using template-directed polymerizations. *Bioorganic Chemistry* 2001, *29*, 308–320.

[69] Sulitzky, C.; Ruckert, B.; Hall, A. J.; Lanza, F.; Unger, K.; Sellergren, B. Grafting of molecularly imprinted polymer films on silica supports containing surface-bound free radical initiators. *Macromolecules* 2001, *35*, 79–91.

[70] Fazal, F. M.; Hansen, D. E. Glucose-specific poly(allylamine) hydrogels – a reassessment. *Bioorganic & Medicinal Chemistry Letters* 2007, *17*, 235–238.

[71] Parmpi, P.; Kofinas, P. Biomimetic glucose recognition using molecularly imprinted polymer hydrogels. *Biomaterials* 2004, *25*, 1969–1973.

[72] Wizeman, W. J.; Kofinas, P. Molecularly imprinted polymer hydrogels displaying isomerically resolved glucose binding. *Biomaterials* 2001, *22*, 1485–1491.